Flexible Microelectromechanical Filters for Telecommunication Electronics

by

MANSOOR NASEER

Submitted to the Graduate School of Engineering and Natural Sciences
in partial fulfillment of
the requirements for the degree of
Master of Science

Sabanci University
Spring 2003

FLEXIBLE MICROELECTROMECHANICAL FILTERS FOR TELECOMMUNICATIONS ELECTRONICS

APPROVED BY

Assist. Prof. Dr. Ayhan BOZKURT .....

Assist. Prof. Dr. Erkay SAVAS .....

Assist. Prof. Dr. Ibrahim TEKIN .....

Assist. Prof. Dr. Thomas Franz BECHTELER .....

Assoc. Prof. Dr. Yasar GURBUZ .....
(Thesis Supervisor)

DATE OF APPROVAL: .....

to Whom Belongs All the Dominion

Acknowledgments

The professors and personnel of microelectronics group deserve a special mention. Each of them with their zest, intelligence and dedication towards their job set an example, provided all too necessary and timely feedback and comments on this work and supported, supplemented and broadened the study's perspective with their constructive ideas. Special thanks to Prof. Ayhan Bozkurt for his supreme genius and utmost interest and help in many of the miscellaneous projects that I have undertaken, and to Yasar Gurbuz, who apart from advising me in the thesis work also distinguished himself with his moral character. I am grateful to my advisor for his objectivity, cool-mindedness, and willingness to help, which proved ever so instrumental during various stages of this journey. May you continue to prosper and progress and be a wonderful company that you are to your students. Ameen.

I am thankful to Thomas Bechteler who shared two paper submissions with me and who also has a central contribution in this thesis. His lively personality encapsulated in objective and critical thinking allowed me the pleasure of having very interesting and fruitful conversations with him. I am also proud of our Lab. Technician Bulent Koroglu who is ever so ready to get involved with any clean room related jobs, not to mention his list of crazy projects, which kept him busy and surely kept me interested. Keep up with assembly, I am sure you will master it one day.

I am most grateful to professors of Faculty of Engineering and Natural Sciences especially Dr. Erkay Savas, Dr. Berrin Yanikoglu, Dr. Mehmet Ali Gulgun and, Dr. Mustafa Unel for their useful comments and eagerness to help. It has been a marvelous experience working on projects with them and learning from them. Dr. Bulent Ozgular and Dr. Mehdi Fardmanesh from Bilkent University deserve a special mention for their helpful references and support when needed and without which, this masters wouldnt have been possible.

My jury members and presentation audiance, with whom I have regularly interacted on a personal and academic basis including Ibrahim Tekin, Mehmet Keskinoz, Ilker Hamzaoglu, Ersin Ozugurlu, Meric Ozcan, Cem Ozturk, Yusuf Menceloglu, Serhat Yesilyurt, and Gokhan Goktug; my very best wishes and warmest regards for you and your future.

There are people who have had a fundamental impact in shaping my level of intellect and outlook during the course of my thesis. Respected Syed Imadudin Qadri sahib, my mentor and guide, who has always been so prompt and resourceful to address my needs. Respected Syed Mahumd sahib and respected Dr. Iftikhar Ahmed sahib and their families, who have been a source of encourgement and constant support during these years of hardship in a foreign country. Thank you very much for your support and comforting company at any times of unsettlement. You will always be a part of my memory.

The people who provided me with friendly company and never gave me a chance to miss my country including Rizwan Akram and Abullah Mirza, Mustafa Parlak, Alisher Kholmatov, Ercument Zorlu, Mustafa Coban, Mehmet Ozdemir, Murat Erman, Ibrahim Ulusoy, Mazhar Adli, Cemal Kocagozoglu, Gokahn Mutcali, Bayram Yenikaya, Bahattin, Veysi, and Ercan bey.

Last but not the least, my respected and most beloved parents who gave me a chance to pursue my ambitions and career and always provided me support and courage through thick and thin. May you remain long to impart happiness and joy around you, Ameen.

I do not know if I will ever get a chance to thank you all those, whom I could and could not mention, enough for bearing with me and being there for me. Thank you, may Allah bless you in this world and the next, Ameen.

FLEXIBLE MICROELECTROMECHANICAL FILTERS FOR TELECOMMUNICATIONS ELECTRONICS

Abstract

The telecommunication electronics sector is under intensive growth and research owing to the much needed expansion in functionality and mobility. As part of this change, more flexible and multi–featured products are gaining popularity, paving the way for uninterrupted and high-speed mobile communications. As the telecommunication devices become lighter, smaller, and smarter, they pose stringent constraints and challenges to the researchers of integrated telecommunication electronics. This thesis addresses one such field of research namely, micromachined resonator based filters and introduces a novel design methodology by providing an overall ease and simplification during the design flow. Present day filter applications are both bulky and off chip. An alternative, in the form of surface micromachined filters, which introduces considerable size reduction, exhibits industry–standard Quality factors and provide on chip capability, is studied and expanded upon.

The aim of this study is twice fold, one to allow the designers a method to design second order filters with greater flexibility than offered by hitherto standards and established procedures; two, to suggest an instructive guideline for extending the design process for higher order filters. The thesis also lays the foundation for fabrication of micromachined filters with mask fabrication, bill of materials, and processing experiments. It furthermore addresses the practical issues and constraints, such as aging, noise, and stability etc., which plague the transition of these research based prototypes to working systems.

Ozet

Haberleşme elektroniği sektörü giderek artan fonkisyonalite ve mobilite ihtiyacından dolayı yoğun bir büyüme ve araştırma çabası altındadır. Bu çabalar sonucu daha esnek ve çok özellikli ürünler giderek popüler olmaya baslamıstır. Bu ürünler bizlere kesintisiz ve yüksek hızlı mobil iletişimin kapılarını açmaktadır. Haberleşme devreleri gün geçtikçe daha da küçlüp, hafif ve akkıllı olmaya başladıkça bu alanda calışan araştırmacılarin önüne aşılması güç engeller ve koşullar getirmektedir. Bu tez bu zorlu alanlardan biriyle, yani MikroElektroMekanik (MEM) Rezonatör bazlı filtrelerle ilgilidir ve tasarım sürecini kolaylaştıran yeni bir tasarım metodu ortaya koymaktadır. Günümüz filtre teknolojisinde filtreler büyük yer kaplamakta ve çip harici üreıtilmektedir. Alternatif bir teknoloji olarak MEMS filtreler daha küçük yer kaplamakta, endüstri standartlarında kalite faktörü sağlamkta, ve elektronik devrelerle aynı çip üzerinde üretilebilmektedir.

Bu çalışmanın iki tane amacı vardır. Birincisi filtre tasarımcılarına normal filtre tasarım ve prosedürlerden daha fazla esneklik tanıyan ikinci dereceden filtre tasarımında yeni bir metod sunmak. Ikinci amaç ise bu filtre tasarım sürecini daha da yüksek derecelere çıkartmak için gerekli temel aşamalrı ortaya koymaktır. Bu tez aynı zamanda MEMS filtrenin fabrikasyonunu, maske üretimini, kullanılan materyalleri ve bu süreçte yapılan deneyleri de kapsamaktadır. Bunlara ek olarak bu tez, prototip üretiminden çalışan bir sisteme geçmek için gerekli pratik konulardan gürültü, yaşlanma ve stabilite vs. gibi konulara da değinmektedir.

Table of Contents

List of Figures

List of Tables

Chapter 1

Introduction

The recent surge in applications of radio frequency transceivers has been accompanied by aggressive design goals such as low cost, low power dissipation and high-speed data transfer. These goals are driven by both the need for better portability and affordability, and the ever-increasing demand for higher-speed data communications. Such objectives, together with the usual bandwidth limitations, not only call for highly integrable transceiver architectures, but also for bandwidth efficient modulation schemes. To address the demand for better portability and affordability, recent research has been focused toward the development of monolithic transceiver architectures.

Most of today's commercially available RF transceivers utilize some variant of conventional heterodyne architecture. In a heterodyne receiver, as shown in Figure 1.1, the RF front-end (preselection) filter serves to remove out-of-band signal energy as well as partially reject image band signals. After this prefiltering, the received signal is amplified by a low-noise amplifier (LNA). The IR (image reject) filter following the LNA further attenuates the undesired signals at the image band frequencies. The desired signal at the output of the IR filter is then down converted from the carrier frequency to a fixed IF by multiplication (mixing) with the output of a local oscillator (LO). Commonly, in heterodyne receivers, high-performance, low-phase-noise voltage-controlled oscillators (VCOs) employed as LOs are realized with discrete components such as high quality factor (Q) inductors and varactor diodes [1].

At the output of the mixer an IF filter, typically followed by a programmable–gain IF amplifier, selects the desired channel and reduces the distortion and dynamic

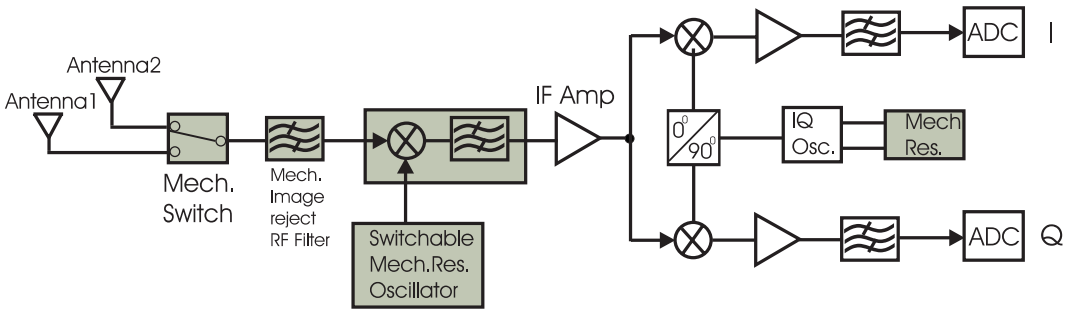

Figure 1.1: System-block diagram for a typical wireless receiver. Greyed out material are potential MEMS replacements

range requirements of the subsequent receiver blocks.

Conventionally, all the filters used in the heterodyne system are high Q discrete component filters, such as surface acoustic wave (SAW) or ceramic filters [2]. The heterodyne receiver has high selectivity, which can be defined as a measure of a receiver's ability to separate the desired band around the carrier frequency from signals received at other frequencies.

Consulting the IEEE standard frequency spectrum [3], RF range can be defined as extending from UHF (300−3000MHz) to S band (2−4GHz) for telecommunications. Similarly the IF filters are expected to work in frequency ranging from 455kHz to 254MHz. The workhorse employed widely in both RF and IF range has been quartz which meets high Q requirements. The quality factor ranges from 20,000 to over 1,000,000, depending upon the frequency and type of SAW and ceramic materials. Used with these characteristics, commercially available wireless systems contain numerous passive, SAW and crystal components. However, the use of these high Q elements does come with some drawbacks. One of the major limitation is that these components are implemented off−chip on the board level and then coupled with the rest of the integrated circuitry. For the off−chip implementations, the series resistance, which directly affects the Q is small, which requires high drive capability for the preceding LNA, inevitably leading to more severe trade−offs between gain, noise figure, stability and power dissipation in the amplifier [4]. The implementations tend to be bulky and hence size reduction is not possible.

Microelectromechanical (MEM) based transducers are considered as potential replacements for some of the bulky components used in the front–end transceiver. If we refer to Figure 1.1 some replaceable components are shaded. Amongst these components are RF filters with center frequencies ranging from 800 MHz to 2.5 GHz; IF filters with center frequencies ranging from 455 kHz to 254 MHz; and high Q, low phase noise oscillators [5], with frequency requirements in the 10 MHz to 2.5 GHz range [6]. There are many factors associated with operation frequency range and it will be discussed shortly.

MEM based filters are considered most suitable for reduced size implementations. Replacing SAW's and ceramics by equivalent MEM devices will result in single chip implementations of large systems hence taking the efforts for attaining miniaturized wireless technology a step further. The substantial size difference between micromechanical resonators, which constitute filters and their macroscopic counterparts is illustrated in Figure 1.2. The comparison consists of a typical SAW resonator with a clamped-clamped beam micromechanical resonator [6] of comparable frequency with a size reduction of several orders of magnitude.

One other attractive option for MEM filters is integrability with conventional CMOS circuitry. Present micromachining techniques allow isolated microstructures to be fabricated over preprocessed conventional CMOS integrated circuitry. This mergence allows for complete systems to be integrated onto a single chip, hence considerably reducing the size of the overall system, for instance, generic heterodyne receiver and its associated transmitter.

There are some issues related to frequency extensions of the devices. First off, it is necessary to understand that as the MEM devices are mechanical, they have a specific mass, which in most cases appears in inverse proportion to the self resonance frequency of the device. In order to successfully implement the devices to meet any frequency criteria, factors such as mass of coupling springs or the shuttle as shown in Figure 1.3 cannot be ignored. The frequency range of these mechanical devices is a function of many factors such as [6]:

1. quality factor, which may change with resonance frequency, material and principle of operation.

2. series motional resistance R_x which contributes to the insertion loss of the

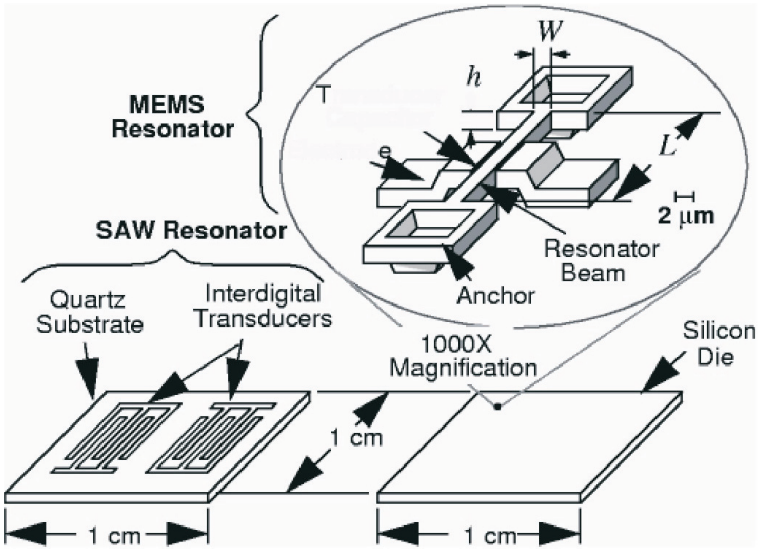

Figure 1.2: Size comparison between present-day SAW resonator technology and the described high Q micromechanical resonator technology [6]

filters, input-referred noise and filter passband distortion due to parasitics [7].

3. absolute and matching tolerances of resonance frequencies, which will both be functions of the fabrication technology and of frequency trimming or tuning strategies.

4. stability of the resonance frequency against temperature variations, mass loading, aging, and other environmental phenomena.

Amongst the above mentioned phenomena, quality factor is the most critical aspect since matching the performance of macro devices requires high Q. Present day research has achieved Q's of over 80,000 under vacuum with proper materials [8]. Furthermore, the series resistance R_x, which appears in the electrical equivalent model causes a sharp increase in insertion loss.

In order to improve the insertion loss, laterally driven devices are much better suited because they offer linear capacitance change and increased coupling with their comb structures [9]. However, the large shuttle mass hinders the chances of increased operating frequency. That is why Free Free beam design [10] are under study, which vibrates lateral to substrate and offers increased operating frequencies due to smaller shuttle mass.

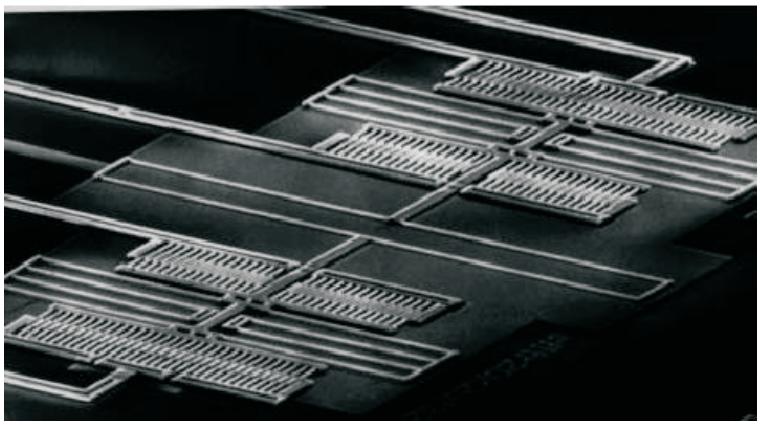

Figure 1.3: SEM of a two-resonator spring coupled micromechanical filter displaying bulky shuttle area

1.1 Overview

The thesis begins with introduction and review where the general biquadratic functions are explained, which can be altered to obtain various filter implementations and bandpass filter characteristics are established. As mechanical and electrical systems, both can represent the same bandpass transfer functions, an analogy function connecting them will be presented. This lays the foundation for evaluating electrical equivalent circuits out of mechanical structures and it will be used for design and analysis of MEM bandpass filters. Next, recent efforts in the design of MEM filters is presented in the form of review. Finally, the chapter concludes with the importance of high Q in the design of filters.

Chapter 2 will present a complete filter design methodology based on electrical equivalent of MEM filters. Both the series RLC and parallel RLC implementations will be discussed. Bandwidth control of filter is presented from electrical equivalent view, which is then translated into the mechanical domain as a device.

Chapter 3 contains information about the device fabrication process along with masks information.

The thesis concludes with Chapter 4, which summarizes the future work and conclusions followed by Appendix.

1.2 General Biquadratic Functions

Second-Order filters, often referred to as *biquads*, are amongst the simplest and the most commonly employed components used in the design of communication and signal processing systems. The general representation of biquadratic function is given in Equation (1.1).

$$T(s) = \frac{N(s)}{D(s)} = \frac{k_2 s^2 + k_1 s + k_0}{s^2 + s(w_0/Q) + w_0^2} \tag{1.1}$$

where the numerator coefficients k_{i} may be positive, negative or zero. It is important to note that transfer function poles of Equation (1.1) are crucial in the filter specifications (in terms of resonance frequency w_0 and Quality factor, Q) and the filter design according to these criteria fixes the poles. However, by placing proper transmission zeros(that is by tuning k_{i} values), different filter types (for instance, low pass, high pass etc) can be obtained by using the same circuit topology.

There are excellent second order filter implementations present in literature and practice which utilize the biquadratic function. Implementations for instance Ackerberg−Mossberg two integrator loop circuit for lowpass and bandpass characteristics, the Sallen−Key circuit for lowpass or highpass characteristics in Figure 1.4, the Delyiannis−Friend single amplifier biquad in Figure 1.5 and GIC filters for bandpass function. Each of these filter implementations are based on manipulation of biquadratic transfer function. Here these circuits are presented just as an example to demonstrate the various implementations of biquadratic transfer function as the same will be used and classified later on to obtain bandpass filter characterisation. For complete treatment, the reader is referred to the original work in [11]−[13].

The Sallen - Key low pass filter has transfer function of the form:

$$T(s) = \frac{KG_1G_2/C^2}{s^2 + s[G_1 + G_2(2-K)]/C + G_1G_2/C^2} = \frac{H\ w_0^2}{s^2 + s\ w_0/Q + w_0^2} \tag{1.2}$$

The filter parameters can be identified and expressed in terms of component values as:

$$\begin{aligned} w_0^2 &= \frac{G_1G_2}{C^2} \\ Q &= \frac{\sqrt{G_1G_2}}{G_1 + G_2(2-K)} \\ H &= K > 1 \end{aligned}$$

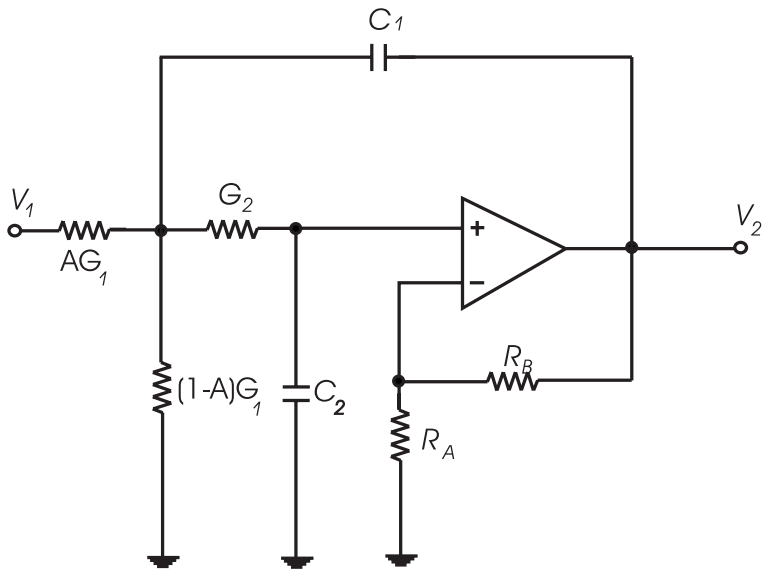

Figure 1.4: Sallen-key low pass filter with DC gain H = aK

From Equation (1.2) we see that the transfer function resort to the general form of low pass filters.

The Delyiannis - Friend bandpass filter has transfer function of the form:

$$T(s) = \frac{sAG_1/C}{s^2 + s2G_2/C + G_1G_2/C^2} = \frac{sH\ (w_0/Q)}{s^2 + s\ w_0/Q + w_0^2} \tag{1.3}$$

The filter parameters can be identified and expressed in terms of component values as:

$$\begin{aligned} w_0^2 &= \frac{1}{R_1R_2C^2} \\ Q &= \frac{1}{2}\sqrt{\frac{R_1}{R_2}} \\ H &= \frac{1}{2}\ A\ \frac{R_2}{R_1} \end{aligned}$$

From Equation (1.3) we see that the transfer function resort to the general form of bandpass filters. A complete transformation scheme is presented in the following section, which channels the filter response according to the parameters in biquadratic function.

1.3 Standard Biquadratic Responses

As mentioned previously, by changing the numerator $N(s)$ in Equation (1.1), that is by generating properly placed transmission zeros in the system without changing

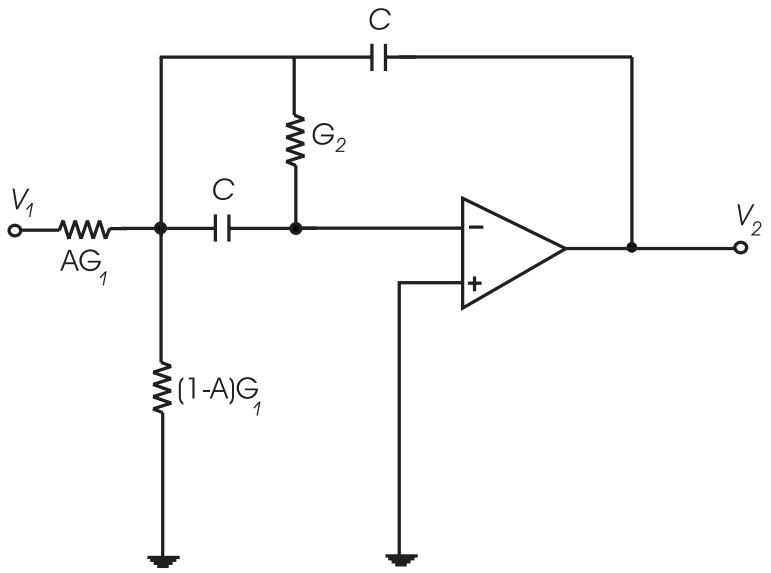

Figure 1.5: Delyiannis-Friend bandpass filter circuit

the poles location, different filter implementations can be obtained. The numerator value $N(s)$ depends on the output node of the filter. For instance the Two-Thomas filter example in Figure 1.6 can have a bandpass and an inverting and non inverting low pass output available at different output nodes [14], [15].

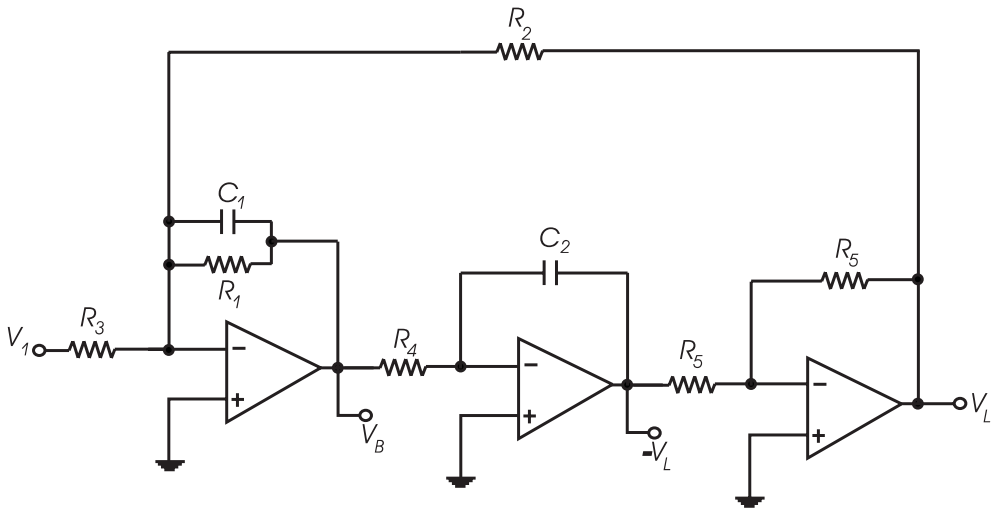

Figure 1.6: The Two Thomas biquad

Individual transfer functions for both low pass and bandpass can be derived from

circuit analysis and are reported below:

$$T_{\mathrm{L}}(s) = -\frac{1/(R_3R_4C_1C_2)}{s^2+s/(R_1C_1)+1/(R_2R_4C_1C_2)} = \frac{w_0^2}{s^2+s\ w_0/Q+w_0^2} \quad (1.4)$$

$$T_{\mathrm{B}}(s) = -\frac{(R_1/R_3)\cdot s/(R_1/C_1)}{s^2+s/(R_1C_1)+1/(R_2R_4C_1C_2)} = \frac{sw_0/Q_0}{s^2+s\ w_0/Q+w_0^2} \quad (1.5)$$

$$(1.6)$$

The filter parameters can be identified and expressed in terms of component values as:

$$w_0^2 = \frac{1}{R_2R_4C_1C_2} \qquad Q = \frac{1}{R_1}\sqrt{\frac{R_2R_4C_2}{C_1}} \qquad H = \frac{R_2}{R_4}$$

There are two ways, which can be used to implement more versatile filters using the structures mentioned in the previous section. The first technique is to use summing of different filter outputs and the second injects the input signal into appropriate nodes and thereby generates full second order numerators in the second order sections. The methods will not be discussed here, however it is more insightful to provide a summary of how numerator zeros can effect the overall filter response. For a detailed treatment reader is referred to [16]. The summary is as follows:

$$T_{\mathrm{LP}} = \frac{w_0^2}{s^2+\left(\frac{w_0}{Q}\right)s+w_0^2}$$

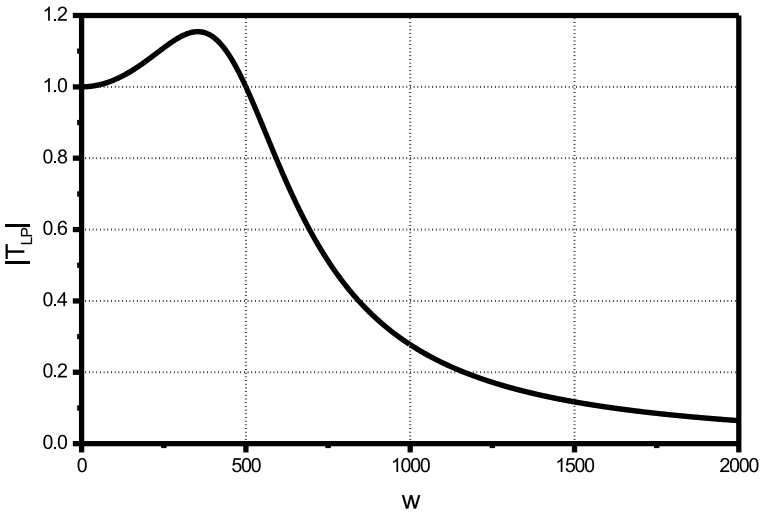

Figure 1.7: Low pass filter characteristics

$$T_{\mathrm{BP}} = \frac{\left(\frac{w_0}{Q}\right) s}{s^2 + \left(\frac{w_0}{Q}\right) s + w_0^2}$$

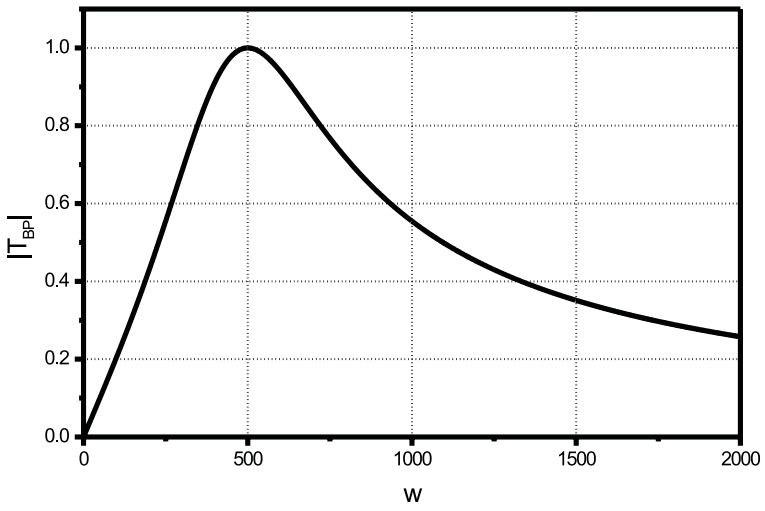

Figure 1.8: Band pass filter characteristics

$$T_{\mathrm{BS}} = \frac{s^2 + w_0^2}{s^2 + \left(\frac{w_0}{Q}\right) s + w_0^2}$$

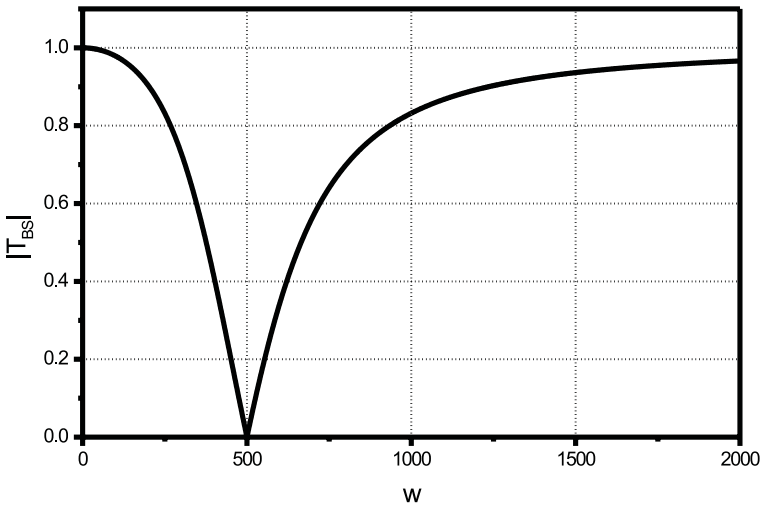

Figure 1.9: Band stop filter characteristics

$$T_{\mathrm{HP}} = \frac{s^2}{s^2 + \left(\frac{w_0}{Q}\right) s + w_0^2}$$

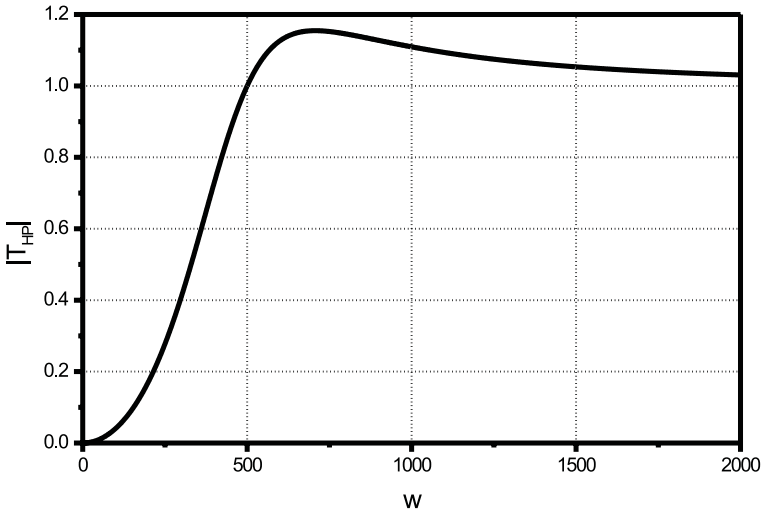

Figure 1.10: High pass filter characteristics

$$T_{\mathrm{AP}} = \frac{s^2 - \left(\frac{w_0}{Q}\right) s + w_0^2}{s^2 + \left(\frac{w_0}{Q}\right) s + w_0^2}$$

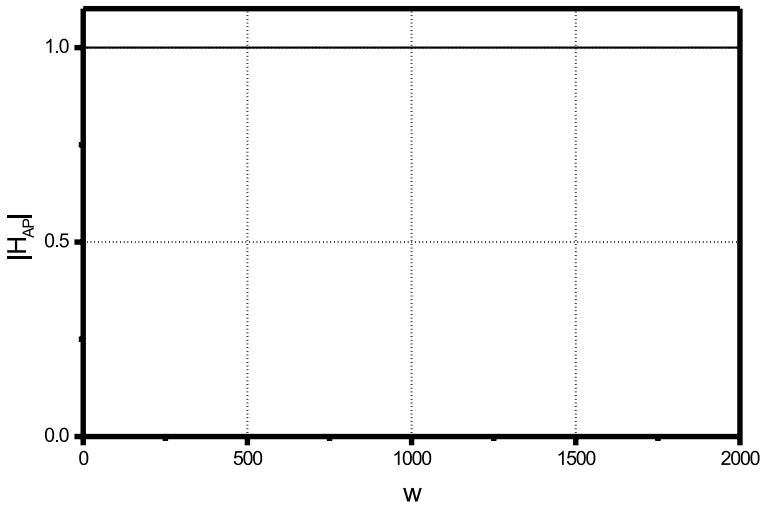

Figure 1.11: All pass filter characteristics

1.4 Analogous Biquadratic Systems

In the previous section different biquadratic responses have been demonstrated to show various types of filtering orientations. There are physical systems which can be represented mathematically by same models, which are called *analogous systems*. Hence, similar transfer functions and integrodifferential equations can describe different implementations of a physical systems. For our case of electromechanical systems, we are only interested in mechanical Mass−Spring−Damper and electrical Resistance−Capacitor−Inductor system calculations of transfer functions leading to biquadratic functions.

We now compare analogous mechanical and electrical systems which will lay foundations of utilizing MEMS as bandpass filters. First some simple mechanical relationships associated with Figure 1.12 are presented in the following:

$$\begin{aligned} \text{Mass}: \quad & f = ma = m\,\frac{\partial^2 x}{\partial t^2} \\ \text{Spring}: \quad & f = kx \\ \text{Damper}: \quad & f = b\,\frac{\partial x}{\partial t} \end{aligned}$$

In order to study mechanical systems through their electrical analogous, we present two electrical analogies namely, the *force−voltage analogy* and the *force−current analogy*.

1.4.1 Force-Voltage Analogy

We will study both the mechanical system of Figure 1.12(a) and the electrical systems of Figure 1.12(b). The external stimulus force, f, in the mechanical system, Voltage V, in the electrical system. The equation for the mechanical system is:

$$m\frac{d^2x}{dt^2} + b\frac{dx}{dt} + kx = f \tag{1.7}$$

whereas the system equation for the electrical system is

$$L\frac{di}{dt} + Ri + \frac{1}{C}\int i\ dt = V$$

Mechanical Systems	Electrical Systems
Force (f)	Voltage V
Mass (m)	Inductance L
Viscous-friction Coefficient (b)	Resistance R
Spring constant (k)	(Capacitance)$^{-1}$, $1/C$
Displacement (x)	Charge q
Velocity (dx/dt)	Current i

Table 1.1: Force-Voltage Analogy [17]

In terms of electrical charge q, this last equation becomes:

$$L\frac{d^2q}{dt^2} + R\frac{dq}{dt} + \frac{1}{C}q = V \tag{1.8}$$

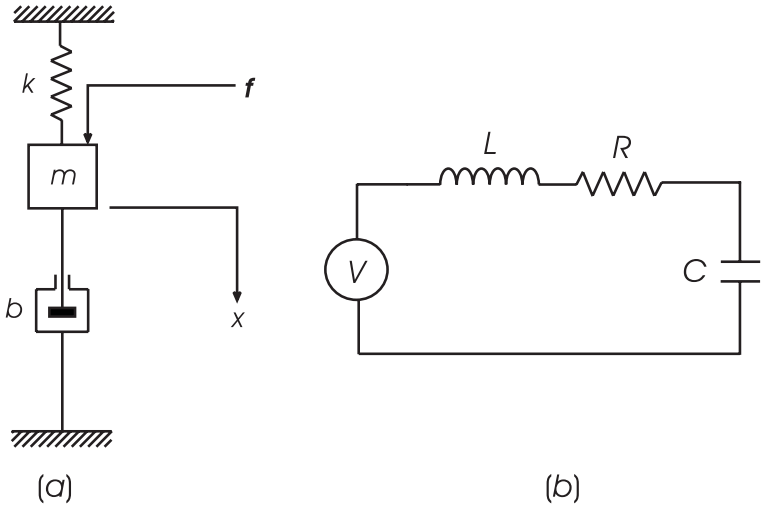

Figure 1.12: Second order mechanical system

Comparing Equation (1.7) and (1.8), we see that the differential equations for the two systems are of identical form which leads to the conclusion of these systems being analogous. The analogous quantities, which are the terms that occupy corresponding positions in the differential equations appear in Table 1.1. The analogy here is also called *mass−inductance analogy*.

1.4.2 Force-Current Analogy

In order to obtain a parallel RLC circuit we can consider again the same mechanical system shown in Figure 1.13(a), where f is the external force. The system equation is:

$$m\frac{d^2x}{dt^2} + b\frac{dx}{dt} + kx = f \tag{1.9}$$

We now derive equations for the parallel RLC electrical system shown in Figure 1.13(b), where i_s is the current source. Application of Kirchhoff's current law gives:

$$i_\mathrm{L} + i_\mathrm{R} + i_\mathrm{C} = i_\mathrm{s} \tag{1.10}$$

where:

$$i_\mathrm{L} = \frac{1}{L}\int V\ dt, \qquad i_\mathrm{R} = \frac{V}{R}, \qquad i_\mathrm{C} = C\frac{dV}{dt}$$

Thus Equation (1.10) can be written as:

$$\frac{1}{L}\int V\ dt + \frac{V}{R} + C\frac{dV}{dt} = i_\mathrm{s} \tag{1.11}$$

Since the magnetic flux linkage ψ is related voltage V by the equation:

$$\frac{\partial\psi}{\partial t} = V$$

in terms of ψ, Equation (1.11) can be written:

$$C\frac{d^2\psi}{dt^2} + \frac{1}{R}\frac{d\psi}{dt} + \frac{1}{L}\psi = i_\mathrm{s} \tag{1.12}$$

Comparing Equation (1.9) and (1.12), we find that the two systems are analogous. The analogous quantities are listed in Table 1.2. The analogy here is also called the *mass−capacitance analogy.*

Using these analogies, we can now derive series and parallel electrical equivalent or RLC circuits from mechanical structures which can be represented as mass−spring−damper systems. The equivalent circuits make the design process convenient while keeping intact the mechanical domain owing to the simple analogies presented in this section. We can now make a review of work done in the field of Microelectromechanical structures to act as filters.

Mechanical Systems	Electrical Systems
Force (f)	Current i
Mass (m)	Capacitance C
Viscous-friction Coefficient (b)	(Resistance)$^{-1}$ $1/R$
Spring constant (k)	(Inductance)$^{-1}$ $1/L$
Displacement (x)	Magnetic Flux Linkage ψ
Velocity (dx/dt)	Voltage V

Table 1.2: Force-Current Analogy [17]

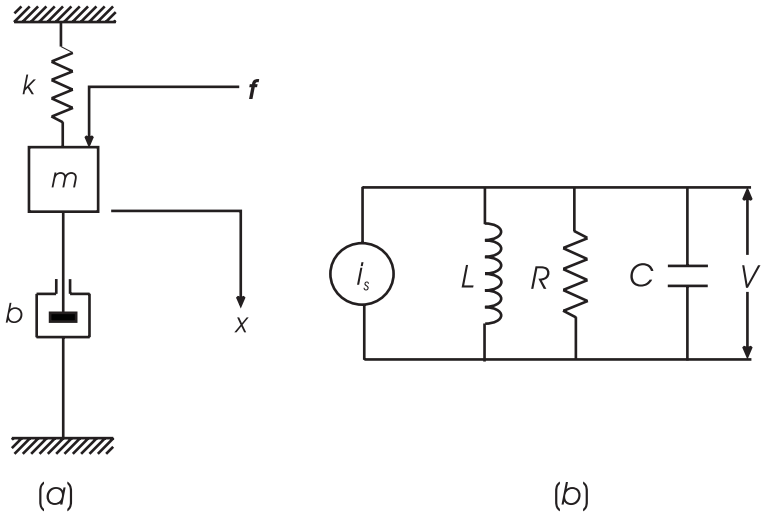

Figure 1.13: Second order electric and mechanic systems

1.5 MEMS Implementation of Bandpass Filters

MEMS based bandpass filters may be excited in lateral and vertical to substrate orientations depending on design choice. There are several excitation methods including piezoelectric, thermal expansion, electrostatic forces and magnetostatic forces. The most commonly adopted method is electric excitation and capacitive detection due to offered advantages such as simplified device design (one mask may define the whole device geometry) and lesser material consumption (compared to piezoelectric or piezoresistive) and hence, reduced stress profile [18].

For electrostatically comb driven resonators/filter such as one shown in Figure 1.14, if the fringing effects are approximated (detailed treatment in section 2.3.1)

then the equations corresponding to change in capacitance with respective distance are given by:

$$\begin{aligned} C(x) &\approx \frac{\epsilon_0 h(L-x)}{g} \\ \frac{\partial C}{\partial x} &\approx \frac{N\epsilon_0 h}{g} \end{aligned} \tag{1.13}$$

where N is the number of finger gaps, g is the gap distance between each finger, h is the fingers thickness, L is the finger length, and ϵ is the permittivity constant.

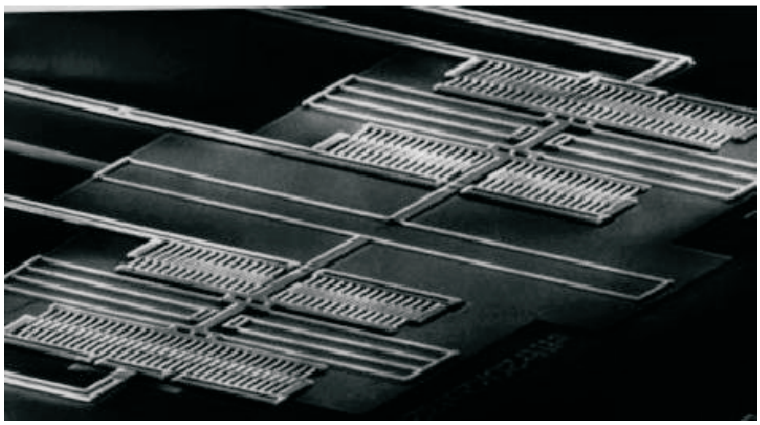

Figure 1.14: SEM of a two-resonator spring coupled micromechanical filter [19]

For vertically driven clamped-clamped structures as shown in Figure 1.15 and implemented in Figure 1.16 the relevant equations of capacitance change with distance, are given by:

$$\begin{aligned} C(x) &= \frac{\epsilon_0 A}{d}\left(1+\frac{x}{d}\right)^{-1} = C_0\left(1+\frac{x}{d}\right)^{-1} \\ \frac{\partial C}{\partial x} &= -\frac{C_0}{d}\left(1+\frac{x}{d}\right)^{-2} \end{aligned} \tag{1.14}$$

where A is the overlap area of beam to sense electrode. Other parameters are shown in Figure 1.15. If we compare Equations (1.13) and (1.14), we can observe that vertically driven structures are less attractive due to their nonlinear capacitance dependence on direction of motion is concerned. Nonlinearity is known to cause several undesirable phenomena for instance DC-bias voltage dependence and distortion on frequency and harmonic distortion in the resonator output current [20].

Another factor, which distinguishes laterally driven structures from the vertically driven structures is the quality factor. As mentioned previously, MEM devices

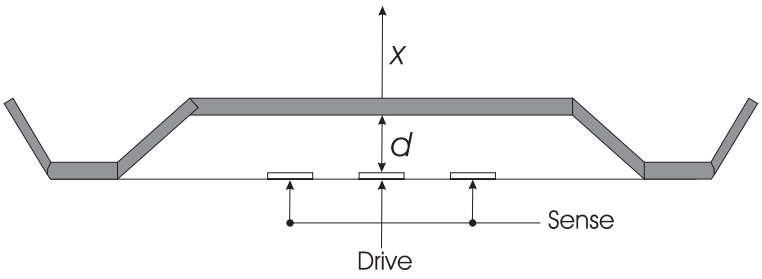

Figure 1.15: Cross section view of clamped-clamped vertically driven resonator

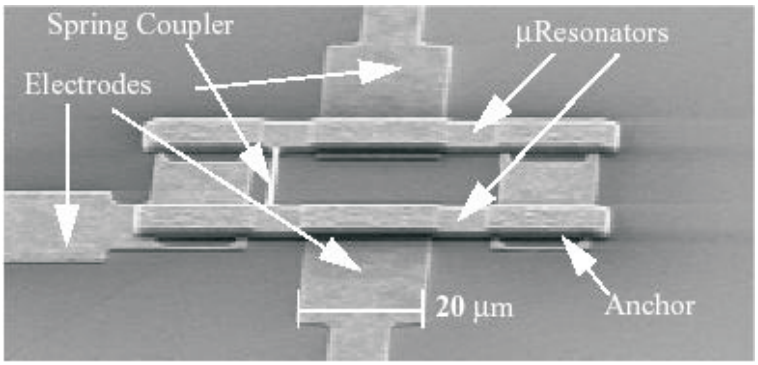

Figure 1.16: SEM of a surface micromachined, two-resonator, spring coupled HF bandpass micromechanical filter [7]

are considered as a potential replacement of quartz resonators and their further implementations. The replacement demands highly selective devices and hence, devices which can beat or at least equal the quality factor ranges of 20,000 to 1,000,000 – which is commonly displayed by the quartz resonator depending upon type or cut and manufacturing quality– is the target.

For vertically driven structures, the squeeze film damping in the thin capacitive gap region is the major energy dissipation factor and hence drastically affects the quality factor at the atmospheric pressure [21]. As far as laterally driven microstructures are concerned, the major factor affecting the quality factor is Couette air flow in the gap between the structure and the substrate and is found as much lesser dissipative compared with squeeze film damping [22]. There has been considerable work towards improvement of the Quality Factor in terms of making it independent of atmospheric pressure by introducing load/termination circuits [8] and modeling

[23].

As a side note, it needs to be pointed out that electrostatically comb driven structures are implemented in this study because the technology under use supports devices at atmospheric pressure. This device geometry decision is also influenced by the fact that nonlinear capacitive detection effects are to be avoided and high quality factor values are needed; hence, the operating frequency is also low.

The equivalent circuit for the parallel driven filter of Figure 1.16 is driven using the mass-spring-damper analogy and is then converted into a series RLC equivalent circuit. This is easily achievable using the techniques established in the previous section with Table 1.1 and Table 1.2. The equivalent circuit is represented in Figure 1.17.

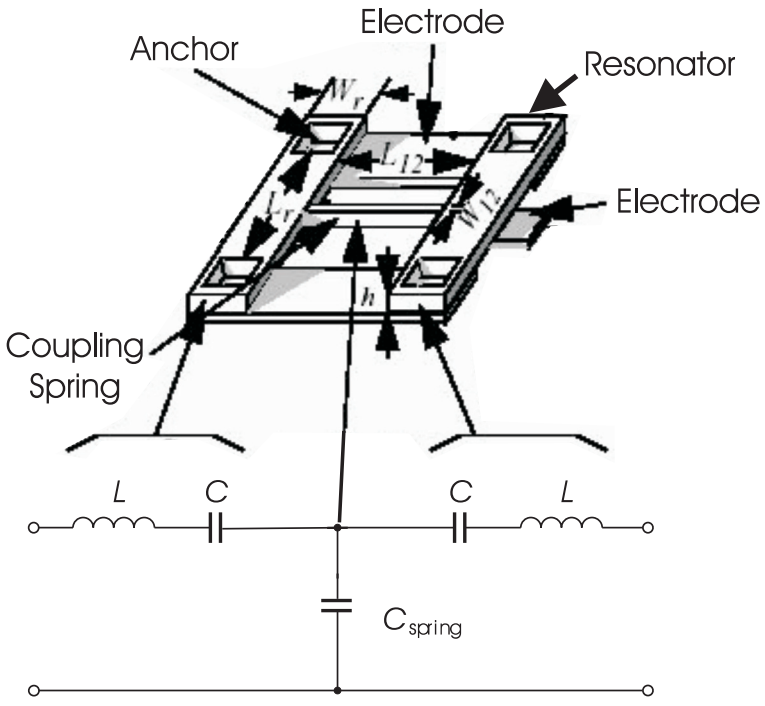

Figure 1.17: Schematic view of two-resonator micromechanical filter of Figure 1.16, along with the equivalent circuit for the filter [7]

In terms of frequency response the vertical driven resonators and filters have been a better choice to address the RF target range due to their operation in megahertz range and it is improving. Electrostatically comb driven resonators and filters

are selected for very high values of quality factors, which not only improves the selectivity of the filters but may also help in the design of phase locked loops, which require ultra stable, fixed frequency and high quality factor constituent resonator.

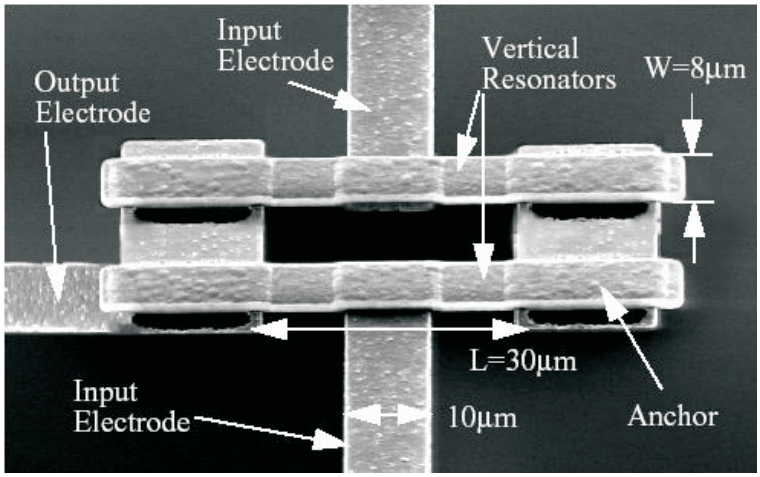

Figure 1.18: SEM of a 14.5MHz parallel filter with labeled critical dimensions [24]

Efforts in the field of MEM filter design continue and one example is shown in Figure 1.18. For lateral design, higher order filters were fabricated and tested by Nguyen et. al. with success.

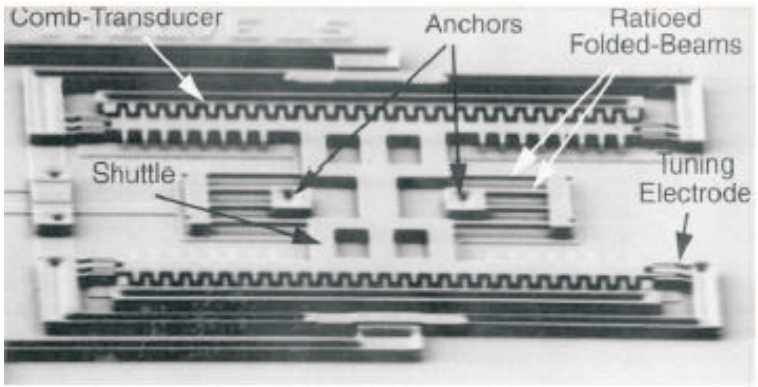

Figure 1.19: SEM of a ratioed folded-beam, comb-transduced micromechanical resonator [25]

The salient feature in this design is the use of double sided comb structures where,

by applying differential voltages, the coupling is doubled as shown in Figure 1.19. Furthermore, the same resonators were coupled via truss instead of the hitherto mass coupled design in as shown in Figure 1.20 and with proper coupling spring velocity adjustment, variable bandwidth and insertion loss is achievable.

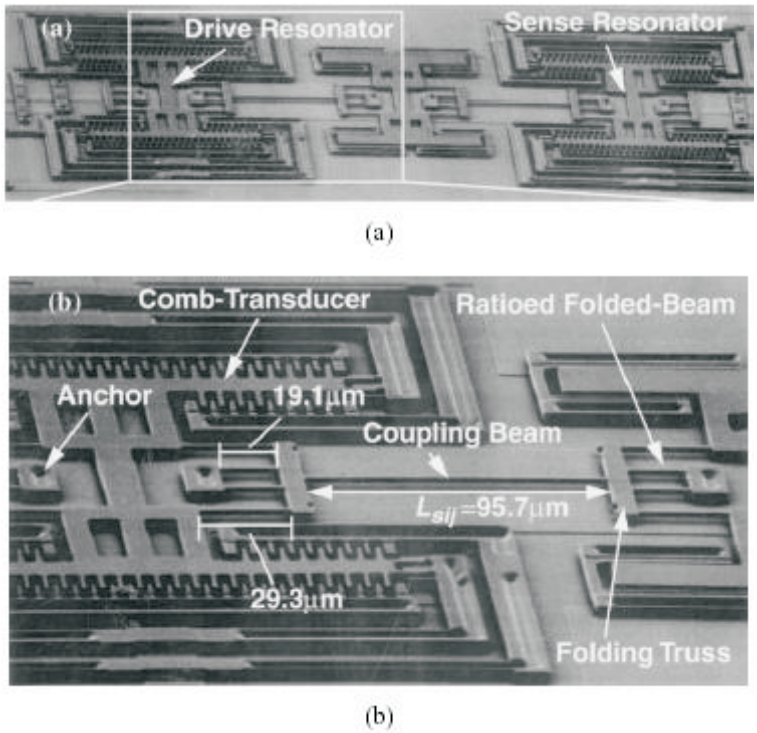

Figure 1.20: SEM of a fabricated ratioed folded-beam micromechanical filter. (a) Full view. (b) Enlarged partial view [25]

The equivalent circuit of the laterally driven filter of Figure 1.20 is shown in Figure 1.21.

In one of the recent designs (2001) cantilever beam based laterally driven resonators are presented which also operate in MHz range. This is an important design since it not only satisfies the criteria of high Q due to only Couette flow present in lateral structures, but also it extends in the high frequency range due to decreased mass unlike the interdigitized comb resonator implementations of Figure 1.20.

A shift from cantilever beam based resonator towards contour based resonator is observed as the frequency ranges moves towards GHz applications. For these implementations piezo materials are used to obtain compression/expansion of the

contour depending upon the applied signal.

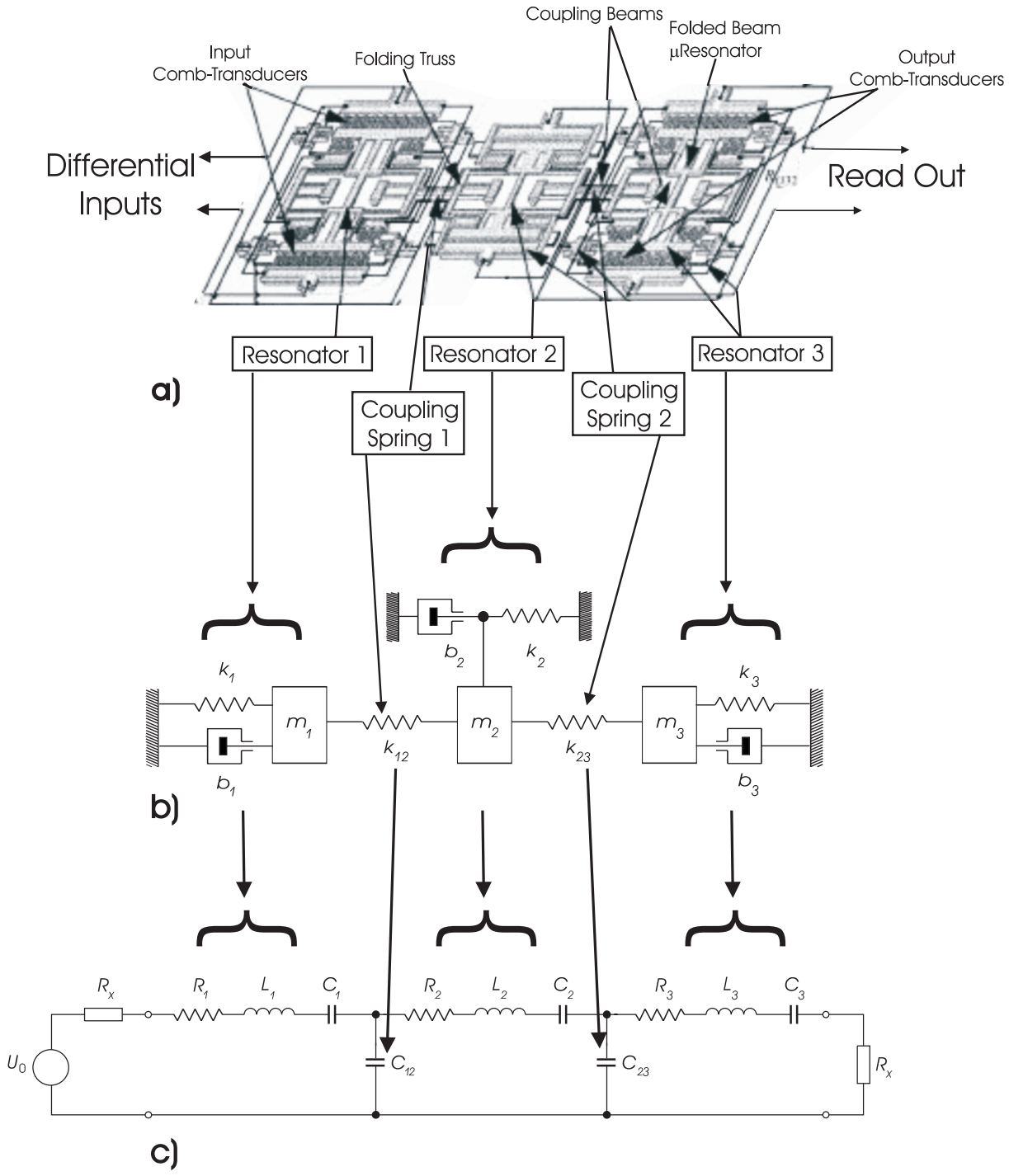

Figure 1.21: (a) Schematic of a folded−beam, three−resonator, micromechanical filter. (b) Mechanical equivalent circuit for the filter of (a). (c) Electrical equivalent circuit for the filter of (a) without parasitic capacitances [25]

As the contour is connected to the ground via an anchor at its center, which effectively has very limited effect on the Q, high levels of Q can be obtained even at the atmospheric pressures. The operating frequency is for first mode 156MHz and 733MHz and Q's as high as 9600 and 7000 respectively for different designs.

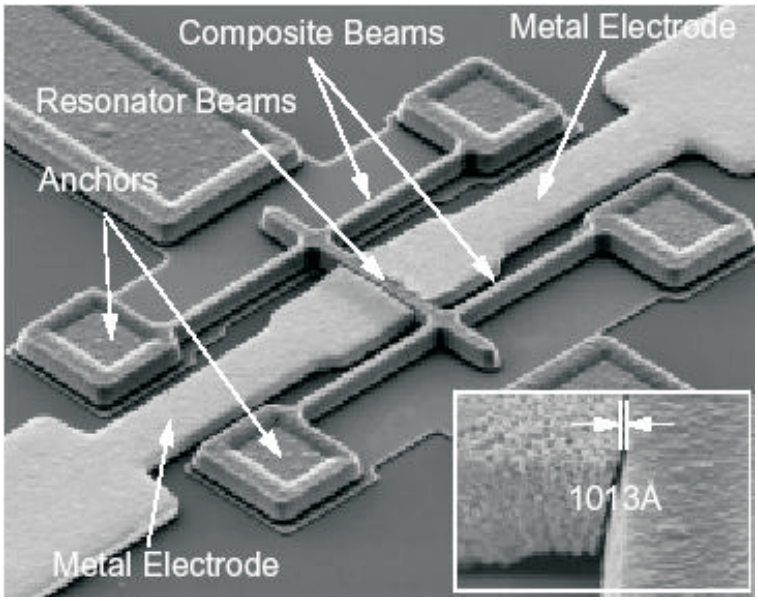

Figure 1.22: SEM of a 10.47MHz lateral free−free beam micromechanical resonator [10]

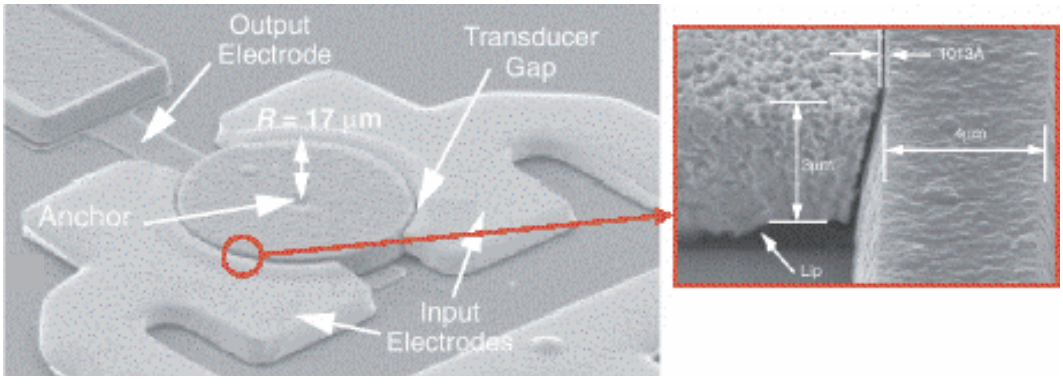

Figure 1.23: SEM of a 156MHz Contour-Mode resonator with Q= 9400 [26]

In this section various implementations of bandpass filters using cantilever beams, a part of MEMS technology, have been presented. Equivalent circuits extracted out

of the mechanical filters are summarized in the section, which are both vertically and laterally driven. We observe that these circuits transform into series RLCs and hence by using circuit analysis on the series RLC equivalents different filter design criteria can be targeted. The transition from electrical to mechanical domain is achieved by using Tables 1.1 and 1.2.

1.6 Importance of High Q in RF devices

The quality factor Q of resonator/filter is defined as follows:

$$Q = w_0/BW \tag{1.15}$$

The laterally driven resonators are considered as a better choice over the perpendicular to the substrate ones because they demonstrate high Q (as high as 80,000 under vacuum [8]). The quality factor is relatively an important criteria for judging device performance especially in filters. As MEMS filters are made of individual resonators, which are mechanically coupled with each other, the Q of individual resonators are of great importance. The resonator Q influences the ability to implement selective IF and RF filters, which may have insertion losses greater than 20dB, which renders them unacceptable for implementation [27]. The simulated effect of Q on an individual resonator response can be shown graphically in Figure 1.24.

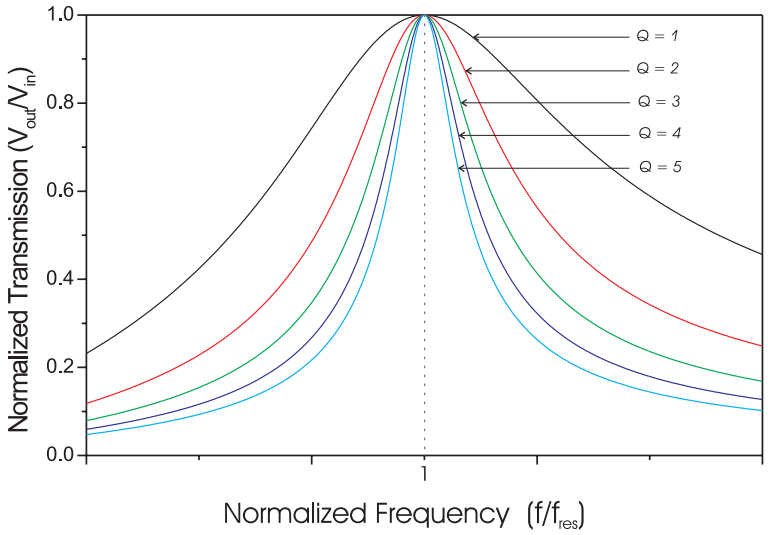

Figure 1.24: Effect of Q variation on normalized transfer function of a resonator

In Figure 1.24 we can see the effect of varying Q on the poll roll off. The response is of a biquad function, which is represented by a single resonator in telecommunication technology. Though the filter Q follows the same idea qualitatively, because of coupling phenomena, there will be attenuation in the pass band as well. As we notice from Equation (1.15) the bandwidth of the resonator decreases as the quality factor increases though the roll off and the attenuation sharpness increases as soon as the passband is cleared in frequency domain. So we may establish a tradeoff criteria between the resonator's and effectively filter's shape factor and the bandwidth. The effects of changing Q onto filters passband is shown in Figure 1.25.

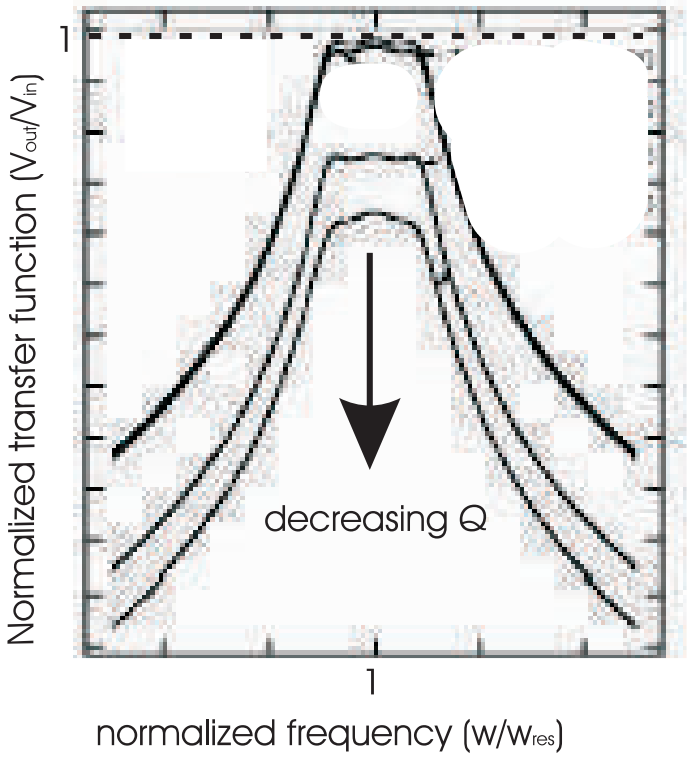

Figure 1.25: Effect of Q variation on a 70MHz bandpass filter

High Q device designs for resonators are filters are under study. The objective of obtaining high Q is tried by using laterally driven structures for instance [10] and by tuning the coupling spring for filter design [28] as well as external control of Q [8].

We will now present theoretical work done for designing filters in various frequency domains.

Chapter 2

Filter Design

In MEM terminology, each resonator adds an order to the filter, which is unlike RF and telecommunication terminology where each resonator or equivalent LC tank circuitry is treated as a separate second order system. Therefore a second order MEM filter composed of two resonators and the capacitive coupling is effectively a second order system. The discussion of general biquadratic systems can be applied to MEM filters only qualitatively as the formulated expressions of section 1.2 treat a resonator tank circuit without including the effects of coupling capacitance. However the treatment and design of bandpass MEM filters is best suited by selecting a filter topology, for instance Butterworth, Chebyshev or Bessel etc., and following the normalized values of coupling and quality factors, k and q respectively. In filter design of MEM also, the choice of filter type is relatively straightforward, and usually Butterworth or Chebyshev filters are preferred owing to maximally flat response and fast pole roll off or decay factor. The theory, which will be presented shortly can be looked at as a transition from Butterworth type response to Chebyshev. The major focus in this chapter is to present a new filter design technique and to be able to fine tune the bandwidth and insertion loss of the filter using coupling spring. Before going into detailed steps, which involve theoretical formulations, let us first layout the major filter design criteria and parameters. We will use some of the most important ones in our discussion of filters while the rest of parameters are considered as ways to better define the filter specifications for the sake of comprehensiveness.

The chapter initiates with discussion of Butterworth and Chebyshev filter types and their responses for the sake of acquaintance of the reader. The following section treats the resonator design in full detail along with the optimization study. Varying

equivalent representations namely series and parallel are considered concurrently and comprehensive set of equations for different filter specifications are evaluated. In the next section the gap between electrical model and mechanical device is bridged by discussion of the coupling spring. Later on, the filter design methodology is summarized and specific design example is given. The chapter is completed with a conclusion section.

2.1 Typical Filter Parameters

For the bandpass filter an important factor is insertion loss which is defined as the maximum response of a filter with respect to the 0dB point. Insertion loss minimization is of fundamental significance in filter design to obtain acceptable responses without the necessity to amplify. The ripples of a bandpass filter (order higher than 2) as shown in Figure 2.1 are usually undesired if they are considerably large in magnitude. However, as we will see in the derivations to follow later, we can allow an acceptable attenuation for achieving equi–ripple Chebyshev like response and achieve a control on the bandwidth in return. The shape factor is similar to pole roll off in filter design terminology, which is actually a measure of how quickly the response attenuates after the operating frequency falls outside the boundaries of the pass band frequencies. These criteria are shown graphically in Figure 2.1.

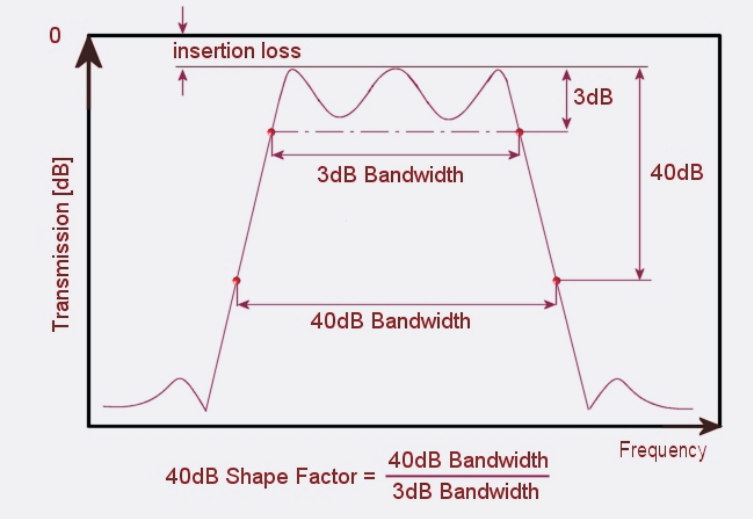

Figure 2.1: Typical bandpass filter response with critical parameters

2.2 Butterworth and Chebyshev Filters

2.2.1 Butterworth Magnitude Response

The Butterworth filter response exhibits a monotonically decreasing transmission with all the transmission zeros at $\omega = \infty$, making it an all-pole filter. The magnitude for a Butterworth filter of the order n with a transition frequency ω_{p} is given by

$$|T(jw)| = \frac{1}{\sqrt{1 + \epsilon^2 \left(\frac{\omega}{\omega_{\mathrm{p}}}\right)^{2n}}} \tag{2.1}$$

In Equation 2.1, ϵ stands for the error function, which varies from 0 to 1 and determines the degree of sharpness from passband to stop band in band pass filters. The Butterworth response is shown graphically in Figure 2.2 for varying values of n. We observe from the figure that as the order increases the degree of passband flatness also increases. It has been shown that at $\omega = 0$ the first $(2n-1)$ derivatives of $|T|$ with respect to ω are zero resulting in a very flat response at $\omega = 0$ also known as *maximally flat response* [29].

In Table 2.1, we see the coefficients of the denominator $B(s)$ of the transfer function which is defined as $|T_n(jw)|^2 = A(w^2)/B(w^2)$. The coefficients are evaluated using the Butterworth transfer function of Equation (2.1).

n	a_0	a_1	a_2	a_3
2	1.0000000	1.4142136		
3	1.0000000	2.0000000	2.0000000	
4	1.0000000	2.6131259	3.4142136	2.6131259

Table 2.1: Coefficients of Butterworth polynomial, $B_{\mathrm{n}}(s) = s^n + \sum_{i=0}^{n} a_{\mathrm{i}} s^i$ [30]

2.2.2 Chebyshev Magnitude Response

The Chebyshev magnitude response is given by similar relationship as that of Butterworth response:

$$|T_{\mathrm{n}}(jw)|^2 = \frac{1}{1 + \epsilon^2 C_{\mathrm{n}}^2(w)}$$

where ϵ is the same error function as used in Butterworth response analysis. Unlike Butterworth response where the pass band is flat, in Chebyshev response there are ripples such that $0< |C_n| <1$. There are two cases such that the transfer function $|T_n|$ oscillates between 1 and $1/\sqrt{1+\epsilon^2}$. In low pass characteristics as demonstrated in Figure 2.3, if n is odd, $|T_n(j0)| = 0$ like n= 1, and if n is even, $|T_n(j0)| = 1/\sqrt{1+\epsilon^2} = 0.5$

n	α	β
1	1.0024	0
2	0.3224	0.7772
3	0.1493	0.9038
	0.2986	0
4	0.0852	0.9465
	0.2056	0.3920

Table 2.2: Coefficients of Chebyshev polynomial for $\alpha_{\max} = 3dB$ [30]

In Table 2.2, α and β are the Chebyshev pole locations.

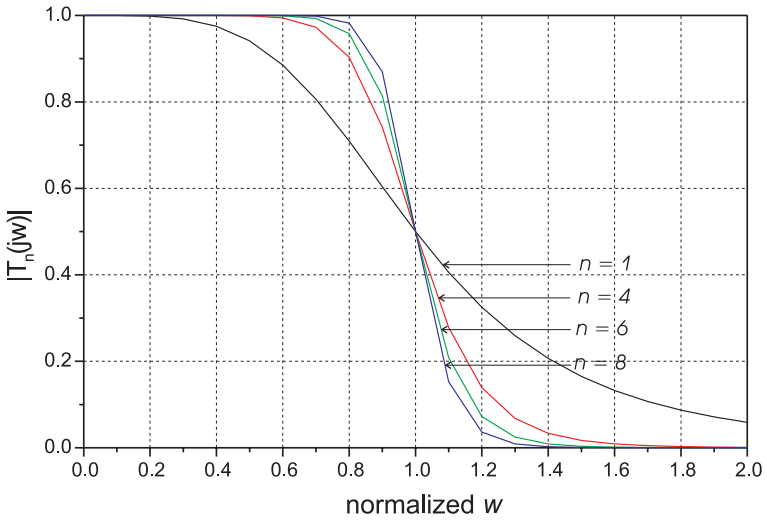

Figure 2.2: Butterworth filter response for varying filter order n

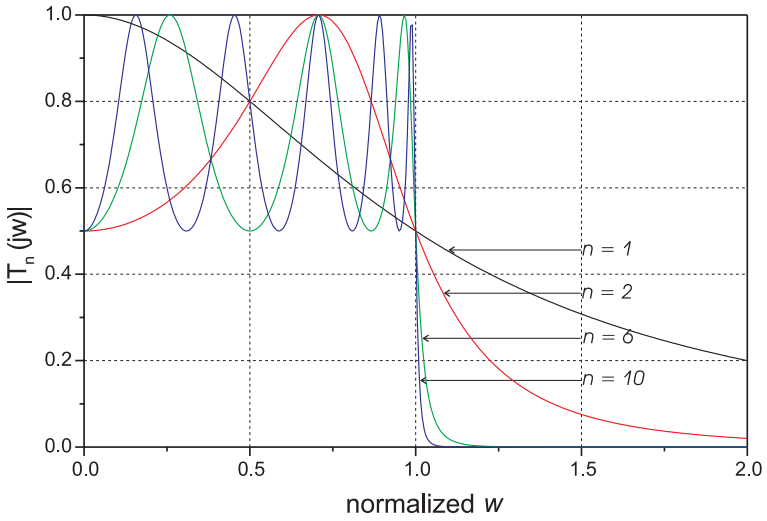

Figure 2.3: Chebyshev filter response for varying filter order n

A comparative analysis yields the fact that the pole roll off in Chebyshev filters is the greater than the Butterworth filter for the same order. This means better passband to stopband transition can be achieved with the Chebyshev filters. These observations are verified in Section 2.8, where an example design of filter shows both the Butterworth or Chebyshev response. Figure 2.4 is the graphical representation of theoretical determined second order bandpass filters.

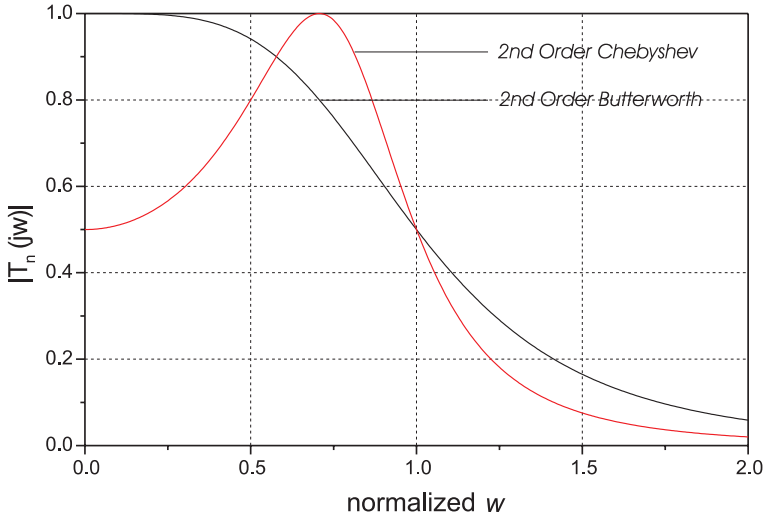

Figure 2.4: Second order Butterworth versus Chebyshev filter transmission characteristics

One of the ways Butterworth and/or Chebyshev filters are realized using passive

components is by following a general narrow band capacitive or inductive coupled resonator filters design strategy. The normalized quality factor and coupling coefficient values (q and k respectively) are tabulated in general filter cook books, for example [30]. Using these values the effective filter design can be conducted by scaling the q and k values according to the center frequency and 3dB bandwidth values. A simple filter design methodology using normalized q and k values for Butterworth as tabulated in Table 2.3, which is converted to a general equivalent circuit as shown in Figure 2.5, is presented in the following [30]:

n	q_1	q_n	k_{12}	k_{23}	k_{34}
2	1.414	1.414	0.707		
3	1.000	1.000	0.707	0.707	
4	0.765	0.765	0.841	0.541	0.841

Table 2.3: Butterworth capacitive coupled resonator

We can relate the k and q values of Table 2.3 with Butterworth/Chebyshev filter poles α and β of Table 2.2 as the translation factor of the form $w_0 = \sqrt{\alpha^2 + \beta^2}, Q = \sqrt{\alpha^2 + \beta^2}/2\alpha$ of a general second order function $s^2 + 2\alpha s + \alpha^2 + \beta^2$.

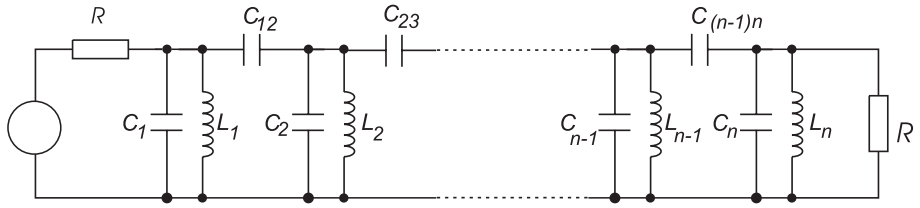

Figure 2.5: General form of capacitive coupled resonator filter

1. Bandpass filter's quality factor is determined from the specifications as

$$Q_{\mathrm{bp}} = f_{\mathrm{m}}/BW_{3\mathrm{dB}}$$

where f_{m} and $BW_{3\mathrm{dB}}$ are the desired center frequency and 3dB bandwidth of the filter, respectively

2. After filter type and order is established, the normalized q and k values are selected to give individual tank's Quality factors Q and coupling coefficients by the following denormalizing steps:

$$Q_1 = Q_{\text{bp}} \times q_1$$

$$Q_n = Q_{\text{bp}} \times q_{\text{n}}$$

$$K_{\text{xy}} = \frac{k_{\text{xy}}}{Q_{\text{bp}}}$$

3. By choosing a convenient inductance value of L the source and load terminations are found from:

$$R_{\text{s}} = w_{\text{m}} L Q_1$$

$$R_{\text{L}} = w_{\text{m}} L Q_n$$

4. The total nodal capacitance is determined by

$$C_{\text{node}} = \frac{1}{w_{\text{m}}^2 L}$$

5. The coupling capacitors are then computed from

$$C_{\text{xy}} = K_{\text{xy}} C_{\text{node}}$$

The design of filters starts with designing high Q constituent resonators, which exhibit low insertion loss and especially fit well with the biquadratic characteristics established in the previous sections. The coupling is done later on to exhibit the bandwidth widening and pass band attenuation. We will now isolate a laterally driven Microelectromechanical resonator, which corresponds to a single tank circuit in the filter, and we will perform a study on its transduction mechanism namely effective Capacitance Evaluation using available Finite Element Modelling (FEM) tools; then a modeled Electrical Equivalent Circuit will be presented as a link between electrical and mechanical domain and lastly, Frequency Optimization will be performed, which will conclude the resonator design.

2.3 Resonator

The resonator presented in Figure 2.6 is actuated using a capacitively coupled mechanism. The direction of vibration is parallel to the substrate, which is preferred over the vertical to the substrate actuation due to reduced lossy mechanisms [21]. The input comb fingers, which are connected to the drive electrode vary linearly with respect to displacement x and hence, the derivative $\partial C/\partial x$ is a constant as given in Equation (2.4) on page 38.

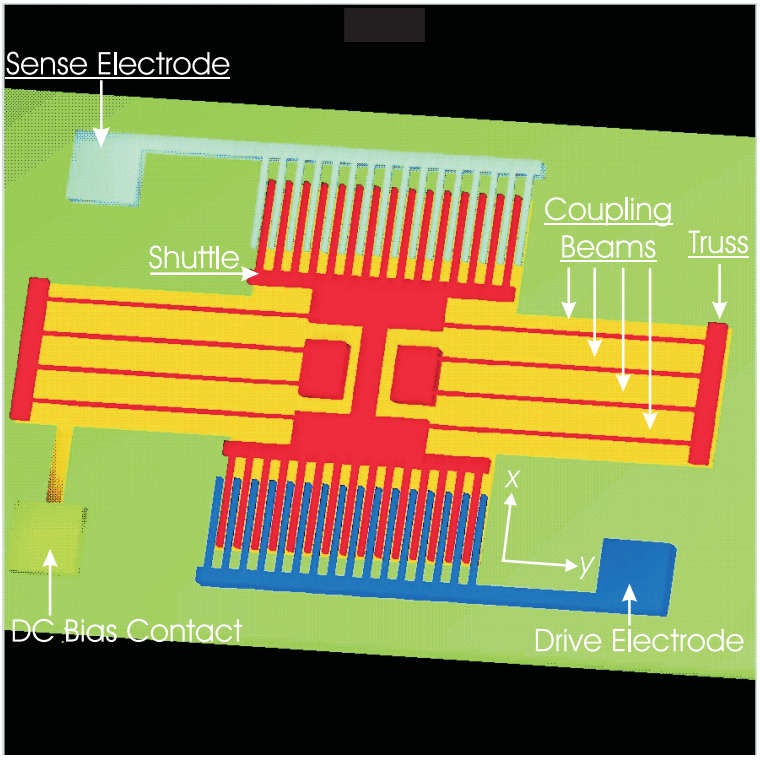

Figure 2.6: 3D view of a laterally driven microelectromechanical resonator

Referring to Figure 2.7, which presents the layout view of the resonator, if a sinusoidal voltage (v_{d}) is applied to the drive electrode on top of a DC bias (V_{D}) of the form $v_{\mathrm{i}}(t) = V_{\mathrm{D}} + v_{\mathrm{d}} sin(wt)$, a push pull force mechanism will be developed on the resonator, which will be detected at the sense electrode. The harmonic coupling at the sense electrode results in a current given as $i_{\mathrm{s}} = V_{\mathrm{sr}}(\partial C/\partial x)(\partial x/\partial t)$ [9] and as $\partial C/\partial x$ is a constant, the rate of vibration determines the coupling; here $V_{\mathrm{sr}} = V_{\mathrm{s}} - V_{\mathrm{r}}$ corresponds to the DC bias of sense electrode (V_{s}) and of resonator

(V_r). The resonator is DC biased to create large electrode to resonator voltages for series resistance minimization [20].

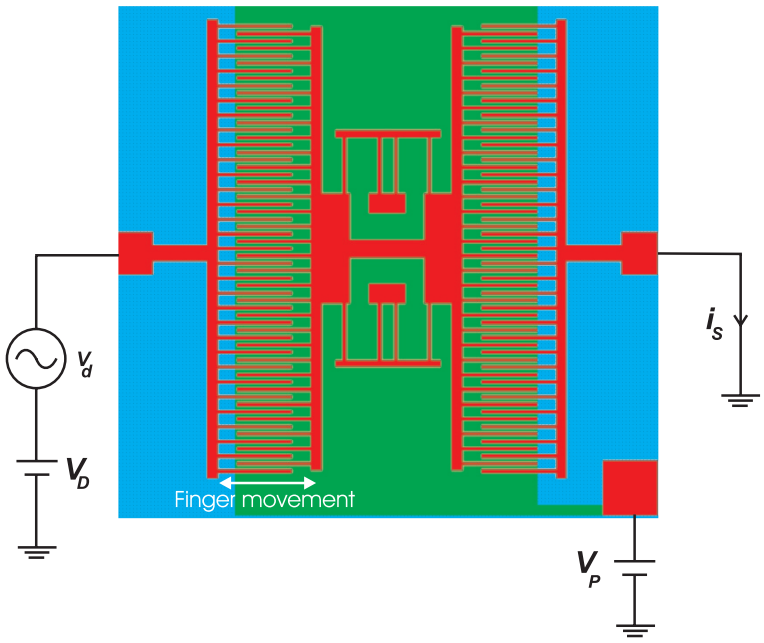

Figure 2.7: Layout view of a laterally driven microelectromechanical resonator

As the main detection and actuation mechanism is capacitive, it is necessary to optimize and calibrate the present circuit simulators and FEM tools for proper capacitive coupled interdigitized comb. The capacitance detection method requires compensation for the fringing effects as reported in [31] and relevant calculations are performed in the next section.

2.3.1 Capacitance Evaluation

Analytical approach towards calculating the capacitance is to assume infinitely long sheets with positive and negative charge and to evaluate net charge and hence, capacitance through Gauss' Law. One important factor, which is ignored in calculation is the fringing effects. Fringing effects are non uniform electric field lines, which originate and terminate at the edges of plates and hence, contribute to the total charge and capacitance, unless the plates are assumed to be infinite. Fringing

effects are graphically shown in Figure 2.8.

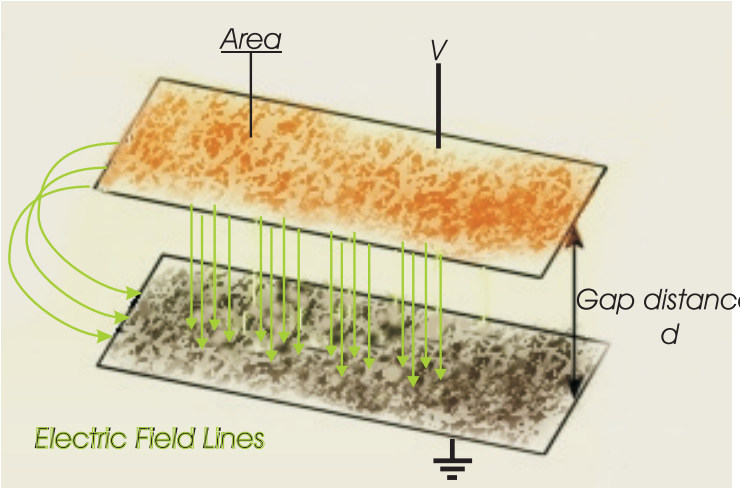

Figure 2.8: Fringing field lines displayed

Ignoring the fringing fields we can evaluate an analytical expression for the "parallel plate" model using Gauss' law which states $C = \epsilon A/d$. Here ϵ is permittivity of air, A is the area of the plate and d is the plate gap. A rough quantitative limit for ignoring the parasitic capacitance due to fringing fields is when the area of plates becomes around 1000 times greater than the plate gap.

In order to test this quantitative approach the plate area was increased while keeping the gap constant and capacitance was computed theoretically and was evaluated using a commercial FEM tool. A plot of varying capacitance versus area is plotted in the Figure 2.9.

We can conclude from this plot that the FEM tool's results approach that of theoretical values when the plate area become large enough than the gap. Here the margin of agreement for the capacitance was taken to be 5% of the theoretical value. As can be seen from Figure 2.9, plate area should be $\approx$ 1000 times greater than the gap before we obtain consonance between FEM results and simplified theory.

Comparative study of FEM and theoretical analysis are extended for the case of comb driven resonators. In the comb structures, we are concerned with the capacitance as a function of distance between fingers and substrate. Previous study has reported an analytical expression for capacitance for an 'n' toothed interdigitized

comb structure to be [32] :

$$C_{\text{comb}} = 2\text{n}\frac{\epsilon\ (L-x)\ t}{g} \tag{2.2}$$

where L is the length of finger, g is finger gap, t is structural thickness and x is the finger distance as shown in Figure 2.10.

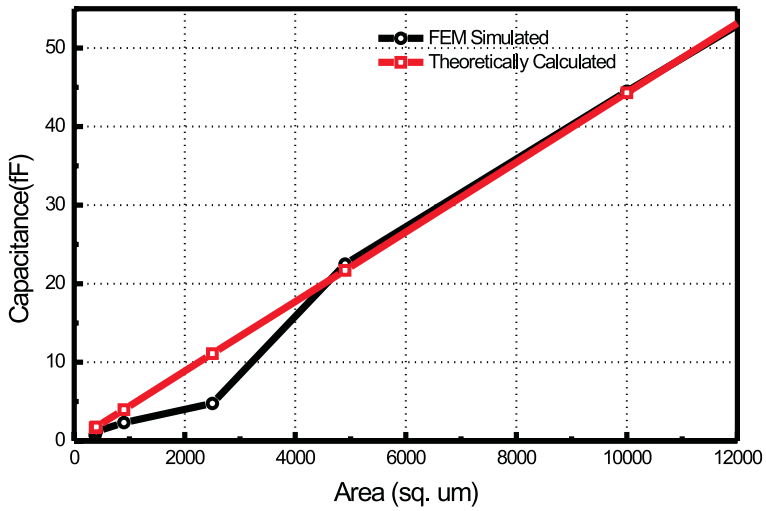

Figure 2.9: Analytically evaluated capacitance using parallel plate approach and FEM simulated capacitance plotted against increasing area. Gap between plates is 2μm

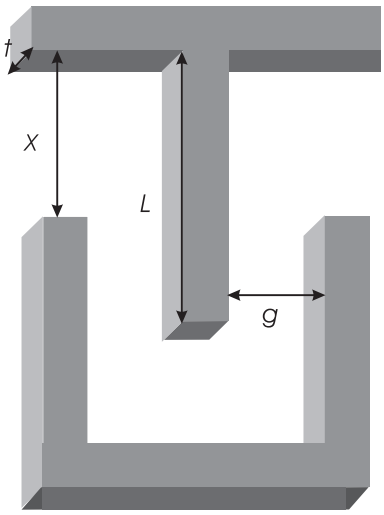

Figure 2.10: Diagram showing the dimension symbols used in Equation (2.2)

In transducers of the sort studied in this work, utilizing comb structure for input/output coupling, the differential factor of capacitance with respect to displacement ($\partial C/\partial x$) is important for calculations; displacement is not considered as a variable while calculating capacitance. However, as Equation (2.2) suggests we can tune the thickness t and gap spacing g to study the capacitance values. The constants are $L = 40\mu$m and $x = 10\mu$m and n = 30. A plot of this equation in both calculated and simulated terms is shown in Figure 2.11.

The difference between the calculated values and FEM simulated values is attributed to the assumption of negligible fringing effects. Coventor [33] is used as an FEM tool for simulating the fringing fields. As displayed in the previous studies of parallel plate (Figure 2.9), the fringing effects calculated using the FEM tool are more accurate. The change is expected since the gap spacing between fingers is in the vicinity, and for some cases equal to or even smaller than the area, let alone it be 1000 times greater as observed in the Figure 2.9.

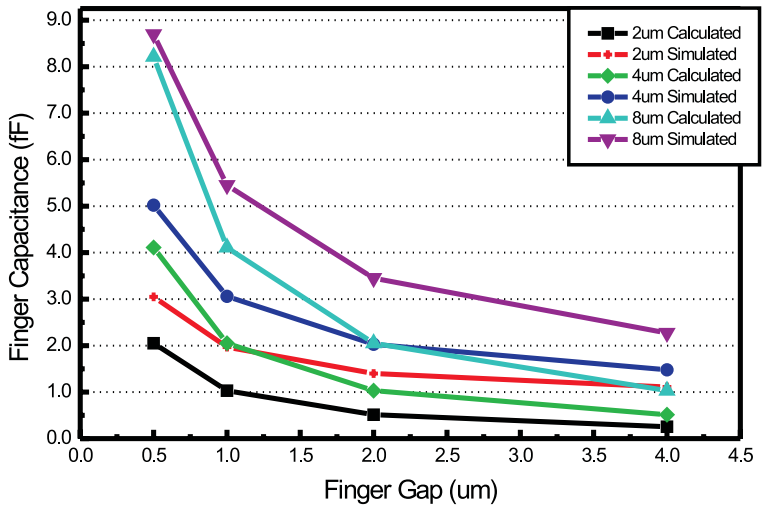

Figure 2.11: Plot of interdigitized finger capacitance versus finger gap for changing finger (structural) thickness

We also see from the plot in Figure 2.11 that the calculated values, which do not take fringing effects into account are a constant magnitude smaller than the FEM simulated results. The compensation factor due to fringing effects can then be incorporated directly into comb capacitance expression. Table 2.4 summarizes the calculated and simulated capacitance versus different gap spacings for different

set of structural thicknesses.

n	$L(\mu m)$	$x(\mu m)$	ϵ (F/cm)
2	20	5.5	8.85x10^{-12}

Thickness (μm)	Calculated C (fF)	Simulated C (fF)	Gap Spacing $g(\mu$m)
2	2.05	3.05	0.5
	1.03	1.93	1
	0.51	1.40	2
	0.26	1.11	4
4	4.11	5.02	0.5
	2.05	3.06	1
	1.03	2.03	2
	0.51	1.48	4
8	8.21	8.69	0.5
	4.11	5.45	1
	2.05	3.45	2
	1.03	2.27	4

Table 2.4: List of all the data values used for creating Figure 2.11

If we observe the trend, the compensation factor α decreases and approaches almost 1 when the thickness increases and the gap spacing decreases. This result agrees with Tang's [31] who presented the comb capacitance as shown in Equation (2.3).

$$C_{\text{comb}} = 2\alpha \text{n} \frac{\epsilon\ (L - x)\ t}{g} \tag{2.3}$$

We can now determine compensation factor α to account for the fringing field effects for our system by studying the decreasing trend of ratio of $C_{\text{simulated}}$ and $C_{\text{calculated}}$ as shown in Table 2.4. There are two immediate observations:

1. For thick plates (= 8 μm), when the gap decreases considerably (0.5μm) the fringing effects become negligible and the system is seen as a flat plate instead of interdigitized combs. Parallel plate calculations are then valid in this case.

2. Structural thickness of our system should be maintained small (more on that in Section 2.3.3 and hence α can vary anywhere from 2.5 to 1.5 and hence we choose an average value of 2.0 for future references.

2.3.2 Electrical Equivalent Model of Resonator

A laterally driven micromechanical resonator is shown in Figure 2.6 with important dimensional parameters. The dimensional parameter tuning is made possible by the previously done work.

Driving mechanical equations are derived in the Equations (2.4) [20].

$$\begin{aligned} k_{\text{sys}} &= 2Eh\left(\frac{W}{L}\right)^3 \\ w_{\text{res}} = 2\pi\ f_{\text{res}} &= 2\pi\ \sqrt{\frac{2Eh(\frac{W}{L})^3}{M_{\text{p}} + 0.3714 \cdot M}} \\ Q &= \frac{d}{\mu A_{\text{p}}}\sqrt{M\ k_{\text{sys}}} \\ C_{\text{comb}} &= \alpha\frac{2n\epsilon_{\text{o}}h(L-x)}{g} \\ \left|\frac{\partial C}{\partial x}\right| &= \alpha\frac{2nh\epsilon_{\text{o}}}{g} \end{aligned} \tag{2.4}$$

An electrical equivalent representation has been evaluated in [20] to model the mechanical components. The resonator system belonging to general transducers family can be represented with an equivalent mass-spring-damper system, which is transformed into equivalent series RLC circuit depicted in Figure 2.12.

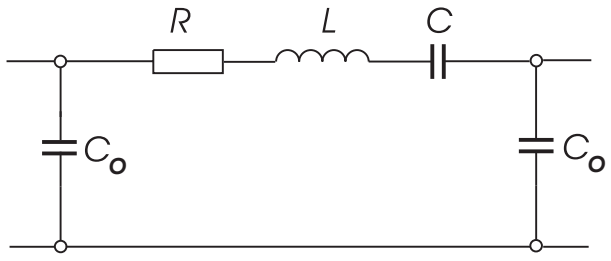

Figure 2.12: Series electrical equivalent model of series resonator circuit

Driving electrical equations are derived in the Equation (2.5) in the following,

which utilizes the Equations (2.4) [20]:

$$\begin{aligned} \eta &= V_{\mathrm{p}} \frac{\partial C}{\partial x} \\ C &= \frac{\eta^2}{k_{\mathrm{sys}}} \\ L &= \frac{m}{\eta^2} \\ R &= \frac{\sqrt{(m\ k_{\mathrm{sys}})}}{Q\ \eta^2} \end{aligned} \tag{2.5}$$

The explanation to the abbreviations used in Equations (2.4) and (2.5) is tabulated in Table 2.5.

A sample design is made for 719kHz to check the validity and verification purposes. Typical values are shown in Table 2.5 on page 41and the corresponding frequency response of the transfer function magnitude is shown in Figure 2.13:

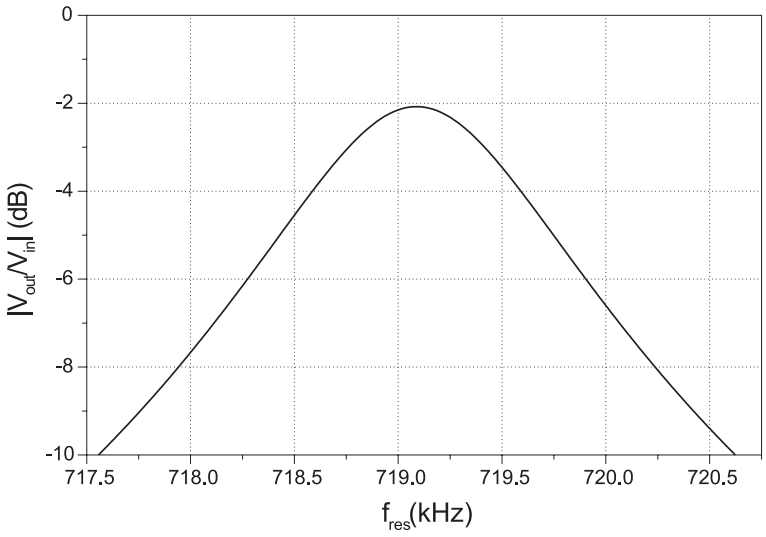

Figure 2.13: Frequency response of electrical equivalent model of a 719kHz micromechanical resonator

We can now optimize Equations (2.4) and (2.5) for increased w_{res} and quality factor.

2.3.3 Operating Frequency Optimization

The main issue addressed in this section is to obtain reasonable device dimensions to account for any frequency requirements. To satisfy the requirement of a more

suitable control over frequency variation and to study the process recursively MATLAB codes were written (Appendix A). The critical dimensions are set according to the CRONOS MUMPS process [35].

The codes of Appendix A were written to calculate the system's mechanical and electrical variables and parameters namely:

1. Mechanical Modeling Coefficients
    - System spring constant (k_{sys})
    - Quality factor (Q)
    - Resonance frequency (f_{r})
2. Electrical Modeling Coefficients
    - Resistance (R)
    - Inductance (L)
    - Capacitance (C)
    - Coupling capacitance for filter (C_{spring})

The results are plotted in Figure 2.14 through 2.16:

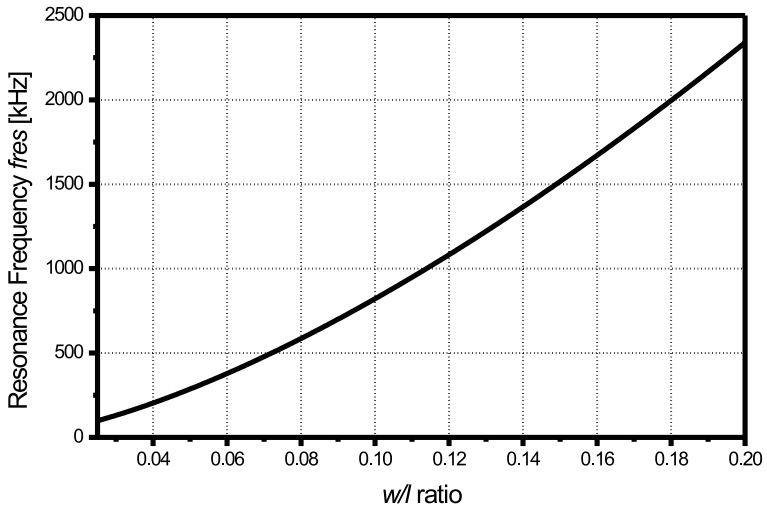

Figure 2.14: Resonance frequency of resonator with respect to varying dimensional ratio

Parameter	Explanation	Sample Values for 17kHz
E	Young's Modulus	150 GPa
μ	Absolute viscosity of air	17.46×10^{-6} Ns/m^2
Folded beam supporting the resonator via anchor:		
h	Structural Thickness	2 μm
W	Beam width	3 μm
L	Beam Length	30 μm
M	Mass (Beam and Truss)	7.23×10^{-12} Kg
d	Folded Beam to substrate gap	4 μm
Shuttle Structure:		
M_{p}	Shuttle Mass	2.69×10^{-11} Kg
A_{p}	Shuttle Area	6018 μm^2
Comb Actuators:		
n	Number of gaps	20
h	Finger Width	3 μm
g	Finger Gap	3 μm
L	Finger Length	20 μm
x	Finger Lateral Distance	15 μm
α	Fringing Effects Correction	1.2
Mechanical Calculations:		
k_{sys}	Mechanical Spring Constant	600 N/m
f_{r}	Resonance Frequency	719.44 kHz
Q	Quality Factor	2508.03
C_{comb}	Finger Capacitance	3.54 fF
$\frac{\partial C}{\partial x}$	Differential Capacitance Change	4.72×10^{-10} F/m
Electrical Calculations:		
V_{p}	DC bias voltage	35 V
C	Series Capacitance	1.63×10^{-19} F
L	Series Inductance	300.53 kHz
R	Series Resistance	540.17 M Ω

Table 2.5: Table explaining the meanings of abbreviations used in Equations (2.4) and (2.5) and values used for the design of 717 kHz resonator

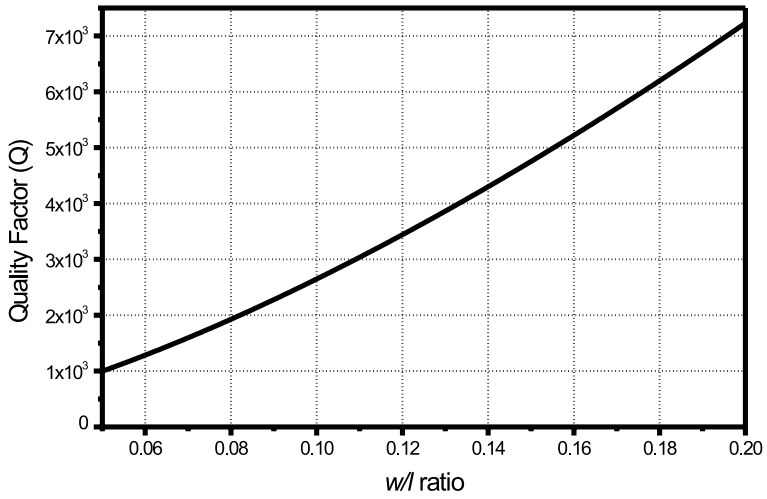

Figure 2.15: Quality factor of resonator with respect to varying dimensional ratio

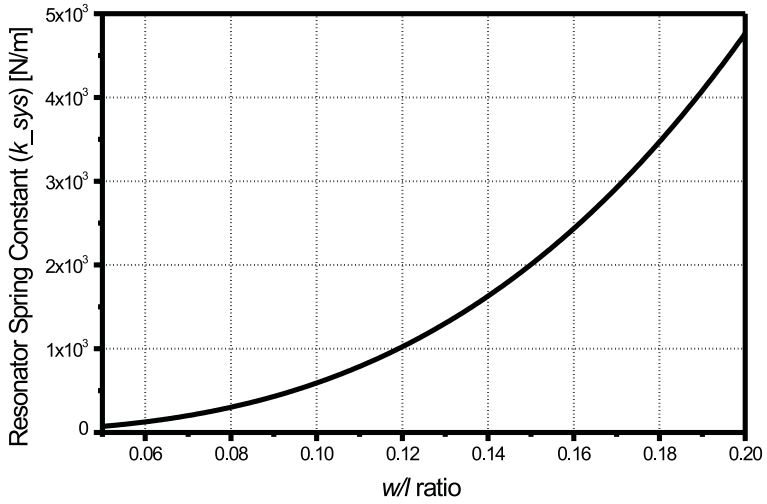

Figure 2.16: System spring constant of resonator with respect to varying dimensional ratio

2.4 Parametric Evaluation

As mentioned previously, a filter is mainly described in terms of its center frequency, bandwidth and coupling coefficient. In this section, we will formulate some relations to address the above mentioned criteria and will link them to critical mechanical device parameters. Bounded Electrical Coupling Coefficient κ will be formulated by real values. An electrical equivalent circuit will be used to model the filter and the transfer function will be evaluated, which will be linked with filter quality factor Q and coupling coefficient κ. Filter bandwidth design criteria and formulae will be presented, which will conclude the design of mechanical filters using electrical equivalent circuits.

2.4.1 Derivation of Transfer Function $|H(f)|^2$

Relevant equations will be presented, which were derived as part of transfer function evaluation and the establishment of relationships between the bandwidth and the insertion loss.

Series RLC

For the transfer function evaluation, we will consider a second order series coupled tank circuit. It should be noted that though an LC tank by itself introduces however, a second order system, we are following the mechanical design in MEMS analogy which implies that each resonator be treated as a single order system. The equivalent circuit is given in Figure 2.17.

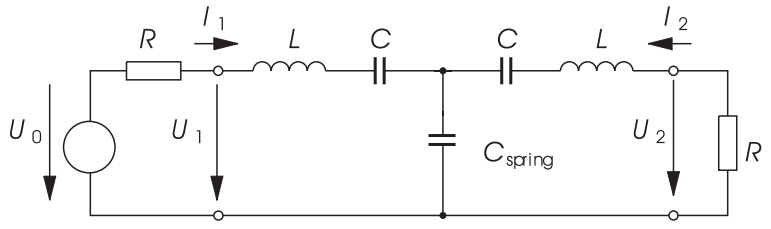

Figure 2.17: Series electrical equivalent circuit of second order MEM filter

From Figure 2.17 we can single out the two individual LC tank circuits each corresponding to an electrically driven mechanical resonator coupled via an equivalent

capacitance C_{spring}, which is the electrical equivalent of the mechanical spring. Some helping definitions are presented in the following to simplify the transfer function calculation.

$$X := \omega L - \frac{1}{\omega C} \tag{2.6}$$

$$X_{\text{k}} := -\frac{1}{\omega C_{\text{spring}}}, \quad B_{\text{k}} := \omega C_{\text{spring}} \tag{2.7}$$

where X is the complex impedance of the tank and X_{k} is the complex impedance of coupling/tether spring. We can write the impedance matrix (Z) of the form with $I_2 = -U_2$ / R and $I_1 = (U_0 - U_1)$/R and the transfer function as $|H|^2 = |U_2/(U_0/2)|^2$. Using the definitions, we can now derive the transfer function of the circuit in Figure 2.17 as follows:

$$H(f) = \frac{j2X_{\text{k}}R}{R^2 - 2XX_{\text{k}} - X^2 + j2R(X + X_{\text{k}})} \tag{2.8}$$

The magnitude of transfer function is then written in the following form:

$$|H(f)|^2 = \frac{(2X_{\text{k}}R)^2}{[R^2 - 2XX_{\text{k}} - X^2]^2 + 4R^2(X + X_{\text{k}})^2} \tag{2.9}$$

and is transformed to a simpler form in terms of definitions as presented in Equations (2.6) and Equation (2.7):

$$|H(f)|^2 = \frac{1}{1 + \left[\frac{R\,B_{\text{spring}}}{2} + \frac{X}{R} + \frac{X^2\,B_{\text{spring}}}{2\,R}\right]^2} \tag{2.10}$$

Having established the transfer function relationship in terms of circuit components in Equation (2.10) we shall relate it to the Quality factor (Q_{E}) and κ. Some abbreviations are needed for simplifying the relations and are summarized in the following:

$$\kappa := \frac{X_{\text{k}}}{R} = -\frac{1}{RB_{\text{k}}}$$

$$\nu := \frac{\omega}{\omega_{\text{res}}} - \frac{\omega_{\text{res}}}{\omega} \tag{2.11}$$

$$Q_{\text{E}} \cdot \nu = \frac{X}{R} = -\frac{1}{R}\sqrt{\frac{L}{C}}\left(\frac{\omega_{\text{res}}}{\omega} - \frac{\omega}{\omega_{\text{res}}}\right) \tag{2.12}$$

$$\omega_{\text{res}} = \frac{1}{\sqrt{LC}}$$

where the parameter ν introduced in Equation (2.11) is called the normalized frequency deviation and is obtained from [3]. Using these abbreviations we can write the simplified final transfer function as presented in Equation (2.13):

$$|H(f)|^2 = \frac{1}{1 + \left[\frac{1}{2\,\kappa} - Q_{\mathrm{E}}\nu + \frac{1}{2\,\kappa}(Q_{\mathrm{E}}\nu)^2\right]^2} \tag{2.13}$$

For detailed derivation steps leading to Equation (2.8) and Equation (2.13) see Appendix B.

Parallel RLC

Parallel RLC filter design in useful when the series resistance of the circuit is very large [34] as in the case of MEM resonators operated at atmospheric pressure. The equivalent circuit is given in Figure 2.18 and represents the dual form of the series RLC circuit.

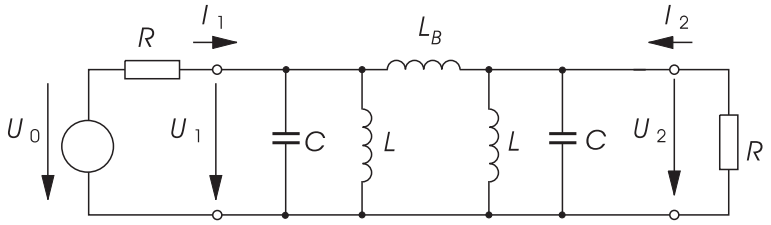

Figure 2.18: Parallel electrical equivalent circuit of second order MEM filter

From Figure 2.18 we can single out the two individual LC tank circuits each corresponding to an electrically driven mechanical resonator coupled via an equivalent inductor L_{B}, which is the electrical equivalent of the mechanical spring. Some helping definitions are presented in the following to simplify the transfer function calculation.

$$\begin{aligned} Y_{\mathrm{A}} &:= j\omega C + \frac{1}{j\omega L} \\ &= \frac{1 - \omega^2 L_{\mathrm{A}} C}{j\omega L_{\mathrm{A}}} \end{aligned} \tag{2.14}$$

$$Y_{\mathrm{B}} := \frac{1}{j\omega L_{\mathrm{spring}}}, \quad B_{\mathrm{B}} := -j\omega L_{\mathrm{spring}} \tag{2.15}$$

where Y_{A} is the complex admittance of the tank and Y_{B} is the complex admittance of coupling/tether spring. We can write the admittance matrix (Y) of the form with $I_2 = -U_2$ / R and $I_1 = (U_0 - U_1)$/R and the transfer function as $|H|^2 = |U_2/(U_0/2)|^2$. Using the definitions we can now derive the transfer function of the circuit in Figure 2.18 as follows:

$$H(f) = \frac{-j2Y'_{\mathrm{B}}G}{(G - j(Y'_{\mathrm{A}} + Y'_{\mathrm{B}}))^2 - (-jY'_{\mathrm{B}})^2} \tag{2.16}$$

where $Y_{\mathrm{B}} = jY'_{\mathrm{B}}$ and $Y_{\mathrm{A}} = -jY'_{\mathrm{A}}$. The magnitude of transfer function is then written in the following form:

$$|H(f)|^2 = \frac{(2Y'_{\mathrm{B}}G)^2}{[G^2 - 2Y'_{\mathrm{A}}Y'_{\mathrm{B}} - Y'^2_{\mathrm{A}}]^2 + 4G^2(Y'_{\mathrm{A}} + Y'_{\mathrm{B}})^2} \tag{2.17}$$

and is transformed to a simpler form in terms of definitions as presented in Equations (2.14) and Equation (2.15):

$$|H(f)|^2 = \frac{1}{1 + \left[\dfrac{G}{2\,Y'_{\mathrm{B}}} + \dfrac{Y'_{\mathrm{A}}}{G} + \dfrac{Y'^2_{\mathrm{A}}}{2\,G\,Y'_{\mathrm{B}}}\right]^2} \tag{2.18}$$

Having established the transfer function relationship in terms of circuit components in Equation (2.18) we shall relate it to the Q_{E} and κ. Some abbreviations used for simplifying the relations are summarized in the following:

$$\begin{aligned} \kappa &:= \frac{G}{Y'_{\mathrm{B}}} = -GB_{\mathrm{B}} \\ \frac{\nu}{Q_{\mathrm{E}}} &= \frac{Y'_{\mathrm{A}}}{G} = -R\sqrt{\frac{C}{L_{\mathrm{A}}}}\left(\frac{\omega_{\mathrm{res}}}{\omega} - \frac{\omega}{\omega_{\mathrm{res}}}\right) \\ \omega_{\mathrm{res}} &= \frac{1}{\sqrt{LC}} \end{aligned} \tag{2.19}$$

where the parameter ν introduced in Equation (2.11) is also used here. Using these abbreviations we can write the final transfer function as presented in Equation (2.20), which is of the same form as the transfer function of the series RLC circuit.

$$|H(f)|^2 = \frac{1}{1 + \left[\dfrac{1}{2\,\kappa} - \nu Q_{\mathrm{E}} + \dfrac{1}{2\,\kappa}\left(\nu Q_{\mathrm{E}}\right)^2\right]^2} \tag{2.20}$$

This is expected since the mechanical filter did not change and both the series and the parallel RLC circuits represent the same device. For detailed derivation steps leading to Equation (2.16) see Appendix B. For the transfer function of both the series and parallel RLC circuits, the only point of difference is the resonator quality factor appearing in inverted form as the dual of each other.

The remaining calculations in the proceeding sections are consequently affected but the final simplified results seem to reflect the same fact of inverted Q without causing any more complexity in the formulation.

2.4.2 Coupling Coefficient (κ) Limitations

If we derivate Equation (2.13) with respect to ν, we can obtain the limits for κ which will correspond to the maximum and 3dB point in terms of frequency response. The objective is to find the maximum range in which κ can be tuned to obtain a minimum and maximum selective bandwidth.

Firstly, for both electrical representations the normalized frequencies ν at which the transfer function H(ν) shows maximum and minimum are calculated. H(ν) and ν are a function of the coupling factor κ.

Series RLC

By using the abbreviation:

$$u = \frac{1}{2\,\kappa} - Q_{\mathrm{E}}\nu + \frac{1}{2\,\kappa}(Q_{\mathrm{E}}\nu)^2$$

and setting:

$$\begin{aligned}
\frac{\partial(|H|^2)}{\partial\nu} &= 0 \\
\frac{\partial}{\partial\nu}\left(\frac{1}{1+u(\nu)^2}\right) &= \frac{(-2u)\ (\partial u/\partial\nu)}{(1+u(\nu)^2)^2} \\
\Rightarrow\ -2u = 0 \quad or \quad \frac{\partial u}{\partial\nu} &= 0 \\
2u = 0 \Rightarrow 2 \quad \times \quad \frac{1}{2\,\kappa} - Q_{\mathrm{E}}\nu + \frac{1}{2\,\kappa}(Q_{\mathrm{E}}\nu)^2 &= 0
\end{aligned}$$

one obtains:

$$\nu_{1,2} = \frac{\kappa}{Q_{\mathrm{E}}} \pm \frac{1}{Q_{\mathrm{E}}} \sqrt{\kappa^2 - 1} \qquad \text{at which H}(\nu_{1,2})\text{is maximum}$$

$$\frac{\partial u}{\partial \nu} = 0 \quad \Rightarrow \quad -1 + \frac{Q_{\mathrm{E}}}{\kappa}\nu$$

and

$$\nu_3 = \frac{\kappa}{Q_{\mathrm{E}}} \qquad \text{at which H}(\nu_3)\text{is minimum}$$

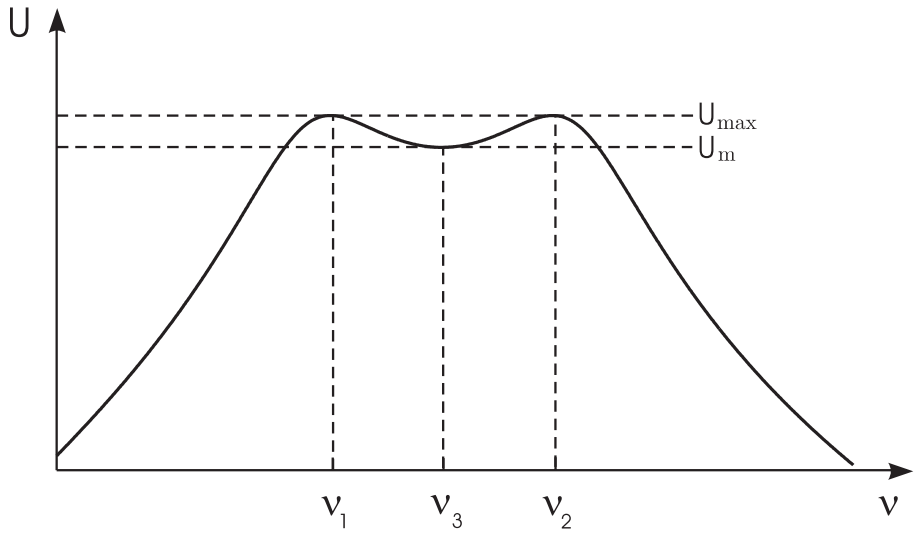

Figure 2.19: ν points on pass band of the frequency spectrum

For the transfer function we now have formulated all the three points (2 for $\mathrm{U_{max}}$ and 1 for $\mathrm{U_m}$) which will correspond to a different κ and hence a different local maxima/minima. These points are displayed graphically in Figure 2.19. For the transfer function to be maximally flat, we would like to have $\mathrm{U_m/U_{max}} = 1$ which, is only possible when κ =1. This marks the lower limit since our objective is to start from the maximally flat response and work towards bandwidth broadening techniques. Furthermore the power magnitude corresponding to ν_3 point is presented in the following:

$$|H(\nu_3)|^2 = \frac{1}{1 + \left[1/\kappa - Q_{\mathrm{E}}\kappa/Q_{\mathrm{E}} + 1/2\kappa \ \ (Q_{\mathrm{E}}\ \kappa/Q_{\mathrm{E}})^2\right]^2}$$

$$|H(\nu_3)|^2 = \frac{1}{1 + \left[\frac{1}{2\kappa} - \frac{1}{2}\kappa\right]^2} \tag{2.21}$$

We can use Equation (2.21) to evaluate the upper limit of κ, which marks the half power point (or the 3dB bandwidth $BW_{3\text{dB}}$) as $|H(\nu_3)|^2 = 1/2$. The upper limit for κ is evaluated as follows:

$$\begin{aligned} |H(\nu_3)|^2 &= \frac{1}{1+1/4\ \left[\kappa - 1/\kappa\right]^2} = \frac{1}{2} \\ &\Rightarrow \quad \kappa - \frac{1}{\kappa} = \pm 2 \\ &\Rightarrow \quad \kappa^2 \pm 2\kappa - 1 = 0 \\ \Rightarrow \kappa_{1,2} = -1 \pm \sqrt{2} \quad &\& \quad \kappa_{1,2} = 1 \pm \sqrt{2} \end{aligned} \tag{2.22}$$

From Equation (2.22) we obtain four results but only one makes physical sense. The only valid choice for the upper limit is $1+\sqrt{2}$. Hence, the limits for coupling coefficient are established as:

$$1 \leq \kappa \leq 1 + \sqrt{2} \tag{2.23}$$

The effects of varying κ onto the transfer function and the graphical justification of upper and lower limits of κ is shown in Figure 2.20. The plotted case for $\kappa = 0.8$ shows that for values of $\kappa < 1$ the insertion loss of the filter becomes predominant and increases with smaller κ values.

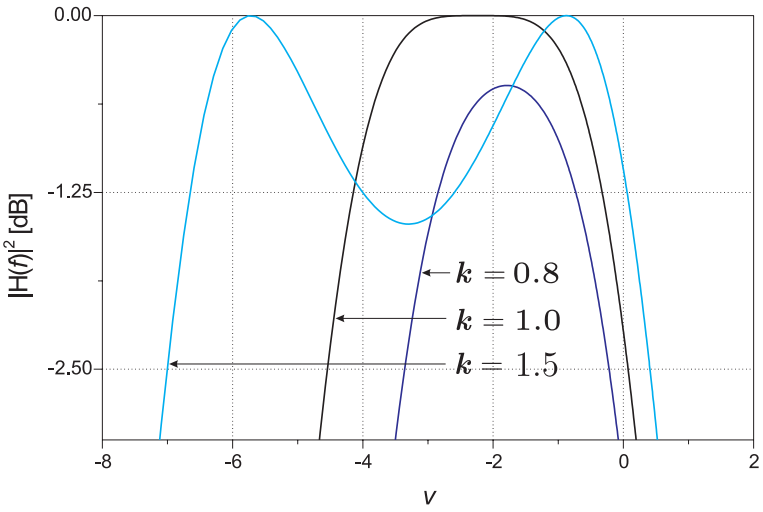

Figure 2.20: Effects of varying κ onto series RLC circuit

Parallel RLC

To find the ν values for maximum and minimum of the transfer function, the same way is followed as described before with the series RLC circuit. Let

$$u = \frac{1}{2\,\kappa} - \frac{\nu}{Q_{\mathrm{E}}} + \frac{1}{2\,\kappa} \cdot \left(\frac{\nu}{Q_{\mathrm{E}}}\right)^2$$

and setting:

$$\begin{aligned}
\frac{\partial(|H|^2)}{\partial\nu} &= 0 \\
\frac{\partial}{\partial\nu}\left(\frac{1}{1+u(\nu)^2}\right) &= \frac{(-2u)\ (\partial u/\partial\nu)}{(1+u(\nu)^2)^2} \\
\Rightarrow\ -2u = 0 \quad or \quad \frac{\partial u}{\partial\nu} &= 0 \\
2u = 0 \Rightarrow 2 \quad \times \quad \frac{1}{2\,\kappa} - Q_{\mathrm{E}}\nu + \frac{1}{2\,\kappa}(Q_{\mathrm{E}}\nu)^2 &= 0
\end{aligned}$$

one obtains three normalized frequency points:

$$\begin{aligned}
\nu_{1,2} &= \frac{\kappa}{Q_{\mathrm{E}}} \pm \frac{1}{Q_{\mathrm{E}}}\sqrt{\kappa^2-1} \qquad \text{at which } \mathrm{H}(\nu_{1/2}) \text{ is maximum} \\
\frac{\partial u}{\partial\nu} = 0 \quad \Rightarrow \quad & -1 + \frac{Q_{\mathrm{E}}}{\kappa}\nu \\
\text{and} \qquad \nu_3 &= \frac{\kappa}{Q_{\mathrm{E}}} \qquad \text{at which } \mathrm{H}(\nu_3) \text{ is minimum}
\end{aligned}$$

For the transfer function we now have formulated all the three points (2 for $\mathrm{U_{max}}$ and 1 for $\mathrm{U_m}$), which will correspond to a different κ and hence, a different local maxima/minima. For the transfer function to be maximally flat, we would like to have $\mathrm{U_m/U_{max}} = 1$, which is only possible when κ =1. This marks the lower limit since our objective is to start from the maximally flat response and work towards bandwidth broadening techniques. Furthermore the power magnitude corresponding to ν_3 point is presented in the following:

$$\begin{aligned}
|H(\nu_3)|^2 &= \frac{1}{1+\left[1/\kappa - Q_{\mathrm{E}}\kappa/Q_{\mathrm{E}} + 1/2\kappa\ \left(Q_{\mathrm{E}}\ \kappa/Q_{\mathrm{E}}\right)^2\right]^2} \\
|H(\nu_3)|^2 &= \frac{1}{1+\left[\frac{1}{2\kappa} - \frac{1}{2}\kappa\right]^2} \qquad (2.24)
\end{aligned}$$

Equation (2.24) referring to parallel RLC turns out to be same as Equation (2.21). So the remaining calculations remain unchanged from the previous case and will not be repeated. The κ limits are the same as presented in Equation (2.23).

The effects of varying κ onto the transfer function and the graphical justification of upper and lower limits of κ is shown in Figure 2.21.

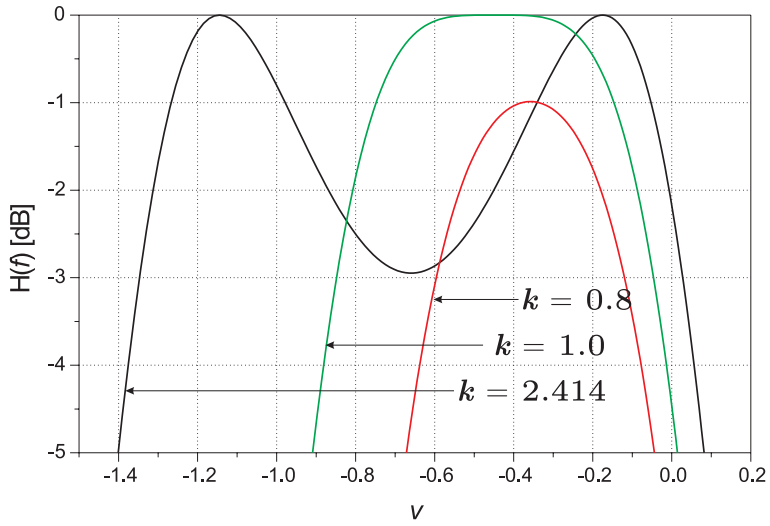

Figure 2.21: Effects of varying κ onto parallel RLC circuit

2.4.3 Half Power Point (ν) Calculations

General bandpass filter characteristics with important parameters are presented in Figure 2.22. The voltage value corresponding to the centre frequency f_{m} is named as the saddle point $\mathrm{U_m}$.

In Figure 2.22, $\mathrm{U_{max}}$ stands out as the maximum voltage for a single resonator. We are interested in finding a closed form relationship for the bandwidth of the filter $BW_{3\mathrm{dB}}$ in terms of external quality factor Q_{E}, normalized deviation ν and the coupling coefficient κ from the transfer function as evaluated in Equation (2.13).

Series RLC

Mathematically this implies:

$$|H(f)|^2 = \frac{1}{2} \Rightarrow 1 + \left[\frac{1}{2\kappa} - \nu Q_{\mathrm{E}} + \frac{1}{2\kappa}(\nu Q_{\mathrm{E}})^2\right]^2 = 2 \tag{2.25}$$

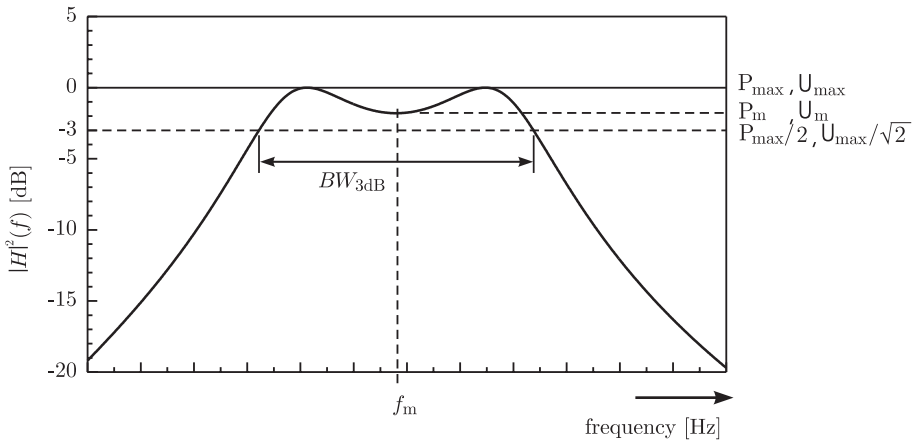

Figure 2.22: Definition of the 3dB bandwidth

Equation (2.25) now yields the conditions for solution of bandwidth, which leads to two cases as:

$$\nu^2 \frac{Q_E^2}{2\kappa} - \nu Q_E + \frac{1}{2\kappa} = \pm 1 \tag{2.26}$$

First Case: $= -1$

$$\nu^2 - \nu \frac{2\kappa}{Q_E} + \frac{1}{Q_E^2} + \frac{2\kappa}{Q_E^2} = 0$$

$$\Rightarrow \nu_{1/2} = \frac{\kappa}{Q_E} \pm \frac{1}{Q_E}\sqrt{\kappa^2 - 2\kappa - 1} \tag{2.27}$$

The equation set presented in Equation (2.27) summarize, the first case. Here, we can observe that the function $f(\kappa) = \kappa^2 - 2\kappa - 1$ become negative for values equal to or greater than 1 as shown graphically in the Figure 2.23. The negative function results in a complex normalized frequency shift from Equation (2.27) which is not physically possible. Hence this case is discarded based on the fact that we must take into account κ =1 case for critically coupled filter design, which is evaluated in Section 2.4.2 and defines the minimum allowed value of κ.

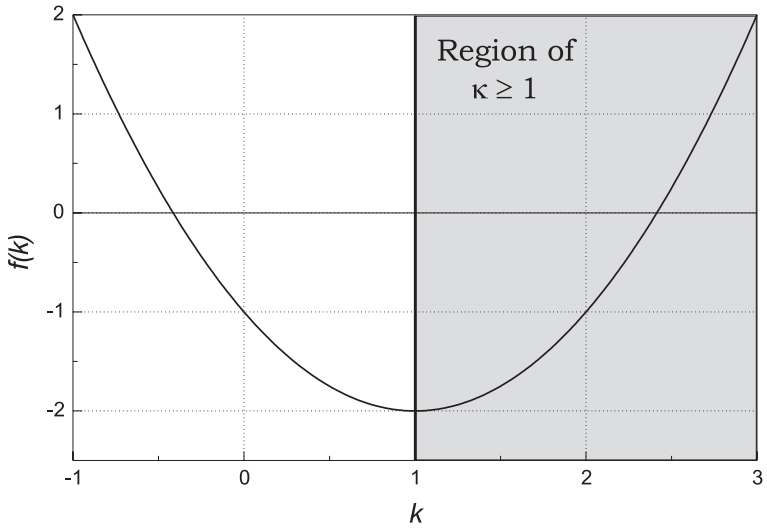

Figure 2.23: Graphic representation of $f(\kappa)$ function versus κ

Second Case: $= +1$

$$\nu^2 - \nu\frac{2\kappa}{Q_{\mathrm{E}}} + \frac{1}{Q_{\mathrm{E}}^2} - \frac{2\kappa}{Q_{\mathrm{E}}^2} = 0$$

$$\Rightarrow \nu_{1,2} = \frac{\kappa}{Q_{\mathrm{E}}} \pm \sqrt{\left(\frac{\kappa}{Q_{\mathrm{E}}}\right)^2 - \frac{1}{Q_{\mathrm{E}}^2} + \frac{2\kappa}{Q_{\mathrm{E}}^2}}$$

$$\Rightarrow \nu_{1,2} = \frac{\kappa}{Q_{\mathrm{E}}} \pm \frac{1}{Q_{\mathrm{E}}}\sqrt{\kappa^2 + 2\kappa - 1} \tag{2.28}$$

The function $f(\kappa) = \kappa^2 + 2\kappa - 1$ is plotted in Figure 2.24. The results allow the inclusion of $\kappa \geq 1$ and hence filter design is supported by this case. We will derive bandwidth from the above mentioned considerations in Section 2.2.4.

Parallel RLC

Mathematically this implies:

$$|H(f)|^2 = \frac{1}{2} \Rightarrow 1 + \left[\frac{1}{2\kappa} - \nu Q_{\mathrm{E}} + \frac{1}{2\kappa} \cdot (\nu Q_{\mathrm{E}})^2\right]^2 = 2 \tag{2.29}$$

Equation (2.29) now yields the conditions for solution of bandwidth, which again leads to two cases as:

$$\frac{1}{2\kappa} - \nu Q_{\mathrm{E}} + \frac{1}{2\kappa} \cdot \nu^2 Q_{\mathrm{E}}^2 = \pm 1 \tag{2.30}$$

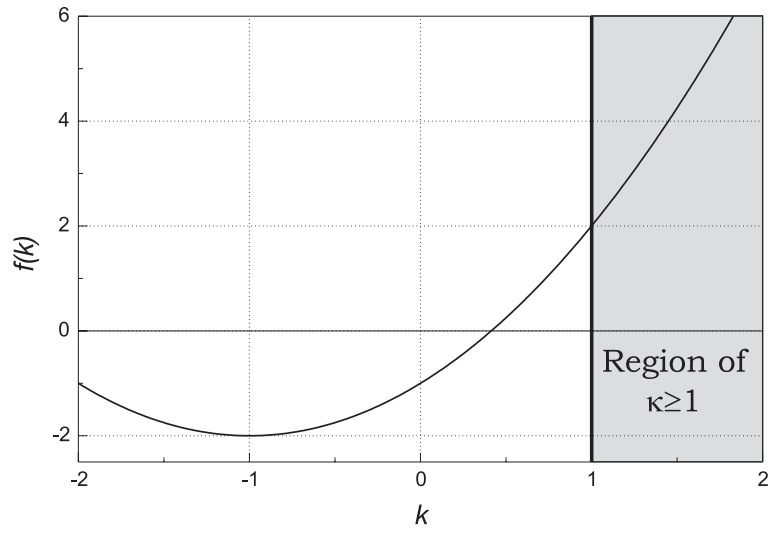

Figure 2.24: Graphic representation of $f(\kappa)$ function versus κ

First Case: $= -1$

$$\nu^2 - \nu\frac{2\kappa}{Q_{\mathrm{E}}} + \frac{1}{Q_{\mathrm{E}}^2} + \frac{2\kappa}{Q_{\mathrm{E}}^2} = 0$$

$$\Rightarrow \nu_{1,2} = \frac{\kappa}{Q_{\mathrm{E}}} \pm \frac{1}{Q_{\mathrm{E}}}\sqrt{\kappa^2 - 2\kappa - 1} \tag{2.31}$$

Second Case: $= +1$

$$\nu^2 - \nu\frac{2\kappa}{Q_{\mathrm{E}}} + \frac{1}{Q_{\mathrm{E}}^2} - \frac{2\kappa}{Q_{\mathrm{E}}^2} = 0$$

$$\begin{aligned} \Rightarrow \nu_{1,2} &= \frac{\kappa}{Q_{\mathrm{E}}} \pm \sqrt{\left(\frac{\kappa}{Q_{\mathrm{E}}}\right)^2 - \frac{1}{Q_{\mathrm{E}}^2} + \frac{2\kappa}{Q_{\mathrm{E}}^2}} \\ \Rightarrow \nu_{1,2} &= \frac{\kappa}{Q_{\mathrm{E}}} \pm \frac{1}{Q_{\mathrm{E}}}\sqrt{\kappa^2 + 2\kappa - 1} \end{aligned} \tag{2.32}$$

The cases are identical to the series counterpart. Taking into account the behavior of κ in Equation (2.31) and Equation (2.32) as well as the allowed boundary points for κ in Equation (2.23) we can validate the second case to be used in 3dB bandwidth calculations.

2.4.4 Bandwidth (BW_{3dB}) Calculation

The bandwidth is defined as $|f_2 - f_1|$ where f_2 and f_1 are frequency points where $|H(f)|^2 = 1/2$. We shall now relate Q_{E} and κ to the bandwidth.

From second case we have already established valid ν roots, which will offer valid κ values for the design. These roots are subtracted and their magnitude is obtained in Equation (2.33), which will be used in comparison with the approximation of Equation (2.34).

$$|\nu_1 - \nu_2| = \frac{2}{Q_{\mathrm{E}}}\sqrt{\kappa^2 + 2\kappa - 1} \tag{2.33}$$

Approximation:

$$\begin{aligned} \nu_1 - \nu_2 &= \left(\frac{w_1}{w_{\mathrm{res}}} - \frac{w_{\mathrm{res}}}{w_1}\right) - \left(\frac{w_2}{w_{\mathrm{res}}} - \frac{w_{\mathrm{res}}}{w_2}\right) \\ &\approx 2\frac{w_{\mathrm{res}} - w_1}{w_{\mathrm{res}}} - 2\frac{w_{\mathrm{res}} - w_2}{w_{\mathrm{res}}} \\ \Rightarrow |\nu_1 - \nu_2| &= \frac{2}{w_{\mathrm{res}}}|w_2 - w_1| = \frac{2}{f_{\mathrm{res}}}|f_2 - f_1| \end{aligned} \tag{2.34}$$

with $f_{\mathrm{res}} = 1/\sqrt{LC}$.

Then, by combining results of Equation (2.33) and Equation (2.34) we can obtain the following relationship of bandwidth:

$$\begin{aligned} \frac{2}{f_{\mathrm{res}}}|f_2 - f_1| &= \frac{2}{Q_{\mathrm{E}}}\sqrt{\kappa^2 + 2\kappa - 1} \\ \Rightarrow BW_{3\mathrm{dB}} &= \frac{f_{\mathrm{res}}}{Q_{\mathrm{E}}}\sqrt{\kappa^2 + 2\kappa - 1} \end{aligned} \tag{2.35}$$

It is important to observe that $f_{\mathrm{res}}/Q_{\mathrm{E}}$ corresponds to a single resonator BW_{E}. Hence we can relate the bandwidth $BW_{3\mathrm{dB}}$ of a MEM filter to that of a single resonator BW_{E} and the coupling coefficient κ as presented in Equation (2.35). The $BW_{3\mathrm{dB}}$ can be controlled by tuning κ. Since an increase in bandwidth accompanies an increase in saddle point $\mathrm{U_m}$ of Figure 2.22 we need to limit $BW_{3\mathrm{dB}}$ to a maximum allowed value, which will offer a mediocre or negligible voltage loss at the output. The criteria for choosing the limits is already established in Section 2.4.2 and will be used for evaluation of limiting cases of the $BW_{3\mathrm{dB}}$. There are following two pre-requisites, which will be helpful:

1. The smallest allowed value of κ should ensure $U_m/\ U_{max} = 1$, which is the critically coupled case and BW_{3dB} should reflect that value.

2. The largest allowed value of κ should not let $U_m/\ U_{max} < 0.707$ because that would correspond to a signal loss greater than 3dB at f_m. Should the value of $U_m/\ U_{max}$ is chosen to be less than 0.707, there will be four values of ν where $|H(\nu)^2|$ will be equal 1/2 and this will violate the bandwidth definition, which works for 2 local maxima and 1 local minima as well as on insertion loss $\geq 3dB$.

The boundary enclosing κ as established in Section 2.2.2 is utilized in evaluating the maximum/minimum obtainable bandwidth of the filter BW_{3dB} as compared to an ideal single resonator case which is also termed as Q_E.

Parallel RLC

For parallel RLC, the calculations are no different than what is presented in Equation (2.34). Furthermore if we are to calculate $|\nu_1 - \nu_2|$ we can consider ν points for case 2 in parallel RLC section.

$$|\nu_1 - \nu_2| = \frac{2}{Q_E}\ \sqrt{\kappa^2 + 2\kappa - 1} \tag{2.36}$$

Then we equate both Equation (2.34) and Equation (2.36) to obtain the following equation for bandwidth:

$$|f_1 - f_2| = \frac{f_{res}}{Q_E}\ \sqrt{\kappa^2 + 2\kappa - 1} \tag{2.37}$$

2.5 Electro-Mechanical Model of Coupling Spring

Similar to the electrical equivalent model of a resonator as discussed in Section 2.3, an electrical equivalent model for the coupling spring has been evaluated. When two resonators are coupled together by a spring as shown in Figure 2.25, the effect is a shift in center frequency f_m as well as a change in bandwidth BW_{3dB}. If the coupling is non elastic (the coupling spring's stiffness can be varied to obtain such characteristics for instance in Figure 2.25 if the spring k_{12} is replaced with a rigid

rod) then both of the constituent resonators act like a single resonator. Hence if the resonators are designed for maximal flatness, the net setup will result in Butterworth implementation.

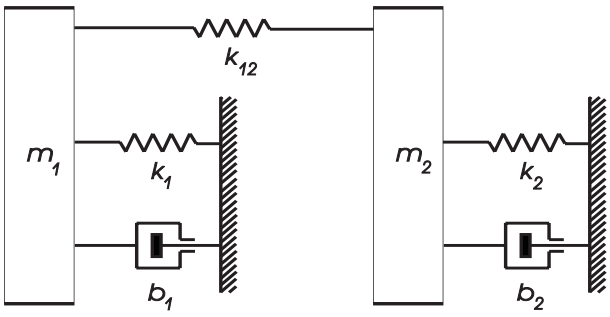

Figure 2.25: Mechanical model of a series N-resonator filter.

The relation between the coupling spring stiffness k_{spring} in the mechanical design and the capacitance C_{spring} in the electrical equivalent circuit is provided by the following Equations (2.38) and (2.39) [36].

Coupling coefficient in electrical equivalent:

$$k_{\text{spring}} = \frac{\eta^2}{C_{\text{spring}}} = \frac{\left(U_{\text{bias}} \cdot \frac{\partial C}{\partial x}\right)^2}{C_{\text{spring}}} \tag{2.38}$$

Coupling coefficient in mechanical equivalent:

$$k_{\text{spring}} = 2 \cdot E \cdot h_{\text{spring}} \cdot \left(\frac{w_{\text{spring}}}{\ell_{\text{spring}}}\right)^3 \tag{2.39}$$

whereas k_{spring} is the stiffness constant, U_{bias} is the applied DC voltage, $\partial C/\partial x$ is the differential change in the coupling capacitance per displacement, h_{spring}, w_{spring} and ℓ_{spring} are the height, the width and the length of the mechanical spring, respectively and C_{spring} is the value for the coupling capacitance in the equivalent circuit. E is a constant known as the Young's modulus and is taken as 150 GPa [35].

As seen in Equation (2.38) k_{spring} is inversely proportional to C_{spring}. The stiffness constant can therefore be taken as a coupling factor as shown by the analogy presented in the next section.

2.6 Linking Electrical and Mechanical Coupling Coefficients

We have established governing equations, which discuss the electrical coupling phenomena κ in the light of transfer function $|H^2(f)|$. On the other hand, we also know that the mechanical coupling spring coefficient k_{spring} is related with electrical equivalent and actual physical parameters, for instance the dimensions as reported in section 2.5. These two facts provide an intuition that we may formulate a direct link between the κ and k_{spring}. This will be another convenient step in understanding the necessary fact that whereas κ in electrical domain is a unit-less quantity, k_{spring} in mechanical domain is effectively represented as Newton/meter. Relevant equations are presented in the following:

As we already know the device-specific k_{spring} in Equation (2.38) we can elaborate

$$k_{\text{spring}} = \frac{\eta^2}{C_{\text{spring}}} = \frac{\eta^2}{\frac{1}{\omega R \kappa}}$$

$$\Rightarrow k_{\text{spring}} = \omega \eta^2 R \kappa$$

Though this direct relationship is not used in our evaluation purposes, it still serves to assert the point that κ is directly proportional to k_{spring}. The dependence on ω is also apparent, however it is not a concerning issue while considering the second order filters because the passband is relatively smaller than the center frequency.

2.7 Filter Design Summary

The treatment in this chapter mainly focuses on transfer functions and when the implementation is presented, it is comprised of electrical components rather than mechanical ones.

The reason for this is that the filter design approach suggested in this work focuses only on the electrical domain which makes it easier for the designer to use readily available electronic circuit simulators. The constituent resonators are designed mechanically. Let us summarize the filter design methodology with the

following tree diagram.

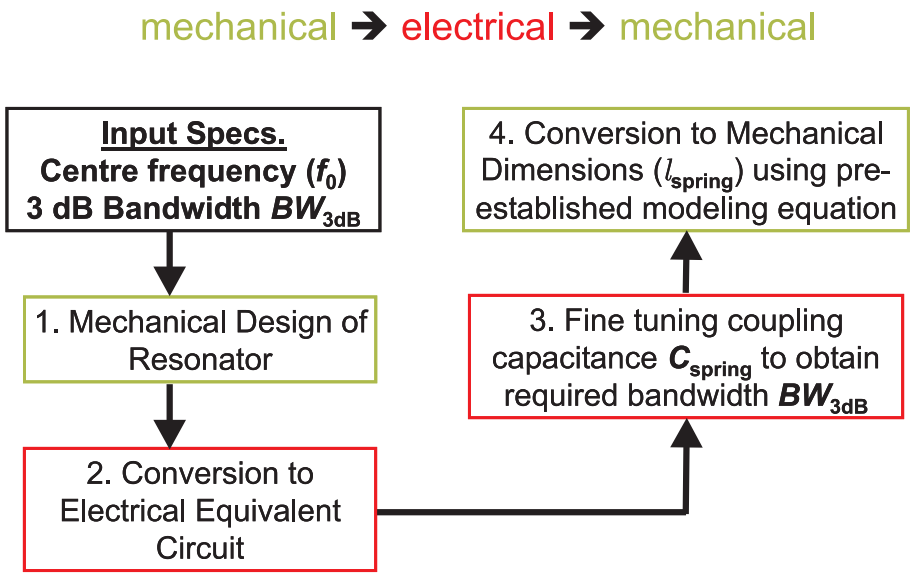

Figure 2.26: Suggested design flow of filter

The filter design will be carried out after:

1. Starting from given specifications of center frequency f_{m} and bandwidth requirements $BW_{3\mathrm{dB}}$ and designing a *mechanical* resonator, which satisfies the center frequency. Symmetric resonators will be coupled, therefore the designed resonators is chosen to have maximally flat passband or a Butterworth like response. The bandwidth requirement will be addressed in the electrical domain.

2. Establishing the working environment (atmospheric pressure/vacuum, applied DC/AC voltage levels, gap to substrate spacing, finger gaps (if applicable) etc...). These values will be used in converting the designed resonator into its electrical equivalent circuit which, for the sake of convenience, should be one of the known configurations as evaluated in this chapter.

3. Tuning the coupling spring to achieve the required filter bandwidth $BW_{3\mathrm{dB}}$. As an extra step, the Q can be calculated here. Furthermore, with the known value of C_{spring}, we can calculate the normalized coupling coefficient κ. This value of κ is matched with the mechanical coupling coefficient as given by

f_{m} [kHz]	κ	BW_{3dB} [Hz/%]	k_{spring} [N/m]	C_{spring} [fF]	ℓ_{spring} [μm]
719.115	1	75 / 0.0104	0.123	2.21	508
719.095	2.414	165.0 / 0.0229	0.296	0.92	379

Table 2.6: Summary of the simulation data

Equation (2.39) or whichever coupling coefficient equation is valid for a given device geometry. Hence knowing the value of κ, which satisfies all the specifications, physical dimensions of the coupling beam can be calculated.

4. By adjusting the process dependent parameters (for instance, in this study, width and height of coupling beam w_{spring}, h_{spring} respectively) mechanical realization of the coupling spring is possible and ultimately the design is transformed back to the mechanical domain.

2.8 Design Example

The base circuit used to verify the theory is the series RLC equivalent as shown in Figure 2.27. The circuit includes the equivalent representation of lossy effects and damping as R_{x}, which results from the mechanical operation of device.

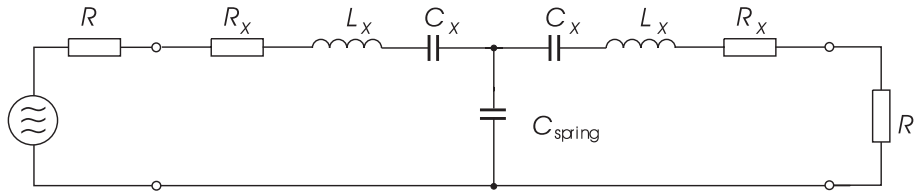

Figure 2.27: Series RLC equivalent of MEM filter after including the effects of damping

With a commercial tool simulations are performed to verify the design of mechanically coupled bandpass structures using the above method. The simulation results for two cases ($\kappa = 1$ and $\kappa = 2.414$) at about $f = 719.1$ kHz are presented in Figure 2.28, with Table 2.6 summarizing the simulation data.

For the two κ cases, reasonable coupling spring lengths ℓ_{spring} are obtained by

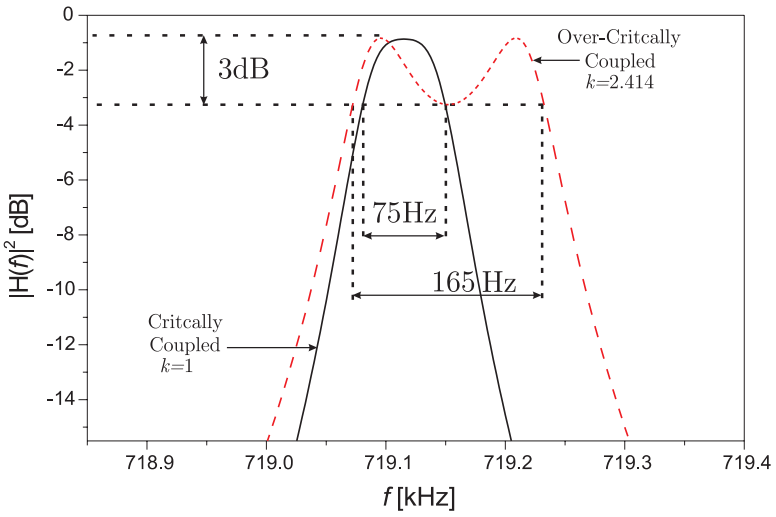

Figure 2.28: Simulation result for the critically and over-critically coupled filter at $f = 719$ kHz

$$\begin{aligned} \text{with} \quad R &= 100.0\ \text{M}\Omega \\ R_{\text{x}} &= 1\ \text{M}\Omega \\ L_{\text{x}} &= 300530\ \text{H} \\ C_{\text{x}} &= 1.63{\cdot}10^{-19}\ \text{F} \end{aligned}$$

Table 2.7: Parameter Values used in calculations

using the method established in Section 2.5. The percentage bandwidth is defined as $BW_{3\text{dB}}/f_{\text{m}} \cdot 100\%$.

As the coupling spring design does not include the effects of series resistance, a simplified value of R_{x} is used for better insertion loss figures. However, upon simulating the filter with real values of R_{x}, the results are consistent with theory and the critically and over-critically coupled cases hold, though the coupling coefficient needs to be tuned due to changing Q values and may not remain bounded by (2.23). Bandwidth can be increased by sacrificing the quality factor Q.

The effects of insertion loss IL and series R_{x} are discussed in [37] where a filter operating at 840kHz with a bandwidth ranging from 0.02% to 0.08% is demonstrated. It is possible that while including the effects of R_{x}, the bandwidth may increase owing to the reduced Q. The coupling in that case can be fine tuned to obtain the desired response without much effort.

2.9 Conclusion

We have presented a concise representation of mechanical filter design using a hybrid mechanical/electrical domain formulations. Using network theory, the mechanical filters, which can be represented both as series or parallel LC tanks circuits. Complete equations are determined to represent the power transfer function for both cases, which are ultimately used for finding closed form relationships for bandwidth in terms of normalized coupling coefficient κ or coupling capacitance C_{spring}. The coupling coefficient is shown to be limited between a certain range, which provides two different responses in the filters, namely maximally flat passband response and equi-ripple passband response. Then κ as well as C_{spring} from electrical design is linked with mechanical coupling coefficient k_{spring}. After the linking procedure, the filter design is couped up in a summary and a complete design example is presented.

It is probably necessary to mention at this conjuncture that the filter design considered in the sections above can be looked upon as exhibiting Butterworth and Chebyshev like filter behaviors.

This study opens a new window of research by first introducing a filter design theory, which is independent of operating frequency and device geometry and then by designing a second order filter. A possible direction would be to extend this concept to higher number of coupled resonators and hence an increased filter order, which is necessary for faster pole roll off. Another concern would be to address the issue of κ and the assumption of it being a constant within the passband. As the filter order increases, this assumption may not necessarily hold true, so some linear approximations should be required to fine adjust the κ value against increasing filter order.

Chapter 3

Device Preparation

The fabrication process for the laterally driven micromachined filters utilizes surface micromachining technology. This chapter highlights the step-by-step fabrication sequence and explains the experiments and discussion regarding thin film deposition and lithography.

3.1 Fabrication Sequence

The fabrication sequence is as follows:

1. Substrate cleaning
2. Deposition of conducting Al layer (500 nm - 1 μm) as ground layer
3. Deposition of Oxide (insulation layer) of thickness 500 nm
4. Spinning photoresist on the device
5. Patterning layer GROUND_DK (dark)
6. Etching 1μm for substrate contact
7. Deposition of metal (Al) of thickness 3μm
8. Spinning photoresist on the device
9. Patterning according to layer GROUND_CL (clear)
10. Etching 1μm of metal for conformal coating
11. Spinning photoresist on the device

12. Patterning according to layer WIRING_CL
13. Etching 1μm of metal for input/output and ground pads
14. Deposition of Polysilicon 1μm
15. Spinning photoresist on the device
16. Patterning according to layer DCPLATE_CL
17. Deposition of PSG 2μm
18. Spinning photoresist on the device
19. Patterning layer ANCHOR_DK
20. Etching PSG 2μm for opening anchor points for shuttle and input/output fingers
21. Spinning photoresist on device
22. Patterning layer DIMPLES_DK
23. Etching PSG 1μm for opening dimples for the shuttle mass
24. Deposition of Polysilicon 4μm
25. Spinning photoresist on the device
26. Patterning according to layer ANCHOR_CL
27. Etching Polysilicon 2μm for conformal layer formation
28. Spinning photoresist on the device
29. Patterning according to layer LEVITATION_CL
30. Release of PSG

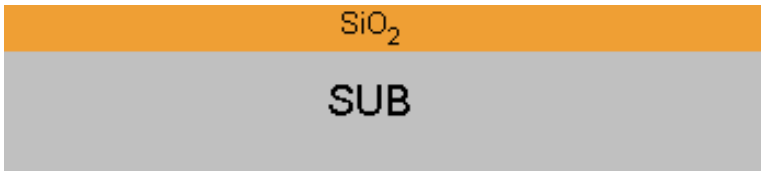

Figure 3.1: Substrate with deposited SiO_2 (step 3)

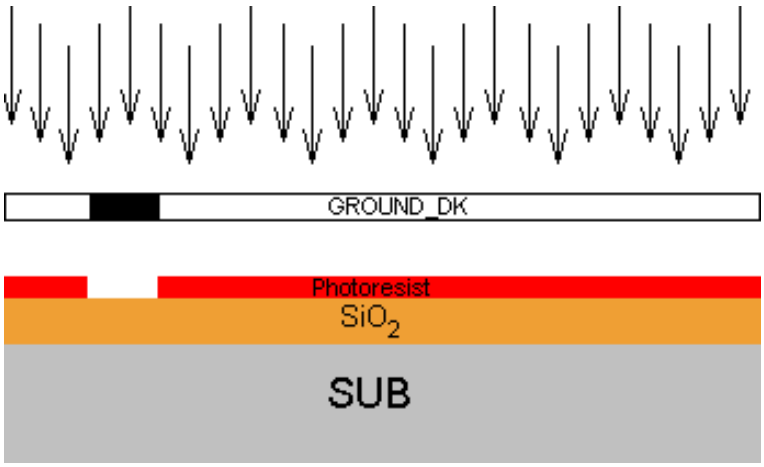

Figure 3.2: Photoresist applied and patterned with Ground mask. (Steps 4, 5)

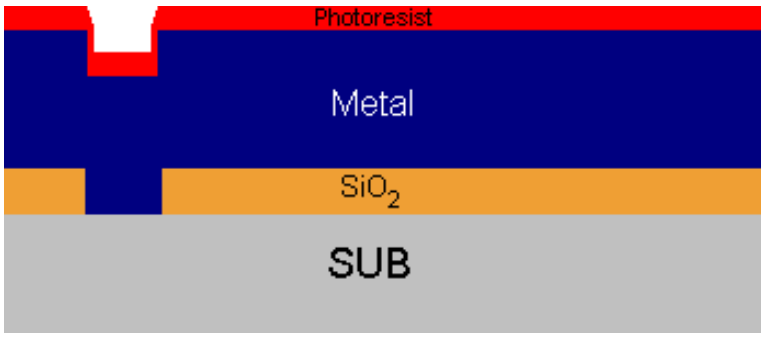

Figure 3.3: Oxide layer etched (1 μm), metal deposited (2 μm) and PR spun (Steps 6 - 8)

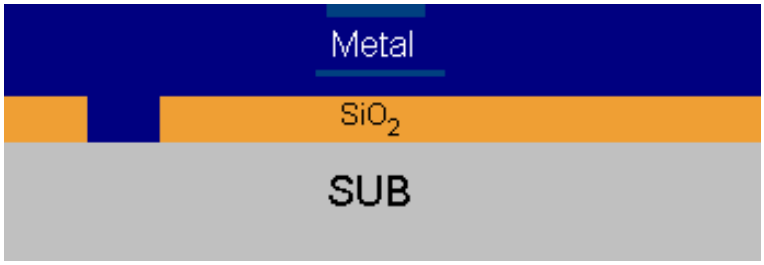

Figure 3.4: Photoresist patterned and etched (1 μm) for conformal metal layer (Steps 9, 10)

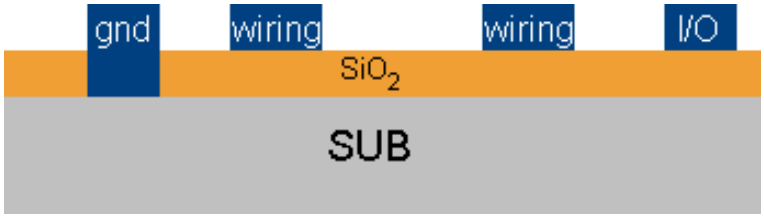

Figure 3.5: Metal etched (1 μm) for routing after PR patterned using wiring mask (Steps 11 - 13)

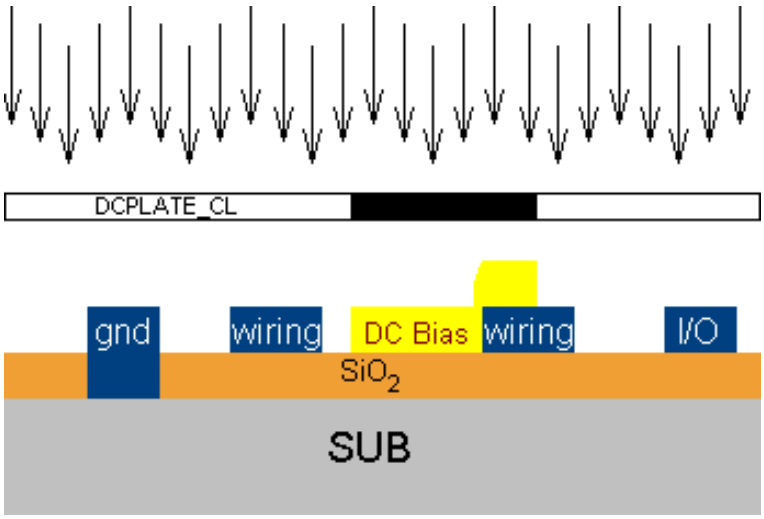

Figure 3.6: Polysilicon deposited (1 μm), patterned and etched to form DC bias plate for the resonator (Steps 14 - 16)

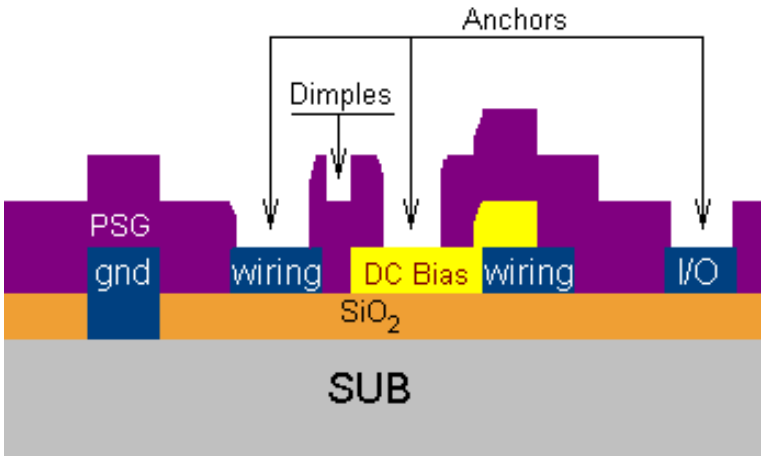

Figure 3.7: PSG deposited (2 μm), patterned and etched to form anchor points and dimples using ANCHOR_ETCH and DIMPLES_ETCH masks (Steps 17 - 23)

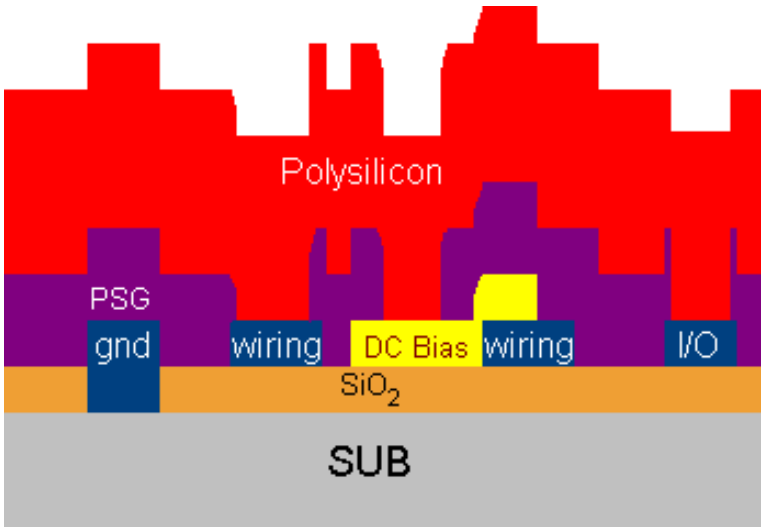

Figure 3.8: Polysilicon is deposited (4 μm), patterned and etched to form a uniform layer using mask ANCHORS_CONFORMAL (Steps 23 - 27)

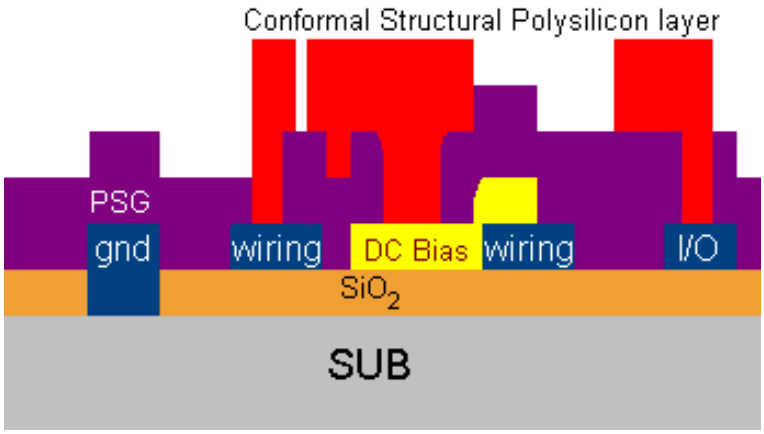

Figure 3.9: PR deposited and patterned for LEVITATION_ETCH layer resulting in levitated structure after Polysilicon etch (Steps 28 - 29)

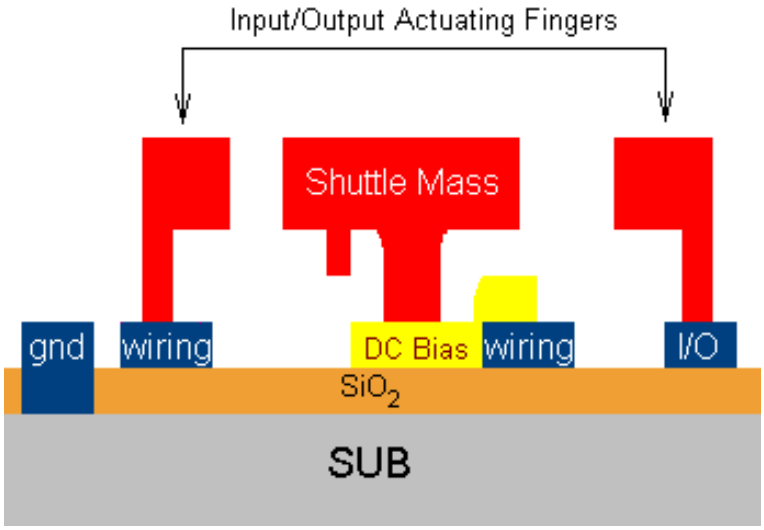

Figure 3.10: Final structure after PSG removal, structure elaborated to incorporate various features (Step 30), figure not scaled

The substrate shown in fabrication illustrations is considered to be conductive and the Al conducting layer is not shown. Furthermore, if conformal deposition can be achieved with thin–film sputtering, then there is no need to use GND_CONFORMAL and ANCHORS_CONFORMAL masks as shown in Table 3.2, hence reducing the processing masks number to 6.

The mask is divided into 4 sets namely:

mask 15:- This set contains 15 devices with varying geometry and shapes according to frequency and levitation considerations. The particulars of these 15 devices are summarized in Table 3.1.

mask 5:-

Components are the same as mask_15. Modifications are decrease in number of elements in each row to one and increase in metal routing spacing to eliminate the parasitic capacitance effect. The devices preserved from mask_15 are numbered 4,14,2,8,11in Table 3.1.

455kHz:-

This set contains five resonators with varying design parameters (finger overlap area, no. of fingers, reduced shuttle mass) all designed for 455kHz to address the needs of another project which aims to use resonators as voltage controlled oscillators.

3filter_2port:-

There are three filters operating at 300kHz, 455kHz and 455kHz respectively. They are different than previous devices since these filters are composed of three resonators unlike previously drawn two resonator filters. An attempt is made to include increased order filters and to study the effects of varying internal and external coupling beams in the shuttle mass. A different coupling phenomenon is present in these 455kHz resonators.

	k_{sys}	$C_{\text{comb}}(pF)$	f_{res}(kHz)	Q	$R_{\text{x}}(M\Omega)$	L_{x}(H)	C_{x} (fF)	w/l	N	Notes
1	600	5.31	614.63	1793	141.11	65,517.7	1.02	3/30	30	
2	600	3.54	717.44	2508	194.46	108,193	4.55	3/30	20	
3	600	3.54	717.44	2508	194.46	108,193	4.55	3/30	20	Avoiding Levitation
4	75	5.31	212.23	772	118.66	68,687.6	8.19	3/60	30	
5	9.38	7.08	69.60	308	254.88	179,303	29.1	3/120	20	L = 40 μm, x = 10 μm
6	9.38	3.54	83.75	308	136.72	124,066	29.1	3/120	20	L = 20 μm, x = 5 μm
7	-	2.48	2,324.4	8225	298.82	168,317	2.78	3/15	14	High Frequency
Filter										
	l_{spring}	C_{comb} = 3.54 pF C_{couple} (pF)	f_{res} (kHz)	Q	$R_{\text{x}}(M\Omega)$	L_{x}(H)	C_{x} (fF)	w/l	N	Notes
8	456	1.64	840.27	357.3	116.54	78,875	0.455	3/30	20	L=20, x=5
9	380	0.951	289.18	151.8	996.36	83,245	3.63	3/60	20	L=20, x=5
10	240	0.238	289.18	151.8	996.36	83,245	3.63	3/60	20	$U_m/U_{max} = 0.707$
11	344	0.704	840.27	357.3	116.54	78,875	0.455	3/30	20	$U_m/U_{max} = 0.707$
12	408	2.28	289.18	151.8	996.36	83,245	3.63	3/60	20	Structural Modifications
13	334	2.84	840.27	357.3	116.54	78,875	0.455	3/30	20	L=20, x=5
14	262	0.299	2,324.2	8225	298.82	168,317	2.78	3/15	14	High Frequency
15	196	0.124	2,324.2	8225	298.82	168,317	2.78	3/15	14	$U_m/U_{max} = 0.707$

Table 3.1: Table listing electrical/mechanical parameters

#	Mask Layer Title	File Name	Kanaga Layer	CD(μ m)	Color
1	GND_ETCH	ground_dk	Hole0	0.5	
2	GND_CONFORMAL	ground_cl	Hole0	0.5	
3	WIRING_ETCH	wiring_cl	Metal	0.5	Blue
4	DCPLATE_ETCH	dcplate_cl	Poly0	0.5	Orange
5	ANCHORS_ETCH	anchors_dk	Anchor1	0.5	Green
6	DIMPLES_ETCH	dimples_dk	Dimple	0.5	Yellow
7	ANCHORS_CONFORMAL	anchors_cl	Poly1	0.5	Red
8	LEVITATION_ETCH	levitation_cl	Anchor1	0.5	Green

Table 3.2: Drawn mask data using Kanaga

The fabrication process involves eight masks, which were drawn with Kanaga MEMS library [39] layer definitions. The purpose was twice fold – first, to obtain accurate micrometer scale masks to be produced and worked upon; and second, to have a layout ready for submission to the foundry, if needed. The mask names, order and, color specifications used in the layout are summarized in Table 3.2.

The masks were drawn on a 0.25 μm grid which caused a problem while merging the layers and separating them at the manufacturer's end, due to their usage of larger grid size (0.50 μm), however the mistake was fixed by aligning the complete mask layout onto the 0.50 μm grid lines before ungrouping and separating the layers.

Figures of individual masks and their array arrangements including the complete mask layout are shown in the appendix C.

The processing after obtaining the masks consists of wafer cleaning and wet etching, wafer exposure, and thin–film deposition.

3.2 Wafer Cleaning

The wafer cleaning is done with 50% HF solution to remove any local oxides from the surface followed by Acetone/Isopropanol and DI water cleaning. The wafer is placed in Acetone and kept under ultrasonic clean for five minutes. Placing the wafer in warm Acetone kept at 55^0C for 10 minutes is another approach [40] followed by transfer to Methanol for 5 minutes followed by DI water rinse. Though the ultra

Figure 3.11: Wetbench for wafer cleaning and wet etching

sonic cleaning releases the dirt particles from the wafer, as the wafer is placed upright, they still remain on the surface while taking the wafer out. A solution to that was to keep the wafer inverted inside a beaker at an angle of 45^0C which ensured all the dirt particles drop down and settle at the bottom. Special care should be taken to not hold the beaker in hands while inside the ultrasonic cleaner. The isopropanol cleaning is carried out by placing the wafer over the contact heater at 115^0C degrees until isopropanol boils. If exploding bubbles are unsettling and disturbing, they can be avoided by placing metallic tweezers in the beaker. From isopropanol the wafer is transferred to DI water while wet. Proper rinsing of wafer with DI water for 2 minutes leaves no marks of isopropanol on the wafer. Afterwards the wafer is dried with nitrogen gun. A strong nitrogen pressure may leave drying marks or water bubbles to appear on the wafer, which must be avoided, also the gun must always be activated from the centre of the wafer [41].

3.3 Lithography

The lithography tool used in this study is Karl Suss MJ653, which is a contact print mask aligner. The exposure energy is fixed at 5.6 mW/cm^2. The masks are designed for +ve tone photoresist. Shipley's S1813 photoresist is used along with

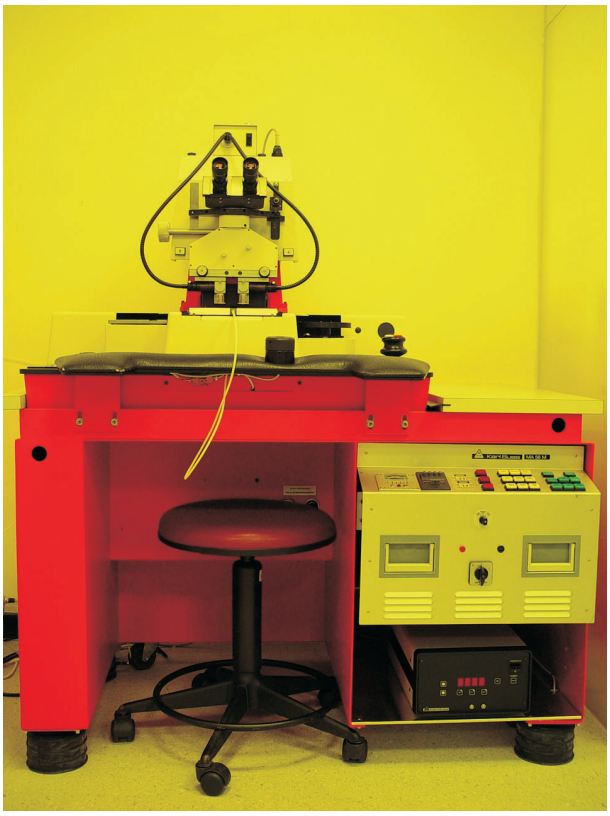

Figure 3.12: Contact print *i*–line lithography system

Shipley's developer. S1813 is low density photoresist, which can achieve 1.8 μm uniform thickness when spun at 4000rpm [42]. While trying to obtain a uniform layer of photoresist on a 5 inch wafer some variations from the recommended rules had to be made. For instance we had to employ an initial spread out time delay for the photoresist of around 30 seconds at 500 rpm before moving to 4000 rpm. The complete spin profile and soft/hardbake sequence is summarized in Figure 3.13.

The soft/hard bake times are different for furnace and contact heater. As depicted in figure 3.13, the soft bake is performed at 90^0C for a duration of 10 minutes in the furnace and 1 minute on the contact heater [43]. Similarly for the hard bake, the wafer is kept at 115^0C in the furnace for typically 20-30 minutes and for 1 minute on the contact heater [45]. The wafer is exposed for 1 minute.

Different spin profiles were tested in order to obtain smaller feature size. Since we have not used HMDS, hexamethyldisilazane adhesion promoter, we were required to cover the wafer completely with photoresist, which was leaving a thick trail on the wafer when spun at 4000rpm. Hence varying ramp (500, 1000)rpm and spin (4000,

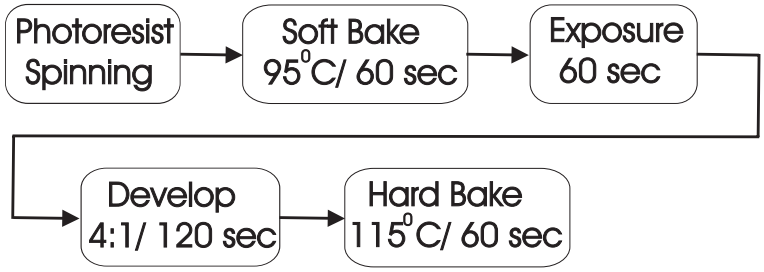

Figure 3.13: Spin Profile and soft/hard bake specs. and spinning flow

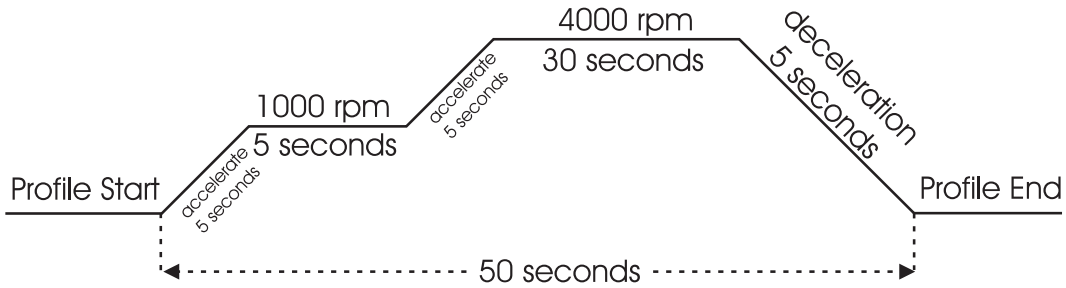

Figure 3.14: Spin profile with spin speeds and ramp times

6000, 10000)rpm speeds were tested. The spin profile is shown in Figure 3.14. The feature sizes obtained after development are shown in Figure 3.15 and Figure 3.16. From the features obtained we can clearly see that the 5 μm features are not sharp as the corners are rounded and hence, require more refinement.

The exposure time is obtained by multiplying the exposure energy with photoresist thickness. Photoresist thickness is obtained from experimentally found data relating photoresist spin speed to photoresist thickness. The most optimized result corresponding to our spin profile is an exposure time of 60 seconds. The developer is diluted 3:1 with DI water (3 parts developer and 1 part DI water). The features appear within two minutes of dipping the exposed wafer in the developer.

The curved rectangles obtained for 5μm dimensions might have resulted due to over–exposure and can be lowered to as small as 1μm with further experimentation.

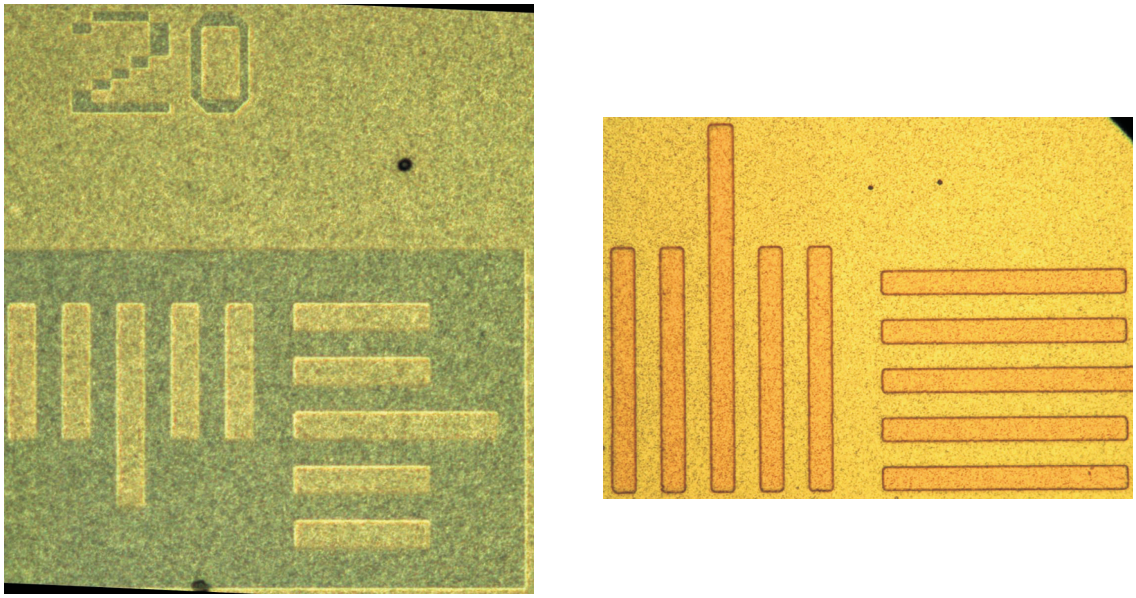

a b

Figure 3.15: Lithography results for (a) 20 μm and (b) 10 μm features

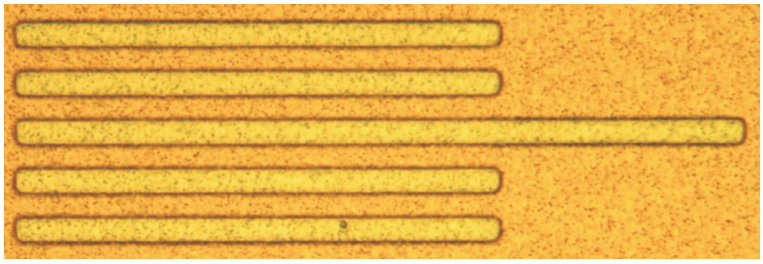

Figure 3.16: Lithography results for 5 μm features

3.4 Deposition

A sputter system is used to deposit thin–films on the device. As the wafer is not conductive with a resistance as high as 500kΩ a thin conductive layer was needed to act as the ground layer.

Initially, work was started with Aluminium and conductive thin films were grown on the wafer. However, aluminium is highly susceptible to oxidation. Hence, when next layer of SiO_2 was reactively grown on the substrate at 300^0C, it resulted in forming an intermediate aluminium oxide layer before continuing with the required SiO_2 layer. The deposition parameters for Aluminium and other materials are pre-

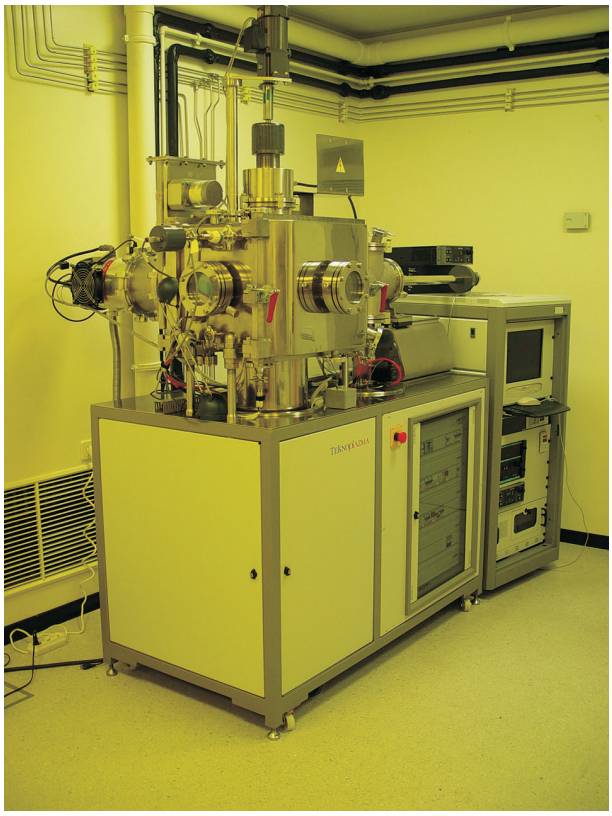

Figure 3.17: DC/RF magnetron sputter system for thin–film deposition

sented in Table 3.4.

A cross–section of the deposited materials was observed to have a fine amorphous layer of different ceramics including the wafer, aluminium, aluminium oxide and finally silicon oxide as shown in Figure 3.18. Hence, the idea of using Al as ground conductor had to be abondened because at the cross–section, starting from Si wafer and Al layer, an Al_2O_3 layer and varying stiometric ratioed SiO_2 layers due to less oxygen present caused by its consumption with Al during earlier stages of reaction [44] were formed, which finally converged to SiO_2. A multiple layer etchant for varying stiometric ratioed SiO_2 layers was not utilized and even if the SiO_2 is etched, it still exposed Al_2O_3 instead of the conductor and hence, required further processing.

Parameters	**Aluminium**	**Palladium**	**Silicon dioxide**
Coating Type	Metallic	Metallic	Semi–Ceramic
Magnetron Used	DC	DC	RF
Oxygen (sccm)	0	0	7
Argon (sccm)	35	20	35
Argon Pressure (mbar)	0.003	0.009	0.002
Substrate Temperature (^{0}C)	50	55	350
Heating Period (min)	3	3	5
Density of Metal (gr/cm^3)	2.700	12.038	2.319
RF Mode	1	1	1
RF Bias (V)	50	50	50
DC Power (W)	150	50	250
RF Power (W)	30	10	35
Sputter Duration (min)	180	180	120
Required Thickness (nm)	500	1000	1000

Table 3.3: Sputtering parameters for materials used in fabrication

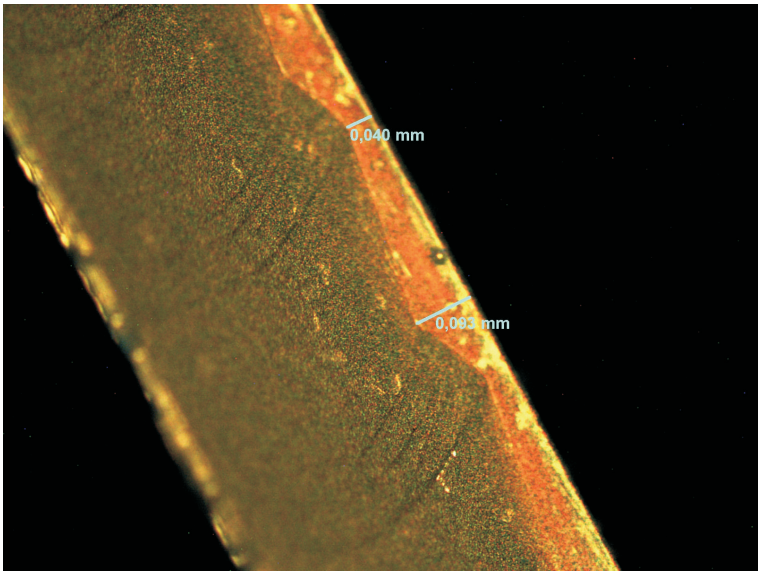

Figure 3.18: Cross section displaying the merged Al-Al_2O_3-SiO_2 layers

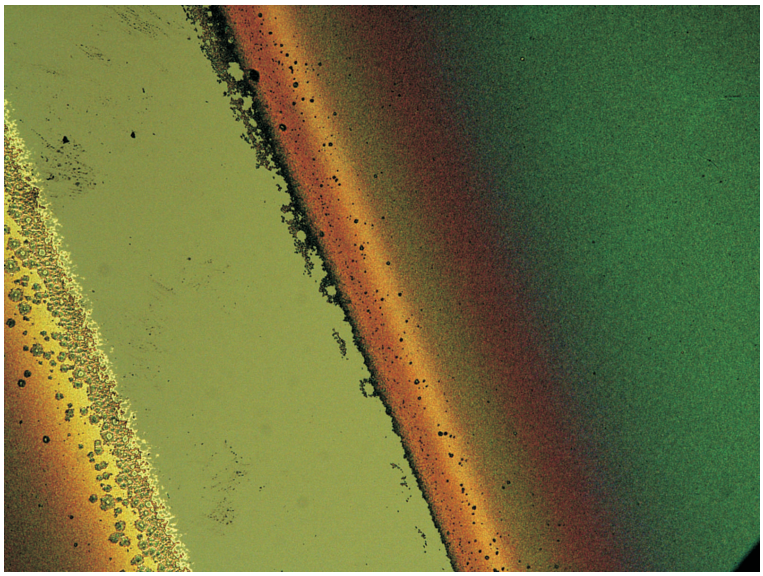

Figure 3.19: Top view of Si-Al-Al_2O_3-SiO_2 layers

Chapter 4

Conclusions and Future Work

We have presented a concise representation of mechanical filter design using a hybrid mechanical–electrical–mechanical domain formulations. The mechanical filters are represented as electrical equivalent models which are used for designing filters according to the center frequency and bandpass specifications. Design equations have been modeled and filter design is summarized in the form of power transfer function for both series and parallel RLC equivalent circuits. Closed form relationships are evaluated to model the passband behavior in terms of Butterworth and Chebyshev filters. The electrical design methodology is linked with mechanical device dimensions hence completing the mechanical filter design. A complete design example is presented to support the theory.

This work concentrates on second order filters operating at 455kHz which is the threshold of IF. The primary concern is to increase the operating frequency of the resonators to make them more suitable for the targeted applications. Present day devices have been shown to operate at 733MHz, however, the center frequency has to increase to 1-2 GHz for the desired performance. This is why, the thesis addresses the filter design issue from a frequency independent perspective by using electrical equivalent models of the resonators.

As the frequency extension necessitates various mechanical device geometries and principles of operation, the readout and signal processing aspect also becomes important. The example worked upon in this thesis uses capacitive readout circuitry, however as other resonator prototypes are developed, different readout mechanisms are becoming important, in particular the piezo-electric and piezo-resistive configurations.

The prototypes of today are potential practical devices of tomorrow. Considering real life operating conditions, stability becomes an imminent issue. The devices should be prone to environmental factors, aging and noise. There are many factors which may distort the resonator performance. In particular, as the resonators are operated in vacuum sealed cavities for better Q, the complete device should be very well immune to jerk or any sudden physical movement, which might fracture the vacuum cavity. Furthermore, the resonators must not self resonate due to environment factors, for instance sound and acoustic vibrations. Moreover, present day applications use the mechanical movement of the device as the actuation method, which reflects upon the aging factor and causes restrictions on the lifetime of the product. Hence, it is better to switch to device geometries, which do not require many moving parts and piezoresistive option becomes more attractive.

Material science is opening new doors of possibilities and a wide variety of materials to choose from while designing the resonators. So far, Si/Poly–Si materials have been employed in developing micromechanical resonators. However, now the focus is shifting to piezo-electric materials. Instead of using the bending and deforming properties, the expansion/contraction or the piezo–electric properties are being employed for designing resonators.

Some fabricatable doped plastics could serve as another alternative and building material for the resonators. In particular, Poly–urethane has already been shown to display impressive stretching properties, and very controlled thickness can be fabricated using electro–spinning [46]. This could serve as new motivation for designing nanoscale resonators and filters. Presently, however, the results of achieving required doping to obtain conductive properties and its consequences on the deforming of polyurethane are unknown.

A follow up of this work, as reported before, will be to extend the filter design and control theory beyond second order filters. Furthermore, the nonlinearity effects, for instance the electrical coupling coefficient κ, assumed to be constant in the passband, can be studied and adjusted for higher frequencies. Similarly the source/load impedances influence the center frequency nonlinearly at GHz frequency range, which can be modeled and studied. Noise analysis is yet another factor which can be used in bringing the design process closer to successful application when the

devices are realized.

In short, the thesis fills a gap in the design of second order micromechanical bandpass filters and provides a more controllable design strategy for obtaining desired passband characteristics.

Appendix A

Matlab Codes

A.1 Main Code for Interfacing and Taking Inputs

```
% Author: Mansoor Naseer, 6050
% The code will take input values for dimensions and
% voltage values and will produce respective results
% for displacement capacitance, resonating
% frequency, Quality factor and spring constant,
% effective electrical model
% values will also be produced

% function s
% Initialize
clear;
close all;

%Defining Constants here:

E = 170e9;
% Young's Modulus as reported by MUMPS rule book rev. 7
u = 17.46e-6;  % Absolute Viscosity of air (Ns/m^2)
d = 4e-6;       % Folded beam to substrate gap - 2u + 1u + 1u (m)
p = 2.23e-15;  % Density of polysilicon (kg/um^3)
h = 2e-6;       % Overall structural thickness (m)
e = 8.85e-12;  % Permitivity of free air (F/m)
s = 1.1;          % Correction factor for fringing effects

% Assuming constant Truss dimensions
w_truss = 4e-6;     % Width of truss (m)
l_truss = 62e-6;    % Length of truss (m)

% Supporting Beam
w_beam = 2e-6; % Width of supporting beam (um)
% Minimum feature size allowed
l_beam = 30e-6;
% Length of supporting beam (um) An initial value
```

```
% Actuating fingers data
% Number of fingers
N = 30;
% Finger length (m)
L = 40e-6;
% Gap from front (m)
x = 10e-6;
% Gap between fingers (m)
g = 2e-6;
w_finger = g;
n = 2*N; % Total # of gaps

% order = 0 for resonator, 1 for filter specifications.
order = input ('Enter "0" for resonator specifications, ...
"1" for filter: ');

% Electrostatic settings
V = 15;%input ('Input Voltage: '); % Voltage at input (V)


% Calculations ...
% 1. System Spring Constant ksys
ksys = 2*E*h*(w_beam/l_beam)^3;

% 2. Displacement ... y = (n*e*h*V^2)/(ksys*g)
y = (n*e*h*V^2)/(ksys*g);

% 3. Capacitance Comb
Ccomb = n*e*h*(L-x)/g;
CperX = n*e*h*s/g;

% 4. Truss Mass Mt (density x volume) kg
Mt = 2*h*w_truss*l_truss*p*1e18;

% 5. Supporting Beam Mass (density x volume) kg
Mb = 8*h*w_beam*l_beam*p*1e18;
M = Mt + Mb;

% 6. Shuttle Mass (fingers mass + other mass) =
%N x L x h x w_finger & Shuttle Area for both resonator and filter.
[Mp,Ap] = shuttle_mass(N, L, x, g, order);

% 7. Resonating Frequency
fr = 1/(2*pi)*sqrt(ksys/(Mp+0.3714*M));

% 8. Quality Factor
Q = d/(u*Ap)*sqrt (M*ksys);
```

```
% to calculate the electrical equivalent depending
% on whether resonator or filter was chosen
[Rx, Lx, Cx, C_spring] =
electrical_eq(V,CperX, ksys, M, Mp, Q, order);

% Printing the result
fprintf('\n ksys = %1g',ksys),fprintf('\n Displacement = %1g',y), ...
fprintf('\n Comb Capacitance=%1g',Ccomb),fprintf(...
'\n fr=%1g',fr), fprintf('\n Q=%1g',Q );

fprintf('\n Rx = %1g',Rx),fprintf('\n Lx = %1g',Lx), fprintf(...
     '\n Cx = %1g',Cx),fprintf('\n Coi= %1g',Ccomb), fprintf(...
'\n Coo= %1g',Ccomb );

fprintf('\n Coupling Capcitance = %1g',C_spring);

% Recursive solutions
fprintf('\n \n Above values were just initial conditions, ...
choose for recursive soln.: ');
fprintf('\n 1. No. of fingers  (N).');
fprintf('\n 2. Dimension ratio  (w/l). ');
fprintf('\n 3. Range of motion (x).');
fprintf('\n 4. Exit.');

selection = input('\n Choice:'); % reading choice

if selection == 1 % only setting up the variables, work
%on them starts later
    min_fingers = input('Enter Min. number "N" of fingers: ');
    max_fingers = input('Enter Max. number "N" of fingers: ');
    selection1
elseif selection == 2
        min_wVSl = input('Enter Min. "w/l"...
ratio of supporting beams: ');
        max_wVSl = input('Enter Max. "w/l" ...
ratio of supporting beams: ');
        step_width = input('Enter number of steps: ');
        [ksys_var, fr_var, Q_var, M] = selection2 ...
        (min_wVSl, max_wVSl, step_width, E, h, Mp, Mt, u, Ap, d, p);
        fprintf('\n \t\t\t\t initial'), fprintf('\t\t final');
        fprintf('\n ksys |'), fprintf('\t\t\t %1g', ...
ksys_var(1)), fprintf('\t\t %1g',  ...
ksys_var(length(ksys_var)));
        fprintf('\n fr   |'), fprintf('\t\t\t %1g', ...
fr_var(1)), fprintf('\t\t %1g',  ...
fr_var(length(ksys_var)));
        fprintf('\n Q    |'), fprintf('\t\t\t %1g', ...
Q_var(1)), fprintf('\t\t %1g',  ...
```

```
Q_var(length(ksys_var)));
    elseif selection == 3
            min_disp = input('Enter Min. displacement of ...
resonator "y" (um): ')*1e-6;
            max_disp = input('Enter Max. displacement of ...
resonator "y" (um): ')*1e-6;
            [v_var] = selection3 (min_disp, max_disp, n, ...
e, h, ksys, g);
            fprintf('\n \t\t\t\t initial'), fprintf('\t\t final');
            fprintf('\n V |'), fprintf('\t\t\t %1g', v_var(1)), ...
fprintf('\t\t %1g',  v_var(length(v_var)));
        elseif selection == 4
            fprintf('\n Exiting... Check the variables ...
from workspace');
        else fprintf ('\n Input between 1-4');

    end;
```

A.2 Selction1: Comb Capacitance versus No. of Fingers

```
%function selection1 (min_fingers, max_fingers)
  diff = max_fingers - min_fingers;
    % for selection 1 the only chart available is for
    % capacitance versus number of fingers
    for i = min_fingers:max_fingers,
        Ccomb1(i-min_fingers+1) = 2*i*e*h*(L-x)/g;
    end
  plot (linspace(min_fingers, max_fingers, (diff+1)), Ccomb1);
  grid on; xlabel ('N (number of fingers)');
  ylabel ('Initial Capacitance (F)');
  %end
```

A.3 Selction2: Q, f_{r} and k_{sys} versus Aspect Ratio (w/l)

```
% Selection 2,
% Author Mansoor Naseer, 6050.
% A code for plotting System Spring constant
% and frequency by changing the W/L ratio

function [ksys_var, fr_var, Q_var, M] = choice2
(min_wVSl, max_wVSl, step_width, E, h, Mp, Mt, u, Ap, d, p)

k = 1;
x = min_wVSl;

while x <= max_wVSl,
```

```
    %Calculating total mass for individual cases

    Mb = 8*h*2e-6*1e-6*p/x*1e18;
% this takes into account the fact that w will always be 2um
    M = Mt + Mb;

    % 1. System Spring Constant ksys
    ksys_var(k) = 2*E*h*x^3;

    % 2. Resonating Frequency
    fr_var(k) = 1/(2*pi)*sqrt(ksys_var(k)/(Mp+0.3714*M));

     % 3. Quality Factor
    Q_var(k) = d/(u*Ap)*sqrt (M*ksys_var(k));

    k = k + 1;
    x = x + step_width;
    y(k-1)=x;
    end
fprintf('selection2 called')

subplot (3,1,1), plot (y, ksys_var, '-');
grid on; xlabel('w/l'); ylabel('Ksys');

subplot (3,1,2), plot (y, Q_var, '-');
grid on; xlabel('w/l'); ylabel('Quality factor');

subplot (3,1,3), plot (y, fr_var, '-');
grid on; xlabel('w/l'); ylabel('Resonance Frequency (Hz)');

%end
```

A.4 Displacement Tolerance

```
% Author: Mansoor Naseer, 6050
% Takes in steps of maximum and minimum
% displacements and computes voltage range
%  possible to achieve the motion, increment is
% 0.1u and hence linear

function [V_var] = choice3 (min_disp, max_disp, n, e, h, ksys, g)

i = min_disp;
k = 1;

while i <= max_disp,
    V_var (k) = sqrt (i*ksys*g/(n*e*h));
    i = i+1e-06;
```

```
    x(k) = (min_disp/1e-06 + k -1);
    k = k +1;
end

figure;
plot (x,V_var);
grid on; xlabel('Displacement (um)');
ylabel('Applied Voltage (V)');
```

A.5 Electrical Equivalent Circuit of a Filter/Resonator

```
% Author: Mansoor Naseer, 6050
% Electrical Equivalent of the previously calculated
% values are shown here.

function [Rx, Lx, Cx, C_spring] = ...
eq(V, CperX, ksys, M, Mp, Q, order);

eita = V*CperX;
Rx = sqrt(ksys*(Mp + 0.3714*M))/(Q*eita^2);
Lx = (Mp + 0.3714*M)/eita^2;
Cx = eita^2/ksys;

if order == 0
    C_spring = 0;
else
    w_spring = 2e-6;
    k_spring = 0.707*1.41/Q;
    l_spring = (170e9*w_spring^3/k_spring*2e-6)^(1/3);
    C_spring = eita^2/k_spring;

end
```

A.6 Device Area and Shuttle Mass versus No. of Fingers

```
% Author: Mansoor Naseer, 6050
% This code determines the shuttle mass of resonator(s).
% The input is number of finger (N), optimized for making
% dC/dx maximum. Another input is order of filter which
% will be taken to be either 0 (resonator) or more than
% one (resonator).

function [Mp,Ap] = shuttle_mass (N, L, x, g, order)

% will try to evaluate total area of shuttle depending on number and
%dimensions of fingers.
```

```
    fingers = N*L*g; % Fingers
    fingers_support = 6e-6*((N-1)*(2*g + g) + N*g + 6e-6);
% here each finger gives 2xfinger gap (g) and
% 1xfinger_width (=g here) + 3um offset from edges

    support_block = 15e-6*60e-6 + 10e-6*20e-6;
% fixed, and no holes will be etched here

    % here area found is converted into volume
    Ap_resonator = fingers + fingers_support + support_block;
    Mp_resonator = ((fingers + fingers_support + support_block)...
 * 2e-6) * 2.23e3;
% We are only calculating shuttle mass for resonator
% with fingers both at input and output
    Ap_filter = support_block + (fingers_support/6e-6 ...
+ 10e-6)*15e-6;
    Mp_filter = ((support_block + (fingers_support/6e-6 ...
+ 10e-6)*15e-6)* 2e-6) * 2.23e3;

if order == 0
    Mp = 2*Mp_resonator;
    Ap = 2*Ap_resonator;
else
    Mp = Mp_resonator + Mp_filter;
    Ap = Ap_resonator + Ap_filter;
end
```

A.7 Series RLC $|H(f)|^2$ wrt ν

```
% Author: Mansoor Naseer
% The code plots transfer function of a series RLC
% circuit with respect to normalized frequency

clear;
R  = 50;
L  = 40e-6;
C  = 80e-9;
QE = 1/R*sqrt(L/C);
wres = 1/sqrt(L*C);
kappa = 0.6;

for i = 1 : 2000
    f(i) = i*300;
    w(i) = 2*pi*f(i);
    nu(i) = w(i)/wres - wres/w(i);
    tf(i) = 1/(1 + (1/(2*kappa) + nu(i)*QE + ...
1/(2*kappa)*(nu(i)*QE)^2)^2);
    tf_db(i)= 20*log(tf(i));
```

```
end
z(:,1) = nu';
z(:,2) = tf_db';
save z_series.dat z -ascii;
```

A.8 Parallel RLC $|H(f)|^2$ wrt neu ν

```
% Author: Mansoor Naseer
% The code plots transfer function of a parallel RLC
% circuit with respect to normalized frequency
clear;
R  = 50;
L  = 40e-6;
C  = 80e-9;
QE = 1/R*sqrt(L/C);
wres = 1/sqrt(L*C);
kappa = 2.5;

for i = 1 : 2000
    f(i) = i*300;
    w(i) = 2*pi*f(i);
    nu(i) = (w(i)/wres) - (wres/w(i));
    tf(i) = 1/(1 + (1/(2*kappa) + nu(i)/QE + ...
 1/(2*kappa)*(nu(i)/QE)^2)^2);
    tf_db(i)= 20* log(tf(i));
end

z(:,1) = nu';
z(:,2) = tf_db';
save z_parallel.dat z -ascii;
```

A.9 All Transfer Function Responses

```
w = 500;
Q = 1;
for i=1:2000
    Tlp(i) = abs(w^2/((j*i)^2 + (w/Q)*(j*i) + w^2));
    Tbp(i) = abs((w/Q*(i*j))/((i*j)^2 + (w/Q)*(j*i) + w^2));
    Tbs(i) = abs(((i*j)^2+w^2)/((i*j)^2 + (w/Q)*(j*i) + w^2));
    Thp(i) = abs((i*j)^2/((i*j)^2 + (w/Q)*(j*i) + w^2));
    Tap(i) = abs(((i*j)^2 - (w/Q)*(j*i) + w^2)/((i*j)^2 + ...
 (w/Q)*(j*i) + w^2));
    m(i) = i;
end

%saving Low pass
lp(:,1) = m';
```

```
lp(:,2) = Tlp';
save Tlp.dat lp -ascii;

%saving bandpass
bp(:,1) = m';
bp(:,2) = Tbp';
save Tbp.dat bp -ascii;

%saving bandstop "notch"
bs(:,1) = m';
bs(:,2) = Tbs';
save Tbs.dat bs -ascii;

%saving high pass
hp(:,1) = m';
hp(:,2) = Thp';
save Thp.dat hp -ascii;

% saving all pass
ap(:,1) = m';
ap(:,2) = Tap';
save Tap.dat ap -ascii;
```

A.10 Effect of Q on Tansmission

```
% Author: Mansoor Naseer
% A code to display the effect of changing Q on bandpass
% filter transfer function
clear all;
close;
w = 500;
%Q = 1;
for Q_factor = 1:5
    for i=1:1000
        Tbp(i) = abs((w/Q_factor*(i*j))/((i*j)^2 + ...
(w/Q_factor)*(j*i) + w^2));
        m(i) = i;
    end
    plot(m,Tbp);
    hold on;
    bp(:,Q_factor+1) = Tbp';
    grid on;
    axis([100 1000 0 1]);
end

%saving bandpass
bp(:,1) = m';
save Q_Tbp.dat bp -ascii;
```

A.11 Butterworth versus Chebyshev Comparison

```
% Author: Mansoor Naseer
% The code is to plot transmission function |(Vout/Vin)|
% of both butterworth and Chebyshev filters for varying
% orders of filters and then a comparison is made for the
% second order filter response between the filter types
clear all;
close all;
% butterworth response for varying n values
for n = 1 : 10,
    i = 1;
    for w = 0:0.1:2,
        butterworth(i) = 1/(1 + w^2^n);
        omega(i) = w;
        i = i + 1;
    end
    plot(omega, butterworth);
    hold on;
    butter_response(:,n+1) = butterworth';
end
butter_response(:,1) = omega';
save butter_response.dat butter_response -ascii;
% Chebyshev response for varying n values
figure;
for n = 1 : 10,
    i = 1;
    for w = 0:0.005:2,
        cheby(i) = 1/(1 + (cosh(n*acosh(w)))^2);
        omega_cheby(i) = w;
        i = i + 1;
    end
    plot(omega_cheby, cheby);
    hold on;
    cheby_response(:,n+1) = cheby';
    if n == 2
        comparison(:,n+1) = cheby';
    end
end
cheby_response(:,1) = omega_cheby';
save cheby_response.dat cheby_response -ascii;
% So now we have chebyshev versus butterworth response for n = 2
% attenuation epsilon = 1 here.
n = 2;
i = 1;
for w = 0:0.005:2,
    butterworth(i) = 1/(1 + w^2^n);
    i = i + 1;
```

```
end
comparison(:,2) = butterworth';
comparison(:,1) = omega_cheby';
figure;
plot(omega_cheby,comparison(:,2),'b-',...
omega_cheby,comparison(:,3),'g-');
grid;
save bvscresponse.dat comparison -ascii;
```

Appendix B

Transfer Function Formulation

B.1 Series RLC

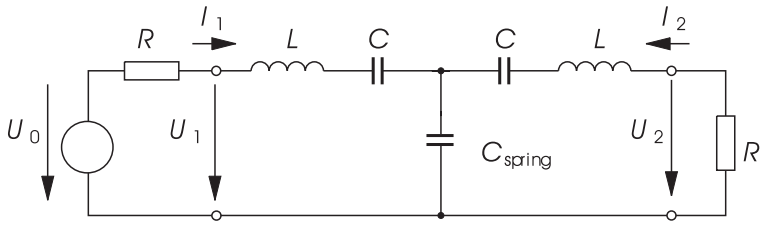

Figure B.1: Series RLC electrical equivalent circuit of second order MEM filter

$$U_1 = j\left(X + X_\mathrm{k}\right) I_1 + jX_\mathrm{k} I_2 \tag{B.1.1}$$

$$U_2 = jX_\mathrm{k} I_1 + j\left(X + X_\mathrm{k}\right) I_2 \tag{B.1.2}$$

$$
\begin{aligned}
U_1 &= j\left(X+X_\mathrm{k}\right)\frac{U_0-U_1}{R}-jX_\mathrm{k}\frac{U_2}{R}\\
RU_1 &= j\left(X+X_\mathrm{k}\right)U_0-j\left(X+X_\mathrm{k}\right)U_1-jX_\mathrm{k}U_2\\
\left[R+j\left(X+X_\mathrm{k}\right)\right]U_1 &= j\left(X+X_\mathrm{k}\right)U_0-jX_\mathrm{k}U_2\\
U_2 &= jX_\mathrm{k}\frac{U_0-U_1}{R}-j\left(X+X_\mathrm{k}\right)\frac{U_2}{R}\\
RU_2+j\left(X+X_\mathrm{k}\right)U_2 &= jX_\mathrm{k}U_0-jX_\mathrm{k}\frac{j\left(X+X_\mathrm{k}\right)U_0-jX_\mathrm{k}U_2}{\left[R+j\left(X+X_\mathrm{k}\right)\right]}\\
\left[R+j\left(X+X_\mathrm{k}\right)\right]^2U_2 &= jX_\mathrm{k}\left(R+j\left(X+X_\mathrm{k}\right)\right)U_0+X_\mathrm{k}\left(X+X_\mathrm{k}\right)U_0-X_\mathrm{k}^2U_2\\
\left(\left[R+j\left(X+X_\mathrm{k}\right)\right]^2+X_\mathrm{k}^2\right)U_2 &= \left[jX_\mathrm{k}R-X_\mathrm{k}\left(X+X_\mathrm{k}\right)+X_\mathrm{k}\left(X+X_\mathrm{k}\right)\right]U_0\\
U_2 &= \frac{jRX_\mathrm{k}}{X_\mathrm{k}^2+\left[R+j\left(X+X_\mathrm{k}\right)\right]^2}U_0\\
H &= \frac{j2RX_\mathrm{k}}{U_0}=\frac{j2RX_\mathrm{k}}{X_\mathrm{k}^2+\left[R+j(X+X_\mathrm{k})\right]^2}\\
H &= \frac{j2RX_\mathrm{k}}{X_\mathrm{k}^2+R^2-(X+X_\mathrm{k})^2+j2R(X+X_\mathrm{k})}\\
H &= \frac{j2RX_\mathrm{k}}{R^2-X^2-2XX_\mathrm{k}+j2R(X+X_\mathrm{k})}
\end{aligned}
\tag{B.1.3}
\tag{B.1.4}
$$

B.2 Q and ν of Equation (2.13)

$$
\begin{aligned}
X &= \omega L-\frac{1}{\omega C}\\
X &= \omega\sqrt{\frac{L}{C}}\sqrt{L\,C}-\frac{1}{\omega}\sqrt{\frac{L}{C}}\frac{1}{\sqrt{L\,C}}\\
X &= \frac{\omega}{\omega_\mathrm{res}}\sqrt{\frac{L}{C}}-\frac{\omega_\mathrm{res}}{\omega}\sqrt{\frac{L}{C}}\\
X &= -\left(\frac{\omega_\mathrm{res}}{\omega}-\frac{\omega}{\omega_\mathrm{res}}\right)\sqrt{\frac{L}{C}}\\
X &= -\nu\sqrt{\frac{L}{C}}
\end{aligned}
$$

B.3 Parallel RLC

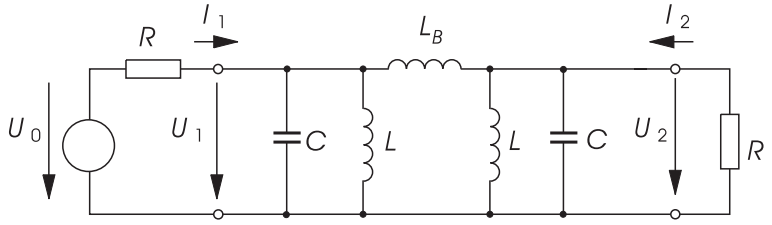

Figure B.2: Parallel RLC electrical equivalent circuit of second order MEM filter

$$
\begin{aligned}
Y_{\mathrm{B}} = \frac{1}{j\omega L_{\mathrm{B}}} \quad &\& \quad Y_{\mathrm{A}} = j\omega C + \frac{1}{j\omega L_{\mathrm{A}}} \\
GU_0 - GU_1 = (Y_{\mathrm{A}} + Y_{\mathrm{B}})\, U_1 + Y_{\mathrm{B}} U_2 \quad &\Rightarrow \quad GU_0 + Y_{\mathrm{B}} U_2 = (G + Y_{\mathrm{A}} + Y_{\mathrm{B}})\, U_1 \\
-Y_{\mathrm{B}} U_1 + (Y_{\mathrm{B}} + Y_{\mathrm{C}})\, U_2 = -U_2 G \quad &\Rightarrow \quad U_1 = \frac{(G + Y_{\mathrm{B}} + Y_{\mathrm{C}})}{Y_{\mathrm{B}}} U_2
\end{aligned}
$$

Solving the above equations :

$$
\begin{aligned}
GU_0 + Y_{\mathrm{B}} U_2 &= \frac{(G + Y_{\mathrm{B}} + Y_{\mathrm{C}})}{Y_{\mathrm{B}}} \cdot (G + Y_{\mathrm{B}} + Y_{\mathrm{C}})\, U_2 \\
\Rightarrow U_2 &= \frac{Y_{\mathrm{B}} G \cdot U_0}{(G + Y_{\mathrm{B}} + Y_{\mathrm{C}})^2 - Y_{\mathrm{B}}^2} \\
H = \frac{U_2}{U_0/2} &= \frac{2 Y_{\mathrm{B}} G}{(G + Y_{\mathrm{B}} + Y_{\mathrm{C}})^2 - Y_{\mathrm{B}}^2}
\end{aligned}
$$

Appendix C

Mask Layouts

C.1 4” Wafer, 600 devices

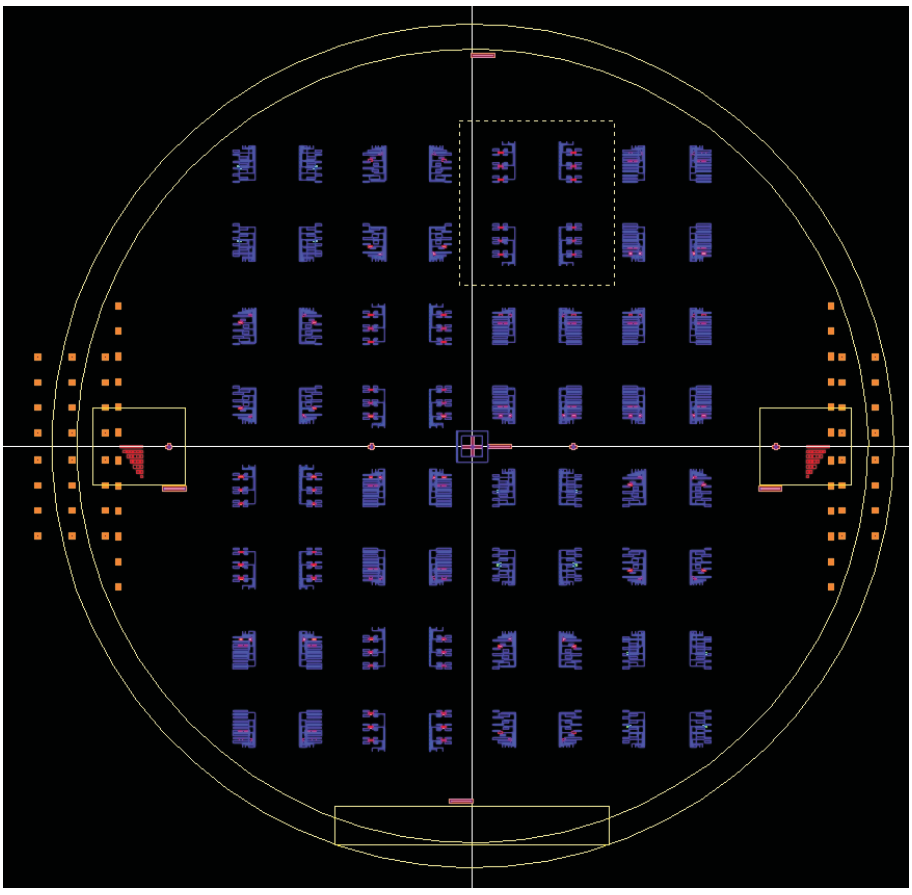

Figure C.1: Complete 4” wafer filled with 256 arrays of 5-15 devices each

C.2 1 x Device array, 15 devices

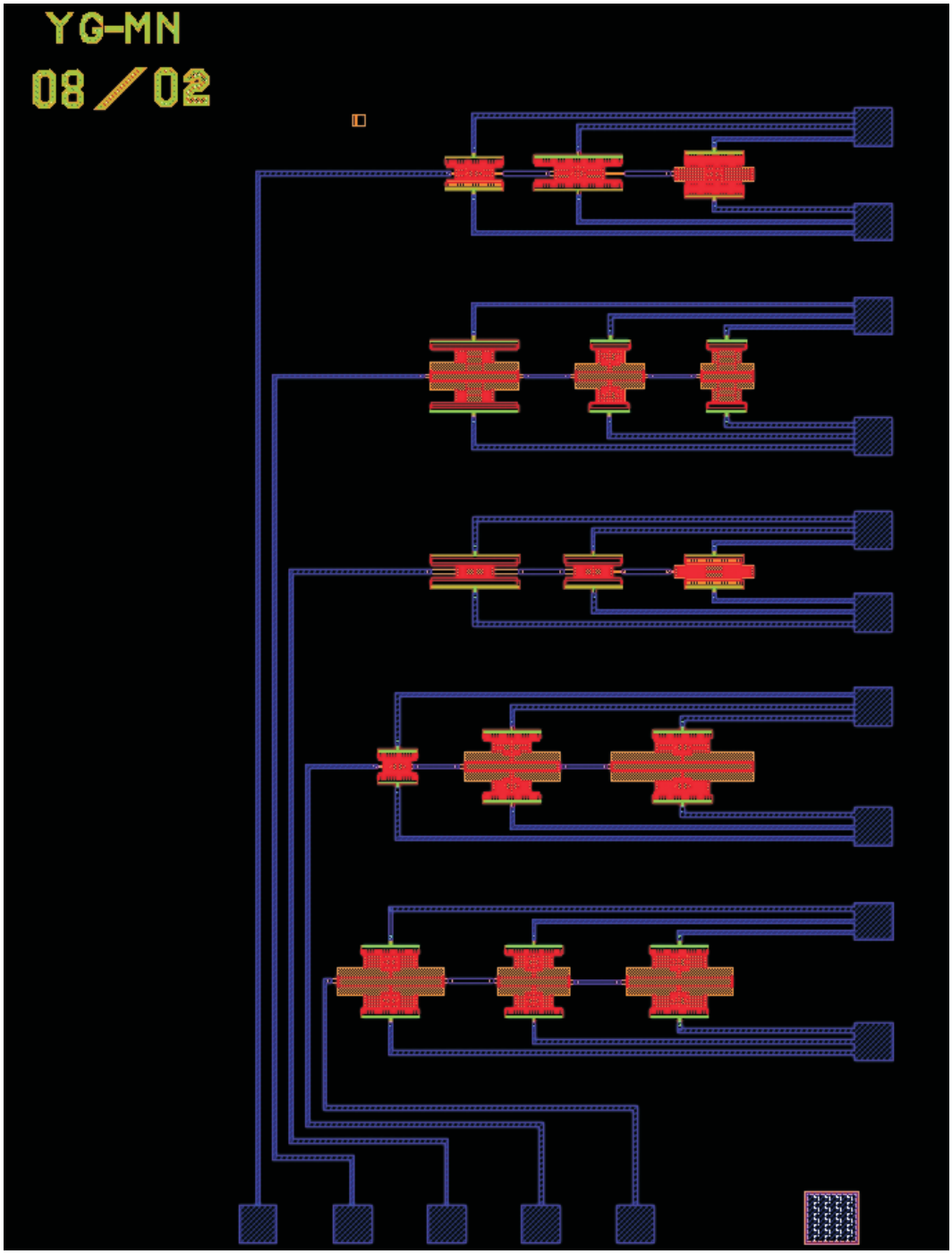

Figure C.2: An array of 15 MEM devices (resonator and bandpass filters) implemented at various frequencies

C.3 Single Resonator

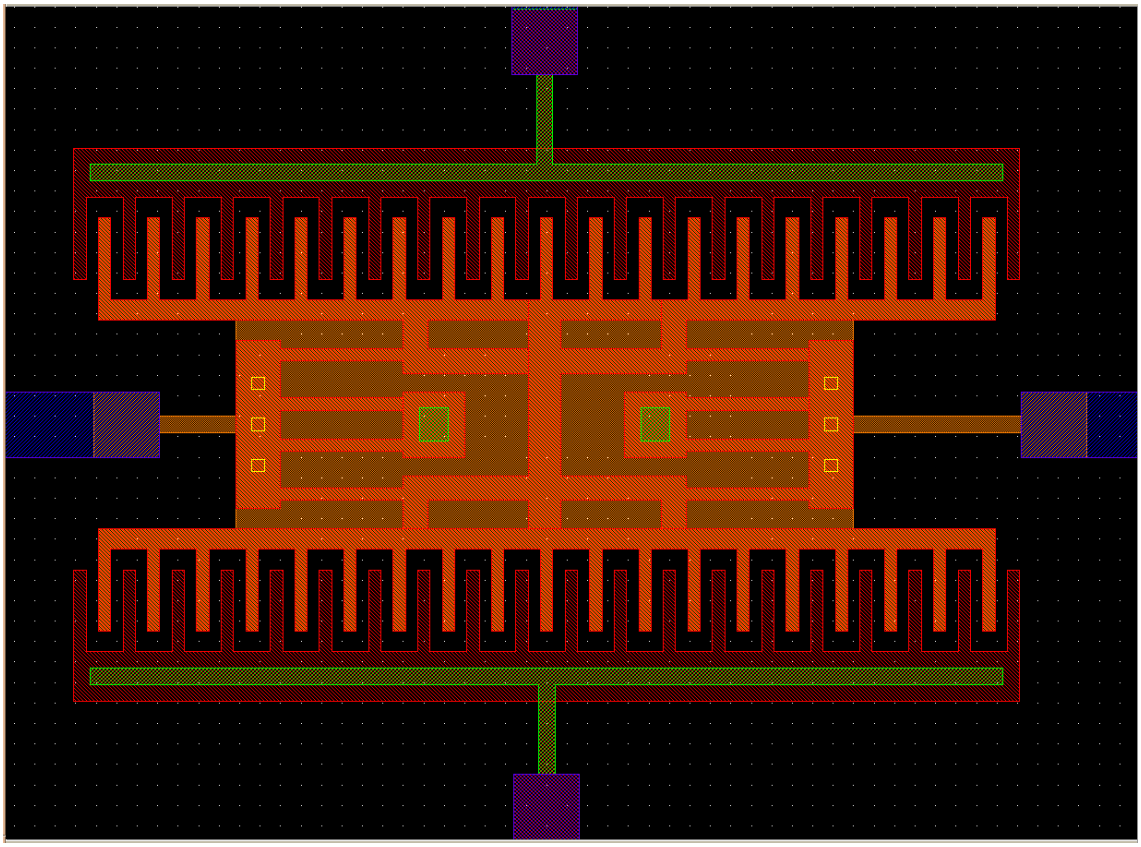

Figure C.3: Single resonator layout drawn using Kanaga (MEMSCAP) design rules

C.4 Alignment Markers

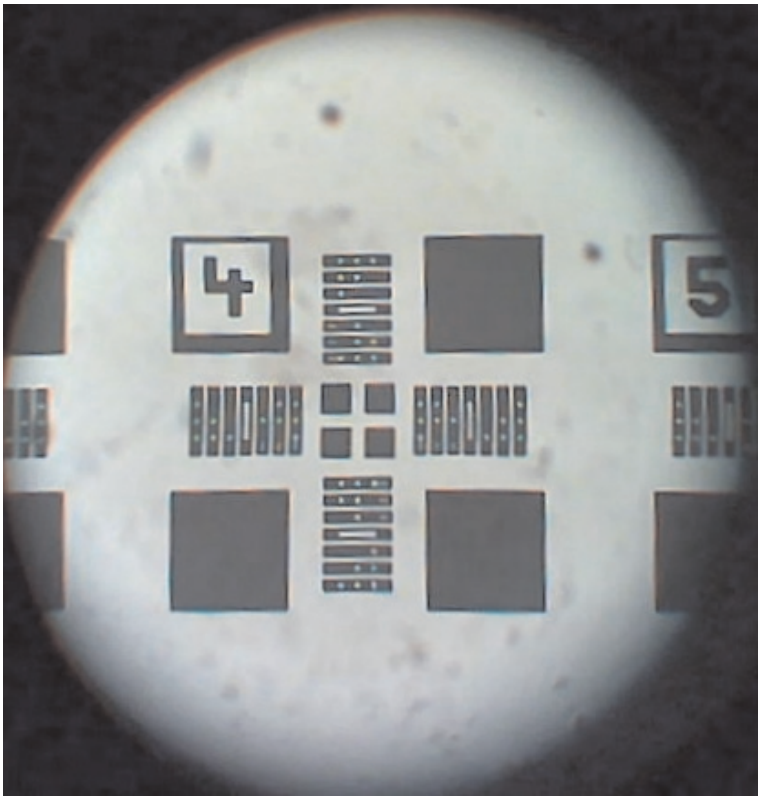

Figure C.4: Alignment markers for the masks

C.5 Devices on Masks

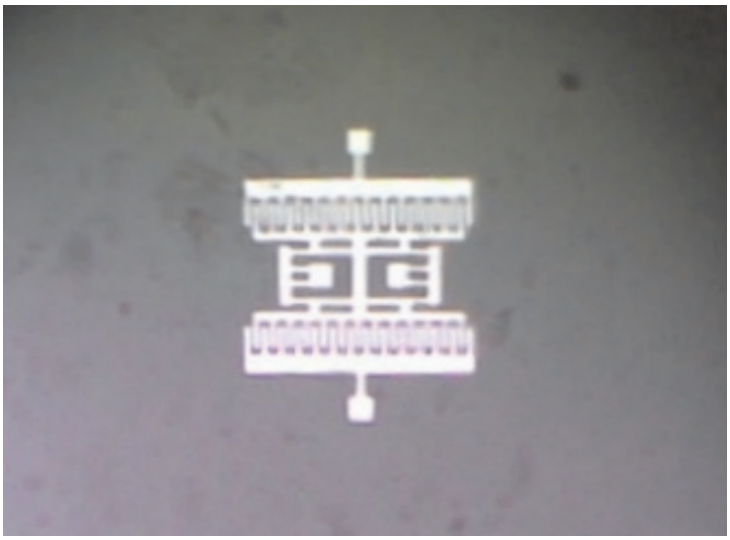

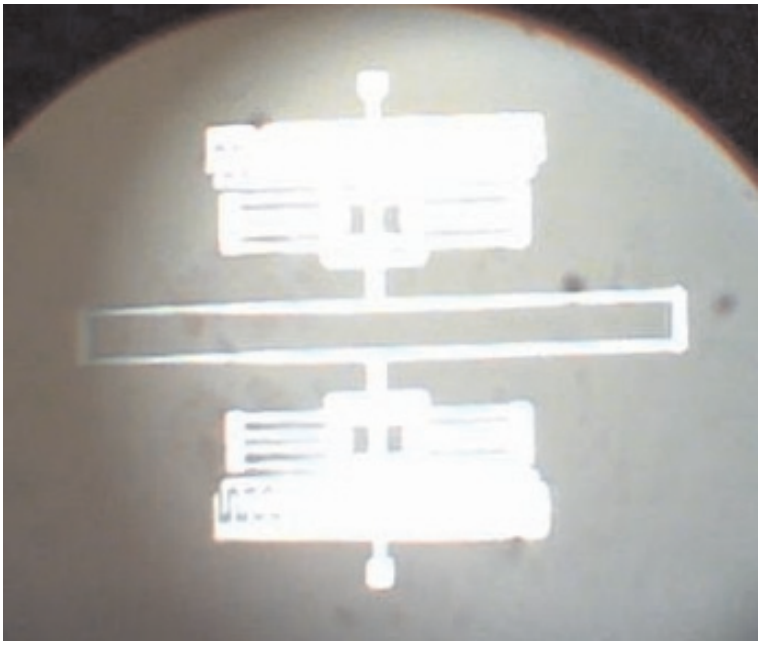

Figure C.5: Single resonator and filter masks

Bibliography

[1] S. Mirabbasi, K. Martin, "Classical and modern receiver architectures", IEEE Comm. Mag., Nov. 2000.

[2] C.T.-C. Nguyen, "Frequency-Selective MEMS for Miniaturized Communication Devices," Proc. IEEE Aerospace Conference, vol. 1, Colorado, pp. 445-460, 1998.

[3] R. Ludwig, P. Bretchko, "RF Circuit Design – Theory and Applications", Prentice Hall, NJ, 2000.

[4] B. Razavi, "RF Microelectronics", Prentice Hall, 1998.

[5] M.Parlak, M. Naseer, Y. Gurbuz, "Design and Simulation of a MicroElectroMechanical Resonator Oscillator" Proc. Nanotech, San Fransisco, pp. 408-411, 2003

[6] C. T.-C. Nguyen, "Frequency-selective MEMS from miniaturized communication devices (invited)", IEEE. Trans. Microwave Theory Tech., vol. 47, pp. 1486-1503, 1999.

[7] F. D. Bannon III, J. R. Clark, C. T. -C. Nguyen, "High frequency microelectromechanical IF Filters", Digest Tech. Papers, IEEE IEDM, San Francisco, pp. 773-776, 1996.

[8] C. T.-C. Nguyen, R. T. Howe, "Quality factor control for micromechanical resonators", Digest Tech. Papers, IEEE IEDM, San Francisco, pp. 505-508, 1992.

[9] W. C. Tang, T.-C. H. Nguyen, R. T. Howe, "Laterally driven Polysilicon resonant microstructures", Sens. Actuators, vol. 20, pp. 25-32, 1989.

[10] W. -T. Hsu, J. R. Clark, C. T. -C. Nguyen, "Q-optimized lateral free-free beam micromechanical resonators", Digest Tech. Papers, pp. 1110-1113, 2001.

[11] T. Delyiannis, "High-Q Factor Circuit with Reduced Sensitivities," Electron. Lett., Vol. 4, p. 577, Dec. 1968.

[12] J.J. Friend, "A Single Operational Amplifier Biquadratic Filter Section", 1970 Digest Tech. Papers, pp. 189, 1970.

[13] R.P. Sallen and E.L. Key, "A Practical Method of Designing RC Active Filters", IRE Trans. Circuit Theory, Vol. CT-2, pp. 74-85, 1955

[14] J. Tow, "Active RC Filters - A State Space Realization", Proc. IEEE, Vol. 56, pp. 1137-1139, 1968.

[15] L.C. Thomas, "The Biquad: Some Practical Design Considerations", IEEE. Trans. Circuits Syst. Vol. CAS-18, pp. 350-357, 1971.

[16] R. Schaumann, M. E. Van Valkenburg, "Design of Analog Filters", Oxford University Press, NY, 2001.

[17] K. Ogata, "System Dynamics", 3rd. Edition, Prentice Hall, 1998.

[18] M. A.Schmidt, R. T. Howe, "Resonant structures for integrated sensors", Tech. Digest, IEEE Solid-State Sensor Workshop, Hilton Head Island, South Carolina, June, 1986.

[19] C. T.-C. Nguyen, "Micromechanical resonators for oscillators and filters", Proc. of IEEE IUS, Seattle, pp. 489-499, 1995.

[20] C.T.-C. Nguyen, "Micromechanical Signal Processors", Ph.D. Thesis, University of California, Berkeley, 1994.

[21] R. T. Howe, R. S. Muller, "Resonant-microbridge vapor sensor", IEEE Trans. on Electron Devices, ED-33, 499-506, 1986.

[22] M. A. Schmidt, R. T. Howe, S. D. Santuria, J. H. Haritonidis, "Design and calibration of a microfabricated floating-element shear-stress sensor", IEEE Trans. on Electron Devices, 35, 750-757, 1988.

[23] Y-H. Cho, A. P. Pisano, R. T. Howe, "Viscous damping model for laterally oscillating microsturctures", JMEMS, vol. 3, no. 2, pp. 81-87, 1994.

[24] J. R. Clark, A. -C. Wong, C. T. -C. Nguyen, "Parallel-resonator HF Micromechanical Bandpass Filters", Digest Tech. Papers, Int. Conference on Solid-State Sensors and Actuators, Chicago, pp. 1161-1164, 1997.

[25] Kun Wang, C. T. -C. Nguyen, "High-Order Medium frequency micromechanical electronic filters", JMEMS, vol. 8, no. 4, pp. 534-557, 1999.

[26] J. R. Clark, W. -T. Hsu, C. T. -C. Nguyen, "High-Q VHF micromechanical contour-mode disk resonators" Digest Tech. Papers, IEEE IEDM, San Fransisco, pp. 399-402, 2000.

[27] C. T.-C. Nguyen, L. P. B. Katehi, G. M. Rebeiz, "Micromachined devices for wireless communications", Proc. IEEE, Vol. 86, No. 8, pp. 1756-1768, 1998.

[28] K. Wang, F. D. Bannon III , J. R. Clark, C. T.-C. Nguyen, "Q-enhancement of microelectromachanical filters via low-velocity spring coupling", Proc. 1997 IEEE Int. Ultransonics Symp., Toronto, Canada, pp. 323-327, 1997.

[29] M. E. Van Valkenburg, "Analog Filter Design", Holt, Rinehart and Winston, 1981.

[30] A. B. Williams, F. J. Taylor, "Electronic Filter Design Handbook", Third Edition, Mc Graw Hill, 1995.

[31] W. C. Tang, "Electrostatic comb drive for resonator sensor and actuator applications", Ph.D. thesis, Dept. EECS, Univ. California, Berkeley, Dec. 1990.

[32] Hector J. Des Los Santos, "Introduction to Microelectromechanical (MEM) Microwave Systems", Artech House, 1999.

[33] CoventorWare Rel. 3.1, www.coventor.com

[34] T. Bechteler, Sabanci University, personal communication

[35] *MUMPS foundry process* design rules version 7. DATE : 2000.

[36] L. Lin, R. T. Howe, A. P. Pisano, "Micromechanical Filters for Signal Processing", JMEMS, vol. 7, no. 3, pp. 286-294, 1998.

[37] M. Naseer, M. Parlak, T. Bechteler, Y. Gurbuz, "Coupling Spring Design and Insertion Loss Minimization of Second Order MicroElectroMechanical Filters" Proc. Nanotech, San Fransisco, pp. 388-391, 2003

[38] A. S. Sedra, K. C. Smith, "Microelectronic Circuits", Fourth Edition, Oxford University Press, 1998.

[39] *Kanaga MEMS design library*, http://www.msc.rl.ac.uk/europractice/univs/memscap.html

[40] M. Bachman, "Cleaning Procedures for Silicon Wafers", INRF Application Note, Spring 2002.

[41] R. C. Jaeger, "Introduction to Microelectronic Fabrication", Vol. 5, Second Edition, Prentice Hall, NJ, 2002.

[42] Shipley S1800 Series Photoresist User Guide. 2000.

[43] M. Bachman, "Spinning Photoresists on Substrates", INRF Application Note, Fall 1999.

[44] M. A. Gulgun, Sabanci University, personal comminucation

[45] S. A. Campbell, "The Science and Engineering of Microelectronic Fabrication" Second Edition, Oxford University Press, NY, 2001.

[46] M. M. Demir, I. Yilgor, E. Yilgor, B. Erman "Electrospinning of polyurethane fibers, Polymer, vol. 43, pp. 3303-3309, 2002.